

Aus dem Biomedizinischen Centrum
der Ludwig-Maximilians-Universität München
Lehrstuhl Molekularbiologie
Vorstand: Prof. Dr. rer. nat. Peter B. Becker

Unraveling Deposition Mechanism and Function of the New Histone H3 Variant H3.Y

Dissertation zum Erwerb des Doktorgrades der Naturwissenschaften
an der Medizinischen Fakultät der Ludwig-Maximilians-Universität München

Lisa-Maria Zink
aus München

2017

Gedruckt mit Genehmigung der Medizinischen Fakultät der Ludwig-Maximilians-Universität München

Betreuerin: Prof Dr. Sandra B. Hake

Zweitgutachter: Prof. Dr. Andreas Ladurner

Dekan: Prof. Dr. med. dent. Reinhard Hinkel

TAG DER MÜNDLICHEN PRÜFUNG: 04.10.2017

Eidesstattliche Versicherung

Ich, Lisa-Maria Zink, erkläre hiermit an Eides statt, dass ich die vorliegende Dissertation mit dem Titel

“Unraveling Deposition Mechanism and Function of the New Histone H3 Variant H3.Y”

selbständig verfasst, mich außer der angegebenen keiner weiteren Hilfsmittel bedient und alle Erkenntnisse, die aus dem Schrifttum ganz oder annähernd übernommen sind, als solche kenntlich gemacht und nach ihrer Herkunft unter Bezeichnung der Fundstelle einzeln nachgewiesen habe.

Ich erkläre des Weiteren, dass die hier vorgelegte Dissertation nicht in gleicher oder in ähnlicher Form bei einer anderen Stelle zur Erlangung eines akademischen Grades eingereicht wurde.

München, den 10.5.2017

.....

(Lisa-Maria Zink)

DANKSAGUNG

Zuerst möchte ich von Herzen Sandra Hake danken. Nie könnte ich mir eine bessere Chefin wünschen! Sie hat mich immer auf ganzer Linie unterstützt, ob es nun wissenschaftliche Durststrecken gab oder ich Unterstützung im Privaten brauchte, Du warst immer da! Du schaffst es mit deiner motivierenden Art einfach immer einen wieder mitzureißen. Danke für die beste wissenschaftliche Betreuung, tolle Teams, lustige Proseccorunden und sehr viel Menschlichkeit!

Ich danke auch Prof. Dr. Peter Becker, der die beste Arbeitsatmosphäre schafft, die man sich wünschen kann. Das gesamte ABI macht es einem leicht jeden Tag gerne in die Arbeit zu kommen und an jeder Ecke Hilfe und Unterstützung zu finden. Außerdem möchte ich meinen TAC Mitgliedern Axel Imhof, Sandro Baldi und Gunnar Schotta für die Unterstützung und den wissenschaftlichen Input danken!

Natürlich möchte ich mich auch bei meinen Kollaborationspartnern bedanken: Erwan Delbarre und Philippe Collas, Eva Keilhauer und Matthias Mann, sowie Marek Bartkuhn. Großen Dank auch an die Praktikanten und Masterstudenten Lucia, Janina und Schmiri. Es war mir ein Fest!

Meine liebsten Kollegen & Freunde! Das alte Northlab plus Sarah hat mir jeden Tag den Gang in die Arbeit versüßt. Ich hatte den größten Spaß mit euch! Seba, der mich in die große weite Welt der Wissenschaft u dieses H3.Ys eingeführt hat, Nils, der immer nur „Artefakt!“ gerufen hat, Corinna, die Schatzmeisterin, Nina, die zwar nur verhältnismäßig kurz bei uns war, dafür immer noch die liebste Freundin ist und natürlich die Leftovers! Ohne euch, Sarah, Maria und Eylisa wäre es sicher nur eine halb so schöne Zeit geworden. Wir hatten so viel Spaß & Salat, ihr habt mit mir Freud und Leid geteilt. Natürlich danke ich auch euch, liebe Hake-Girls! Ramona, die sich immer aufopfernd um alles und jeden kümmert, Stephi, die schuhverrückte Reiswaffeltante und natürlich Martina, deren Tiramisu ich wohl nie vergessen werde. Ich war sehr gerne euer Sonnenschein!

Selbstverständlich danke ich auch meiner Familie. Meiner Mama, meinem Papa, Bruder, Oma und Opa, sowie Tanten und Onkeln. Mama, Papa, ihr habt mich immer unterstützt und mich spüren lassen wie stolz ihr auf mich seid. Oma & Opa, ich könnte mir keine besseren Großeltern wünschen. Ihr wart immer für mich da. Opa, was wären meine Präsentationen ohne dich?

Der allergrößte Herzensdank geht an meinen Kopf- und Seelenverwandten Götz. Für allzeit bereitwilliges Unterstützen in jeglichen Lebenslagen, ständiges Zuhören, fürs Beruhigen, für unzählige Illustrator lessons, für romantische Dates an der Ecke. Du bist der Hummer!

TABLE OF CONTENTS

SUMMARY	1
ZUSAMMENFASSUNG	2
1 INTRODUCTION	4
1.1 CHROMATIN STRUCTURE	4
1.2 COMPLEXITY OF CHROMATIN	7
1.2.1 HISTONE POSTTRANSLATIONAL MODIFICATIONS.....	9
1.2.2 HISTONE VARIANTS.....	11
1.2.3 HISTONE VARIANT H3.3.....	15
1.2.4 HISTONE VARIANT H3.Y.....	19
1.2.5 H3 SPECIFIC CHROMATIN REMODELER & HISTONE CHAPERONES	21
1.2.6 NUCLEOSOME-FREE H3.Y INTERACTOME/CHAPERONES.....	27
1.3 OBJECTIVES	29
2 MATERIALS AND METHODS	30
2.1 MATERIALS	30
2.1.1 TECHNICAL DEVICES	30
2.1.2 CHEMICALS AND CONSUMABLES	31
2.1.3 KITS, ENZYMES & MARKERS.....	33
2.1.4 ANTIBODIES.....	34
2.1.5 PLASMIDS.....	35
2.1.6 OLIGONUCLEOTIDES.....	35
2.1.7 BACTERIAL STRAINS & CELL LINES	36
2.1.8 SOFTWARE	38
2.1.9 STANDARD BUFFERS & SOLUTIONS.....	38
2.2 MOLECULAR BIOLOGICAL METHODS	39
2.2.1 MUTAGENESIS OF H3.Y CONSTRUCTS.....	39
2.2.2 CLONING OF H3.Y MUTANT CONSTRUCTS INTO DESTINATION VECTOR PIRENEO-EGFP.....	40
2.3 BIOCHEMICAL METHODS	41
2.3.1 SDS POLYACRYLAMIDE GEL ELECTROPHORESIS (SDS-PAGE)	41
2.3.2 COOMASSIE STAINING OF POLYACRYLAMIDE GELS.....	41
2.3.3 IMMUNOBLOTTING	41

2.3.4	MONONUCLEOSOME PREPARATION	42
2.3.5	PURIFICATION OF MNASE DIGESTED DNA.....	42
2.3.6	MONONUCLEOSOME-IMMUNOPRECIPITATION (MNASE-IP).....	43
2.3.7	MNASE-IP FOLLOWED BY QUANTITATIVE MS (MNASE-IP-QMS)	43
2.3.8	CHROMATIN IMMUNOPRECIPITATION (CHIP) OF CROSSLINKED & SONICATED HK CELLS	45
2.3.9	ILLUMINA SEQUENCING	47
2.4	CELL BIOLOGICAL METHODS.....	47
2.4.1	MAINTENANCE OF HUMAN HK & MESENCHYMAL STEM CELL LINES.....	47
2.4.2	GENERATION OF STABLE EGFP-H3.Y MUTANT HK CELL LINES	48
2.4.3	TRANSFECTION OF HUMAN MESENCHYMAL STEM CELLS.....	48
2.4.4	IMMUNOFLUORESCENCE (IF) OF HK CELLS & MESENCHYMAL STEM CELLS	48
2.4.5	FLOW CYTOMETRY ANALYSIS OF TRANSFECTED HUMAN CELL LINES.....	50
2.4.6	PREPARATION OF CHROMATIN-FREE EXTRACTS.....	50
2.4.7	IMMUNOPRECIPITATION OF EGFP-H3 VARIANTS IN CHROMATIN-FREE EXTRACTS.....	51
2.5	BIOINFORMATICS.....	52
2.5.1	MNASE-IP-QMS ANALYSIS.....	52
2.5.2	CHIP-SEQ ANALYSIS	52
3	RESULTS.....	54
3.1	H3.Y ONLY INTERACTS WITH THE HIRA COMPLEX BUT NOT DAXX/ATRX.....	54
3.2	H3.Y NUCLEOSOMES ARE DEPLETED FROM H3K9ME3 ENRICHED SIMPLE REPEAT SITES.....	57
3.3	CHROMATIN INTERACTOME OF H3.Y-CONTAINING NUCLEOSOMES	61
3.4	RESIDUES IN THE H3.Y CORE & C-TERMINUS ARE NECESSARY FOR DAXX INTERACTION	67
3.4.1	MUTATION OF THE SINGLE Q59E RESIDUE IN H3.Y IS NOT SUFFICIENT FOR DAXX BINDING.....	67
3.4.2	REPLACING CORE RESIDUES IN H3.Y DOES NOT ENABLE DAXX INTERACTION	70
3.4.3	H3.3 & H3.Y TAIL SWAP MUTANT CONSISTING OF N-TERMINAL H3.Y & H3.3 CORE/ C-TERMINUS ALLOWS STABLE DAXX INTERACTION	72
3.5	H3.3-DAXX INTERACTION: A DEFINED COMBINATION OF AMINO ACIDS MATTERS.....	76
3.6	DAXX BINDING TO H3.Y MUTANTS INFLUENCES CHROMATIN INCORPORATION SITES	81
4	DISCUSSION	86
4.1	H3.Y ONLY INTERACTS WITH THE HIRA COMPLEX & LOCALIZES TO EUCHROMATIC SITES.....	87
4.2	H3.Y NUCLEOSOMES ARE ENRICHED IN TRANSCRIPTION-ASSOCIATED INTERACTION PARTNERS.....	90
4.3	A COMBINATION OF CORE & C-TERMINAL H3.3 RESIDUES DETERMINES DAXX INTERACTION.....	94

REFERENCES	102
ABBREVIATIONS.....	124
APPENDIX.....	I
CURRICULUM VITAE	V

SUMMARY

The nucleosome is the basic subunit of chromatin, the packaging of DNA in the nucleus in an eukaryotic cell. Nucleosomes consist of DNA that is wrapped around a histone octamer. This octamer in turn contains 2 copies of each histone: H2A, H2B, H3 and H4. One mechanism how DNA-related processes such as transcription or DNA repair can be regulated involves the exchange of canonical histones with so-called histone variants. The incorporation of the variant counterparts is carried out by histone chaperone complexes. Various chaperones interact with the respective variants and determine their deposition into distinct genomic sites. Thus histone chaperones contribute to the regulation and plasticity of the chromatin landscape by introducing a variety of histones. To date eight different human histone H3 variants are described with H3.3 being the best-studied H3 variant. H3.Y on the other hand is a relatively new variant and so far knowledge about its function in chromatin remained limited. Comparing H3 variant amino acid sequences, H3.Y shows the highest similarity to H3.3, and especially shares the same so-called chaperone recognition site with H3.3. The chaperone recognition site is a four-amino acid stretch that determines the interaction of H3 variants with distinct chaperones complexes. Whereas H3.3 interacts with two distinct chaperone complexes, namely DAXX/ATRX and HIRA, our group surprisingly only identified the HIRA complex as a binding partner of H3.Y. In my PhD thesis, I initially confirmed that H3.Y indeed does not interact with DAXX/ATRX. In order to identify the amino acids in H3.Y that prevent DAXX binding I generated multiple H3.3/H3.Y mutants that exhibit amino acid exchanges of H3.Y with H3.3 residues. I could show that apart from the chaperone recognition site a combination of H3.3 core and C-terminal residues contributes to the specific recognition and/or binding of the histone chaperone DAXX to its substrate.

DAXX/ATRX is responsible for the deposition of H3.3 to heterochromatic genomic sites while the HIRA complex mediates H3.3 incorporation into euchromatic regions. Since H3.Y does only interact with the HIRA complex I speculated about its incorporation into open, euchromatic sites. Indeed, I could show by ChIP-seq that H3.Y localizes only to H3K4me3-positive euchromatic regions and is excluded from DAXX dependent H3K9me3-positive and simple repeat sites. Correspondingly, H3.Y nucleosomes are enriched with the transcription-associated FACT complex and depleted of the repressive H3K9me3 mark.

In conclusion I could demonstrate that a combination of core and C-terminal residues prevents H3.Y's interaction with the histone chaperone DAXX, explaining its exclusive localization to euchromatic sites and absence from heterochromatic sites.

ZUSAMMENFASSUNG

Das Nukleosom ist die grundlegende Einheit von Chromatin, der Verpackung der DNA in einer eukaryotischen Zelle. Nukleosomen bestehen aus DNA, die um ein Histonoktamer gewickelt ist; dieses Oktamer wiederum besteht aus 2 Kopien jedes der Histone H2A, H2B, H3 und H4. Ein Mechanismus wie DNA bezogene Prozesse wie Transkription oder DNA Reparatur reguliert werden können, beinhaltet den Austausch der kanonischen Histone mit sogenannten Histonvarianten. Der Einbau dieser Varianten wird von Histon-Chaperon-Komplexen bewerkstelligt. Verschiedene Chaperone interagieren mit den entsprechenden Varianten und bestimmen deren Einbau an unterschiedliche genomische Stellen. Histon-Chaperone tragen somit, indem sie eine Vielzahl an Histonen an bestimmten genomischen Stellen einfügen, zur Regulation und Plastizität der Chromatinlandschaft bei. Bis heute sind acht verschiedene humane Histon H3 Varianten im Menschen beschrieben, von denen H3.3 die am besten untersuchte Variante darstellt. H3.Y wiederum ist eine relativ neue Variante und bisher ist das Wissen um ihre Funktion im Chromatin begrenzt. Vergleicht man die Aminosäuresequenzen der H3 Varianten, zeigt H3.Y die größte Ähnlichkeit zu H3.3 und weist insbesondere die selbe sogenannte Chaperonerkenngungssequenz, ein vier Aminosäuren langer Abschnitt, der die Interaktion von H3 Varianten mit verschiedenen Chaperonkomplexen bestimmt, wie H3.3 auf. Während H3.3 mit zwei unterschiedlichen Chaperonkomplexen interagiert, und zwar DAXX/ATR und HIRA, hat unsere Gruppe überraschenderweise nur den HIRA-Komplex als Bindungspartner von H3.Y identifiziert. In meiner Dissertation habe ich zunächst bestätigt, dass H3.Y tatsächlich nicht mit DAXX/ATR interagiert. Um herauszufinden welche Aminosäuren in H3.Y die Bindung an DAXX verhindern, habe ich diverse H3.3/H3.Y-Mutanten generiert, die Aminosäureaustausche von H3.Y mit H3.3 Resten aufweisen. Ich konnte zeigen, dass abgesehen von der Chaperonerkenngungssequenz auch eine Kombination von H3.3-Resten in der Mitte und am C-terminus der Sequenz zur Erkennung und/oder Bindung von DAXX an sein Substrat beitragen.

DAXX/ATR ist verantwortlich für den Einbau von H3.3 an heterochromatische genomische Stellen, während HIRA die Inkorporation in euchromatische Regionen vermittelt. Da H3.Y nur mit dem HIRA-Komplex interagiert, habe ich über dessen Einbau in offene, euchromatische Stellen spekuliert. Tatsächlich konnte ich durch ChIP-seq zeigen, dass H3.Y nur an H3K4me3 positiven euchromatischen Regionen lokalisiert und von DAXX abhängigen H3K9me3 positiven und simple repeat Stellen ausgeschlossen ist. Entsprechend sind H3.Y-

Nukleosomen angereichert mit dem transkriptionsassoziierten FACT-Komplex und abgereichert mit der repressiven Modifizierung H3K9me3.

Zusammengefasst konnte ich zeigen, dass eine Kombination aus innenliegenden und C-terminalen Resten die Interaktion von H3.Y und dem Histonchaperon DAXX verhindert, was die ausschließliche Lokalisierung in euchromatischen Regionen und den Ausschluss von heterochromatischen Stellen erklärt.

1 INTRODUCTION

1.1 CHROMATIN STRUCTURE

The development from a single zygote to a multicellular organism includes the differentiation into various cell types, each containing the same DNA sequence. Nuclear transfer experiments in mice revealed that the contribution of both the paternal and maternal genomes plays a role to successfully develop an embryo (1, 2). It was concluded that the DNA alone does not provide sufficient information to allow the completion of mouse embryogenesis (3-5). Moreover, since the sequencing of the human genome in 2001 (6, 7) it became apparent that unraveling the genetic code of the DNA can not account for every process. Thus, it is crucial to understand how the genetic information is interpreted in different cell types. Here, chromatin comes into play. In eukaryotes, the DNA is not present as a naked molecule in the cell but exists as a nucleoprotein complex, so-called chromatin. The basic repeating subunit of chromatin is the nucleosome (8, 9), comprised of a nucleosome core particle (NCP) and the linker DNA. The NCP is a disc-shaped complex of 145-147 bp of DNA that are 1.65 times wrapped around a histone octamer in a left-handed manner (10) (Figure 1). This octamer consists of two copies of each histone H2A, H2B, H3 and H4. Histones, in turn are basic proteins that are composed of a N-terminal tail and a globular domain containing the histone fold domain, the region where nucleosomal histones interact with each other and the DNA (10, 11).

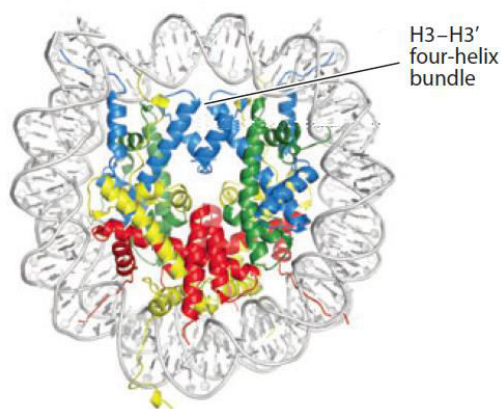


Figure 1: Crystal structure of a nucleosome, looking down the DNA superhelix. Histone H2A is depicted in yellow, H2B in red, H3 in blue and H4 in green, respectively. The interaction of the two H3-H4 dimers by the formation of a H3-H3'-4-helix bundle is highlighted. Adapted and reprinted with permission from Annual Reviews (12).

INTRODUCTION

Although lacking sequence similarity, the histone fold domains (HFD) of the four different histones all share a structural motif: they compose of three alpha-helices $\alpha 1 - \alpha 3$ connected by two unstructured loops, L1 and L2. Two histone H3-H4 dimers interact with each other via a 4-helix bundle of the HFD of H3 and H3' to form a tetramer (see Figure 1). In the presence of DNA or under high salt conditions this (H3-H4)₂-tetramer associates with the two H2A-H2B dimers by the formation of a 4-helix bundle and additionally by the interaction of the H2A docking domain and H3 (12). NCPs are connected by the linker DNA and arranged in an array, thereby making up the primary so-called 'beads on a string' structure (Figure 2) with a diameter of ca. 10 nm (13-16).

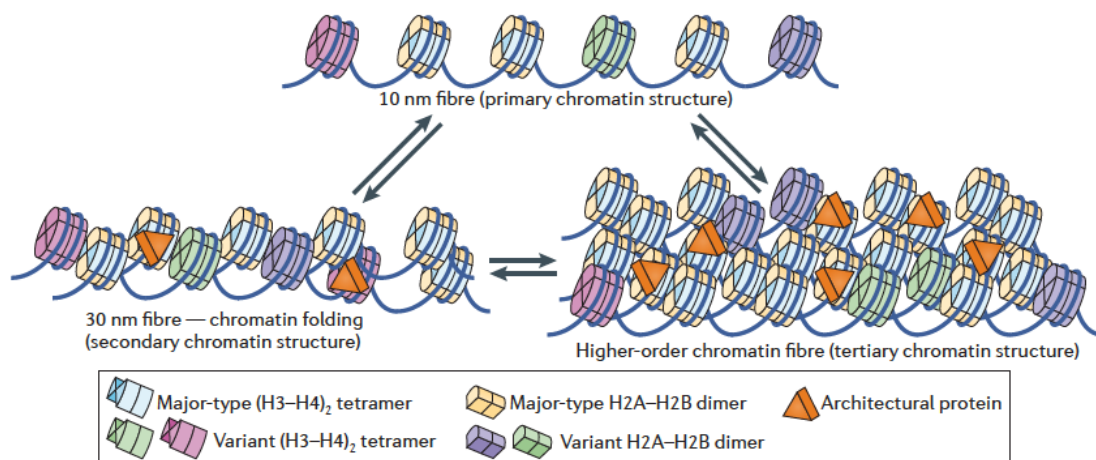


Figure 2: Primary, secondary and tertiary structures of chromatin. Chromatin is thought to be organized in these three structural states. First, an array of nucleosomes defines the primary structure, with nucleosomes consisting of either canonical histones (in light blue and yellow) or variant histones (in green and purple, see chapter 1.2.2). The 30 nm fiber describes the secondary structure whereas long-range interactions between different 30 nm fibers determine the tertiary structure. Secondary and tertiary structures are influenced by the presence of architectural proteins like the linker histone H1 and heterochromatin binding protein 1 (HP1) (see section 1.2) Adapted and reprinted with permission from Nature Publishing Group (13).

Chromatin secondary structure results from short-range interactions between neighboring nucleosomes (17) resulting in a predicted and in *in vitro* experiments observed 30nm fiber (15). Two competing models for this higher order structure of chromatin exist: first the solenoid model and second the zigzag model (Figure 3). The solenoid model proposes that nucleosomes are arranged linearly along a helical turn that is composed of 6 nucleosomes (18-20). It was suggested to be the most stable structure. Yet, later studies revealed a zigzag conformation of the 30 nm fiber where nucleosomes interact with every second neighbor (15, 21, 22). The zigzag model was additionally supported by the crystallization of a tetranucleosome that revealed a zigzag conformation (22).

INTRODUCTION

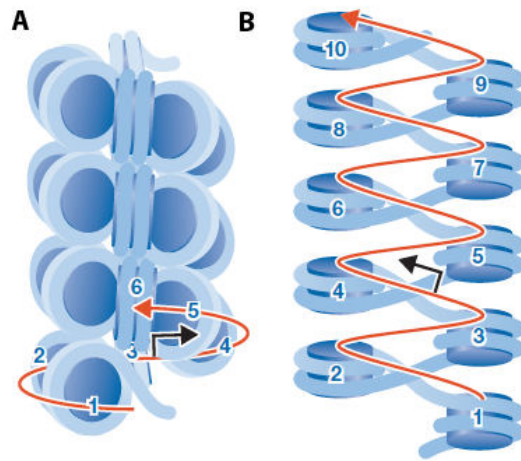


Figure 3: Two models of a 30 nm fiber. (A) Solenoid model of the 30 nm fiber. Nucleosomes are arranged in a helical turn. (B) Alternatively, the Zigzag model exists to describe the conformation of the 30 nm fiber. Here nucleosomes are arranged in a zigzag shape. See text for details. Adapted and reprinted with permission from John Wiley and sons (23).

However, the existence of a 30 nm fiber *in vivo* is under debate (24-27). Rhodes et al. observed that different linker lengths give rise to different conformations of higher order chromatin structures (28). 30 nm fibers have been demonstrated by different *in vitro* approaches, most of them with uniform linker length and precise nucleosome positioning. *In vivo*, however, variable linker length, DNA sequences and heterogeneous histone octamers exist that influence the folding of higher order structures (29, 30). Indeed, the existence of a heteromorphic 30 nm fiber with a mixed conformation of both models was observed (31). Still, recent studies suggest instead of a 30 nm fiber rather the folding into a polymer melt (32) where nucleosome arrays are disordered and in a interdigitated state.

In general, chromatin tends to localize in different compartments according to its functional state (14, 33). Two major functional states of chromatin have been described: on the one hand the repressed heterochromatin and on the other hand the active euchromatin (34). It is believed that differential chromatin compaction between eu- and heterochromatin accounts for the distinct accessibilities to the DNA template and thus its repressed or active transcriptional state.

1.2 COMPLEXITY OF CHROMATIN

As mentioned in 1.1 two major states of chromatin exist: eu- and heterochromatin. Heterochromatin can be subdivided further into facultative and constitutive, determining its either temporary (facultative) or permanent (constitutive) transcriptional repression (35).

Not only during transcription but also during other DNA-related processes such as replication or DNA repair, access to the DNA has to be granted. The balance between maximal compaction of DNA during mitosis and accessibility of DNA is highly complex and regulated by DNA methylation, long noncoding RNAs, architectural proteins, chaperones, ATP-dependent chromatin remodelers and thus nucleosome positioning, posttranslational modifications (PTM) of histones or the incorporation of histone variants (36-47).

DNA methylation is one way to regulate chromatin. It occurs mainly at cytosines (5mC), especially at CpG dinucleotides, and was initially associated with gene silencing (48). However, more recent studies suggest that depending on the position in the gene, DNA methylation can also function in gene activation (49). Whereas methylation around the transcriptional start site (TSS) accounts for transcriptional repression, methylation of the gene body, in contrast, activates transcription (50). Moreover, additional biological functions such as the recruitment of transcription factors (TF) (51), nucleosome positioning (52, 53) and splicing (54) have been linked to 5mC. It has also been demonstrated that methylation is important for genomic stability since it is required for silencing of transposable elements (55), imprinting (56) and chromosomal stability (57). Sequential oxidation of 5mC generates the demethylation intermediates 5-hydroxymethylcytosine (5hmC), which can be further converted into 5-formylcytosine (5fC) and 5-carboxylcytosine (5caC), respectively (58). 5hmC has been found at enhancers, promoters and gene bodies of active genes and is therefore considered as an active mark (59). 5fC alters in contrast to the other modified cytosines the conformation of the DNA double helix structure and might thus influence the binding of diverse proteins (60). Its function is so far unknown but it has been detected at active and poised enhancers in mouse embryonic stem cells (mESCs) (61). A recent study suggested that 5caC serves to decelerate the transcription machinery, thereby fine tuning transcriptional elongation (62).

In addition to cytosine, the methylation of adenine in mouse embryonic stem cells was described in 2016, resulting in silenced LINE transposons and neighboring enhancers and promoters (63). It is becoming obvious that DNA methylation is highly complex and has differential outcomes regarding the circumstances: localization of the methylation mark in the transcriptional unit (TSS versus gene body) or elsewhere in the genome (centromeric

INTRODUCTION

and pericentromeric localization) as well as methylation timing during development results in different effects (56).

In addition to DNA methylation chromatin can also be regulated by long noncoding RNAs (lncRNAs). These are defined as “non-protein coding transcripts longer than 200 nucleotides” (nt) (64) and are often expressed tissue- and developmental stage-specific (65). They can influence chromatin regulation by either recruiting chromatin modifying enzymes such as DNA methyltransferases or histone modifying enzymes to establish DNA methylation and histone posttranslational modifications, or control nucleosome positioning (47).

A third way to regulate chromatin structure is achieved by the presence of architectural proteins. These proteins have the property to bind chromatin and thus modulate higher-order chromatin structures (13, 66) (see also Figure 1). Shaping the 3-dimensional organization of the genome functions through binding of the linker histone H1 that stabilizes higher-order structures (18, 67) as well as through Polycomb group proteins that are responsible for the establishment of facultative heterochromatin (16). Furthermore, CCCTC-binding factor (CTCF) has been demonstrated to mediate long-range interactions in the genome and by that e.g. enables enhancer-promoter-interactions (68, 69). Several architectural proteins have been identified, but introduction and discussion of these go beyond the scope of this thesis. For more details see (68, 70, 71).

Diverse biological processes such as transcription, replication or DNA repair require access to the DNA. Normally DNA is occluded in nucleosomes, thereby providing hurdles for these processes and regulating them. One way to gain access happens via ATP-dependent chromatin remodeling (36). Chromatin remodelers are multiprotein complexes that modify chromatin structure by sliding or evicting nucleosomes or exchanging histones with their variants (see 1.2.2) (39). They can be grouped in four families depending on the domain structure surrounding their ATPase domain: SWI/SNF (switch/sucrose non-fermentable), CHD (chromodomain helicase DNA-binding protein), ISWI (imitation switch) or INO80 (inositol-requiring 80). All these enzymatic subunits pair with a variety of different proteins thereby building diverse chromatin remodeling complexes with distinct characteristics. SWI/SNF remodelers are capable of sliding and/or evicting nucleosomes, ISWI remodelers are involved in nucleosome spacing, chromatin assembly and gene silencing by compacting chromatin in higher order structures. Depending on the associated proteins and the complex, ISWI can also be involved in transcriptional activation highlighting the diverse nature of the different complexes (72). Similarly, CHD remodelers are also associated with diverse functions ranging from transcriptional repression to activation and nucleosome

INTRODUCTION

sliding (73, 74). INO80 remodelers exhibit helicase activities and regulate the exchange of H2A/H2A.Z-H2B dimers. Moreover they can evict and slide nucleosomes and are involved in DNA repair (75-79).

In the further sections other ways of chromatin regulation will be discussed in detail.

1.2.1 Histone Posttranslational Modifications

As mentioned earlier, not only the DNA but also histones can be modified in various ways to influence chromatin packaging and accessibility. Among the posttranslational modifications are at least: acetylation, methylation, phosphorylation, deimination, glycosylation, ADP-ribosylation, ubiquitination, SUMOylation, propionylation, formylation and crotonylation (80-82). Histone PTMs are established by “writers”, enzymes that set the respective modification and can be removed by so-called “erasers” (83). There are two ways how PTMs affect chromatin: they can either directly modulate chromatin structure or recruit other “readers” thereby indirectly mediating changes in chromatin structure through other effector chromatin proteins (40, 80). PTMs can occur on the N-terminal tail of the histones, or on the other hand on the histone core. So far, studies mainly focused on modifications of the histone tails; however, more and more data reveal the functions of core histone modifications (84). Here, I will discuss the best-studied PTMs, especially on H3 as the thesis focuses on this histone type.

Acetylation, in general, appears on lysines and causes a charge neutralization of this positively charged amino acid, thereby weakening the interaction of the histone and the negatively charged DNA (80). This is believed to induce changes in chromatin structure and facilitate access to the DNA. In general, this modification is set by so-called histone acetyltransferases (HATs) or alternatively called lysine acetyltransferases (KATs) and associated with transcriptional activity (85). Removing acetylation by histone deacetylase (HDACs) is thought to stabilize chromatin, therefore HDACs are generally associated with gene silencing (86). Histone acetylation occurs on the N-terminal tail as well as on core residues of the histones (40, 84): histone H3 lysine 4 acetylation (H3K4ac), H3K9ac, H3K14ac, H3K18ac, H3K23ac, H3K27ac, and H3K36ac all correlate with transcriptional activation (40, 87-92). Additionally, H3K14ac and H3K18ac facilitate DNA repair (93, 94), illustrating the complexity of PTMs depending on the chromatin context. This modification also occurs on histone core residues, e.g. H3K56, H3K64, H3K115, and H3K122 were demonstrated to be acetylated (95, 96). Both, H3K56ac and H3K64ac mark active chromatin and are believed to

INTRODUCTION

destabilize the nucleosome (97). H3K115 and H3K122 are located at the dyad axis of the nucleosome where the strongest contacts between histone and DNA occur. Acetylation might enable nucleosome disassembly (98). Both residues have been shown to be acetylated, although functional studies for H3K115ac are missing so far. H3K122ac is enriched around the TSS and involved in transcriptional activation in agreement with its ability to facilitate nucleosome eviction (99, 100).

In addition to acetylation, histones can also be methylated at lysine (mono-, di- and trimethylation) and arginine residues (mono- and dimethylation; symmetric or asymmetric). H3 lysine 4 di- or trimethylation are both associated with euchromatin (101, 102), whereas H3K9me3 and H3K27me3 mark transcriptionally silent regions (103, 104). Additionally, enriched H3K9me3 is found in imprinted regions (105), while H3K27me3 is involved in X-inactivation in mammals (106). Trimethylation of H3K36 is involved in transcriptional elongation (107). H3R42 is located at the DNA entry/exit site of the nucleosome and methylation at this position might disrupt the histone-DNA binding. Dimethylation of R42 has been demonstrated *in vivo* in human and mouse cells and results in enhanced transcription in *in vitro* transcription assays (108). Moreover, H3K56 and H3K64 are not only acetylated but also methylated. Trimethylation of the two residues is a heterochromatic mark, localized at pericentromeric repeats and might play a role in compaction of chromatin (40, 109). Both, H3K56me3 and H3K64me3, partly overlap with H3K9me3, again supporting their function in heterochromatin (109, 110). Finally, H3K79 can be mono-, di- and trimethylated. This residue is located on the solvent-exposed site of the nucleosome and therefore easily accessible. All H3K79 methylation states have been linked to transcription and accordingly H3K79 hypomethylation correlates with heterochromatic loci in yeast (111-114).

Last but not least, serine, threonine and tyrosine residues can be phosphorylated. Among the best-studied phosphorylated H3 residues are H3S10 and H3S28. Both have opposing roles and are either associated with transcriptional activation of immediate early genes or on the other hand involved in chromosome condensation during mitosis (115-118).

It is getting more and more clear that depending on the chromatin context, spatiotemporal dynamics and the crosstalk between PTMs different outcomes derive from the same histone modification. Indeed, the “histone code hypothesis” was brought forward years ago where it is postulated that the combination of PTMs on one or different tails of the histones establishes a histone code that affects different biological processes by recruiting different reader proteins (119). This hypothesis is still highly debated since only a limited number of

INTRODUCTION

combinations occurs *in vivo* (120). Nonetheless, it is clear that several combinations of PTMs have been demonstrated to result in different biological outcomes: the repressive H3K27me3 and the active mark H3K4me3 occur together at bivalent genes in mESCs to enable transcriptional activation while keeping the genes in a generally repressed state (121). The antagonistic modifications do not necessarily have to be on one tail, but can also appear on the two copies of H3 in one nucleosome with one H3 tail carrying H3K27me3 and the other one carrying H3K4me3 (122).

Apart from that, it has also been demonstrated that in some cases specific modifications are prerequisites to establishing additional marks. Trimethylation of H3 lysine 27 in *Drosophila melanogaster* is dependent on phosphorylated H3S28. Mutating H3 serine 28 to alanine that can not be phosphorylated anymore results in a global reduction of H3K27 methylation (123). Moreover, the methylation of H3K4 and H3K79 are both dependent on ubiquitinated H2BK123 (124).

All in all, it becomes obvious that different PTMs and combinations thereof depend on developmental or cell cycle stages, modification timing, genome localization, and histone residues, thereby establishing another complex layer to the regulation of chromatin structure.

1.2.2 Histone Variants

To complicate the regulation of chromatin even more, the canonical core histones H2A, H2B and H3 exist in a variety of variants. So far no H4 variants have been discovered in humans and higher eukaryotes (125). Canonical histones and histone variants differ in some general aspects. Multiple gene copies of canonical variants are organized in gene clusters that are transcribed only during S-phase thereby ensuring the high histone demand for packaging when doubling the amount of DNA. In contrast, histone variant genes are present in only one or two copies outside of histone gene clusters and are expressed throughout the cell cycle, except CENP-A whose expression peaks in Gap 2 (G2) phase (126). Whereas genes of histone variants often contain introns that can give rise to splice isoforms, again providing more complexity, canonical histones lack introns. Similarly, mRNAs of canonical histones lack a poly A tail and instead contain a stem-loop structure at the 3' end that is suggested to regulate histone supply according to the cell's needs (127). The differences in protein sequence between histone variants and their canonical counterparts can be minimal but also tremendous, ranging from single amino acid substitutions to the exchange of whole

INTRODUCTION

domains. Generally speaking, the exchange of canonical histones with their variants in chromatin can have two different effects: first, the incorporation of variants can result in changes in nucleosome structure and stability or second, the chromatin landscape can be affected by the recruitment of alternative readers and/or different PTMs that in turn recruit other readers.

1.2.2.1 Histone H2A family

So far, the H2A family consists of most variant members. Besides H2A eight variants exist in humans: H2A.Z.1, H2A.Z.2.1, H2A.Z.2.2, H2A.X, macroH2A1.1, macroH2A1.2, macroH2A2, and H2A Barr body deficient (H2A.Bbd). Generally, H2A variants differ mostly in their C-terminus reaching from differences in sequence to alternative length of C-termini (128).

H2A.Z is probably the best-characterized variant. It is highly conserved from yeast to humans and has been shown to be essential in *Tetrahymena*, *D. melanogaster*, frog, and mouse (128).

Although H2A and H2A.Z differ considerably in their primary sequence, the overall nucleosome structure between the two is remarkably similar. However, these minimal changes in nucleosome structure account for H2A.Z's decreased stability. Especially the combination of H2A.Z and the histone H3 variant H3.3 in one nucleosome leads to a significant reduction in stability. Accordingly, H2A.Z localizes around the TSS of genes and is implicated in transcription initiation but also localizes to enhancers and insulators (129-132). H2A.Z is also an important player in DNA repair. Initially, the rapid accumulation of H2A.Z after a DNA double strand break was thought to generate an open chromatin configuration, thereby allowing the repair machinery to gain access to the damaged site (133). However, more recent data support the view, that only after H2A.Z removal, an open chromatin state is established. The initial incorporation of H2A.Z together with the recruitment of heterochromatic factors like HP1 serves as a safety net to prevent transcription of the damaged site and keep the damaged DNA ends in close proximity (133, 134).

Moreover, H2A.Z is implicated in genome organization. First, it was demonstrated to preserve chromatin boundaries and prevent heterochromatin spreading (135). Second, H2A.Z has been shown to be essential for genome integrity. After its depletion mouse and monkey cell lines exhibited chromosome segregation defects with chromatin bridges and lagging chromosomes (136). Third, H2A.Z seems to be implicated in centromere formation. With the onset of mitosis, the localization of H2A.Z changes from promoter regions to the centromere, arguing for a role in centromere structure (137, 138).

INTRODUCTION

MacroH2A is approximately three times larger than H2A and has a unique domain structure with an N-terminal histone-like domain, a linker domain and a non-histone macro domain, that is able to bind nicotinamide adenine dinucleotide (NAD) metabolites (139). MacroH2A is generally considered as a repressive variant (140) conferring gene silencing by three mechanisms. First, it was shown to inhibit chromatin remodeling (141), although this is in conflict with another study that demonstrated no differences in macroH2A remodeling (142). Second, binding of TF is inhibited by the presence of macroH2A in nucleosomes (143). Third, macroH2A reduces histone acetylation by directly inhibiting acetylation and by physically interacting with HDACs (139, 141). MacroH2A is not only implicated in transcriptional repression but is also found at the promoters of both, active and repressed genes and is implicated in the transcriptional activation of some target genes (144, 145).

H2A.Bbd is an unusual, smaller histone and shows only 50% similarity to H2A (146). It is lacking the C-terminal tail and part of the docking domain thereby nucleosomes containing H2A.Bbd result in an altered nucleosome structure with more relaxed chromatin, that binds DNA less tightly (147, 148). Concomitant with this reduced stability, H2A.Bbd is associated with open chromatin such as sites of active transcription and DNA replication (149, 150). Depletion of H2A.Bbd results in changes in gene expression and altered splicing patterns, arguing for roles in transcription and mRNA splicing (150).

H2A.X is the H2A variant with the most specialized function and defined by its unique C-terminus with a so-called SQ(E/D) Φ motif (Φ stands for a hydrophobic residue). It is referred to as the “histone guardian of the genome” (151). Shortly after a double strand break (DSB) H2A.X gets phosphorylated at serine 139 (γ H2A.X). γ H2A.X accumulates then in nuclear foci, which spread along the sites of the DSB, in mammals up to several Mb (152). H2A.X and especially γ H2A.X are believed to mark the damaged sites in the genome and rather than recruiting, are more likely responsible for preserving the repair machinery at the damaged spot. Several studies argue for a role in chromatin destabilization, thereby allowing the repair machinery to gain access to the DNA damage (128).

1.2.2.2 Histone H2B family

In humans H2B has two testis-specific variants, namely TH2B and H2BFWT. In mice, H2BE was identified as the newest variant and is expressed solely in olfactory neurons. Strikingly, its presence is correlated with the life span of olfactory neurons with elevated H2BE levels showing a decreased lifespan (153).

INTRODUCTION

TH2B differs from canonical H2B in 19 amino acids (aa) with most of the replacements at the N-terminal tail, thus resulting in an overall similar nucleosome structure than an H2B-containing nucleosome. It is expressed in testis and involved in histone-protamine exchange during spermatogenesis, but also in the oocyte where it contributes to the reprogramming of the paternal genome (154, 155).

H2BFWT reveals despite its similarity of only 45% with H2B a very comparable nucleosome structure with the same stability. The biggest differences to H2B are located in the N-terminal tail of H2BFWT. Boulard et al. suggested a function in telomere identity but evidence for this is still missing (156, 157).

In general, it has been demonstrated that different combinations of H2A variants together with H2B variants result in different nucleosome structures and stabilities with a large set of variations accounting for the complex needs in various biological processes (158).

1.2.2.3 Histone H3 Family

In humans, the H3 family consists of the canonical histones H3.1 and H3.2 and the variants H3.3, H3.X, H3.Y, CENP-A (cenH3), H3.1t and H3.5. Some of these variants are universal and highly conserved, whereas others are tissue- or species-specific.

CENP-A shares only ca. 45% similarity with its canonical counterparts, with the histone fold domain that shares 62% identity and the more divergent N-terminal tail (159). CENP-A is the most specialized histone variant: it defines a centromere (160). The presence of CENP-A at the centromere is necessary and sufficient for centromere formation but also for the assembly of a kinetochore (161). Although its function as a centromeric variant is highly conserved, its sequence is mildly conserved and rapidly evolving (162).

Due to its divergence in sequence, the CENP-A nucleosome structure differs from canonical nucleosomes. Whereas H3.1- or H3.2-containing nucleosomes wrap 145-147 bp of DNA, CENP-A nucleosomes wrap only 121 bp (163). Despite revealing more flexible DNA ends a CENP-A-containing nucleosomal array is more densely packed than H3-containing ones (164). Moreover, it has been shown that the CENP-A gene is essential. CENP-A knockout mice die 6.5 days after fertilization and reveal mitotic defects like micro- and macronuclei and nuclear bridges (165).

CENP-A is crucial for proper centromere function. Misregulation in CENP-A expression and thus disturbed CENP-A levels can account for defects in chromosome segregation and result in aneuploidy, a hallmark of cancer. Hence, it is not surprising that elevated CENP-A levels

INTRODUCTION

were detected in various cancer types such as lung, ovarian, colorectal or breast cancer and correlates in some cases with poor patient outcome (166). These elevated levels of CENP-A are suggested to establish neocentromeres at ectopic sites, thereby causing chromosome breaks, leading to genomic instability (167).

H3.1t and H3.5 are testis-specific H3 variants (168, 169). So far only little is known about the function of H3.5. It is generally associated with euchromatin and in agreement with this excluded from the repressive chromatin regions revealing H3K9me3 and HP1 (169).

The histone variants H3.3 and H3.Y will be discussed in greater detail in 1.2.3 and 1.2.4, respectively since they are the main focus of this thesis.

1.2.3 Histone Variant H3.3

H3.3 is evolutionary highly conserved from yeast to humans. In yeast, only one noncentromeric H3 variant exists and this resembles H3.3 (170). In humans, it is encoded by two genes, *H3f3a* and *H3f3b*, resulting in the same protein but with distinct untranslated regions (UTRs). These differences are responsible for discrete expression patterns, depending on the tissue, developmental stage and cell type (161, 171, 172).

H3.3 differs in humans from the canonical H3.1 and H3.2 in five or four amino acids, respectively. One exchange lays in the N-terminal tail at position 31. Alanine in H3.1/H3.2 is replaced by a serine in H3.3 that can be posttranslationally modified, namely phosphorylated. This phosphorylation occurs in mESCs at both telomeres and pericentric satellite repeats. In differentiated cells, the phosphorylation at telomeres disappears and persists on pericentric heterochromatin. There, the mark is set during mitosis in late prometaphase and metaphase by the Aurora B and CHK-1 kinase (173-176). The other aa differences between H3.1/H3.2 and H3.3 are located in the HFD, more precisely, at position 87, 89 and 90. Overall, these differences do not result in structural changes of the nucleosomes containing either H3.3 or H3.1 (177). In line with this, H3.3-containing mononucleosomes exhibit comparable stabilities than H3.1-containing ones (178, 179). However, these results are in conflict with *in vivo* data from Jin et al. who demonstrated reduced stability for H3.3-containing nucleosomes, especially in the combination with H2A.Z. Indeed, H3.3 und H2A.Z have been demonstrated to co-localize at the TSS of active promoters and other regulatory sites and displayed higher turn over rates *in vivo* (130, 180, 181). Additional *in vitro* studies revealed H3.3's effect on chromatin structure. Nucleosomal

INTRODUCTION

arrays containing H3.3 showed reduced folding of higher-order chromatin structures whereas H2A.Z nucleosomal arrays were able to efficiently compact chromatin. Arrays containing both variants demonstrated intermediate folding states, suggesting that H3.3 is able to antagonize H2A.Z mediated compaction (178). Accordingly, H3.3 could counteract the binding of the linker histone H1 in *D. melanogaster*, supporting H3.3's role in relaxed, open chromatin (182). All of this highly supports the idea of H3.3 as a destabilizing variant, that localizes to nucleosome-depleted regions of active promoters, enhancers and insulators and is able to generate an accessible chromatin environment where TFs can bind.

Conflicting opinions exist about H3.3's contribution to transcription. Whereas some studies unravel the positive effect of H3.3 on transcription (178, 183-185), others report that H3.3 depletion does not cause any transcriptional changes, arguing that H3.3 has no effect on transcription (186-188). In *D. melanogaster*, depletion of both H3.3 genes results in transcriptional defects. To overcome the loss of H3.3, flies upregulate the expression of canonical H3. Similarly, exogenous expression of canonical H3 at one of the endogenous H3.3 loci can compensate the transcriptional defects caused by H3.3 loss (189). In contrast, the double knock out mouse does only show mild transcriptional abnormalities, suggesting only a minor function for H3.3 in transcription in the mouse. Unlike in *D. melanogaster*, no elevated level of canonical H3 was detected, thus the general loss of histones by depleting H3.3 is not compensated (187). Inducible genes, however, reveal impaired transcriptions after H3.3 knockdown, arguing that H3.3 positively influences their expression (178, 184). In general, H3.3 is associated with active PTMs and marks of ongoing transcription like the presence of RNA Polymerase II (190). Recent studies suggest, that deposition of H3.3 at transcribed loci happens due to a "gap-filling mechanism". H3.3 is expressed and available throughout the cell cycle and can therefore be deposited during transcription when nucleosomes get disrupted and "gaps" in chromatin appear. This suggests that H3.3 can be deposited anywhere in the genome where nonnucleosomal DNA occurs and might therefore be important for genome integrity (191).

As mentioned above, H3.3 differs only in a few aa from the canonical variants (see Figure 4). Although the exchanges in the HFD do not alter the nucleosome structure they are sufficient for the differential localization of the variants. Whereas H3.1 and H3.2 are deposited throughout the genome during replication H3.3 is deposited at distinct genomic regions. Mutating the canonical specific residues to the corresponding H3.3 residues in *D. melanogaster* abolishes replication-dependent deposition and allows incorporation

INTRODUCTION

throughout the cell cycle, arguing that not the expression time but the sequence determines the differential deposition modes (192).

On the one hand H3.3 gets deposited at euchromatic and nucleosome depleted sites like promoters and enhancers, at TF binding sites, at the gene body of actively transcribed genes, at transcriptional end sites of highly transcribed genes but also localizes to heterochromatic sites like pericentric heterochromatin, telomeres and retroviral elements (130, 175, 190, 191, 193-200). Here H3.3 is associated with gene repression. In mESCs H3.3 is present at a subset of repetitive endogenous retroviral elements and there co-localizes with the repressive histone mark H3K9me3. Depletion of H3.3 results in loss of H3K9me3 and upregulation of certain nearby genes. Additionally, H3.3 has been shown to be essential for the establishment of the heterochromatic H3K9me3 mark at telomeres. Knockout of either *H3f3a* or *H3f3b* in mESCs resulted in reduced levels of the silencing modifications H3K9me3 and H4K20me3, accompanied by increased transcription of the telomeric repeat-containing RNA TERRA (190, 197). The tumor suppressor ZMYND 11 was shown to simultaneously bind H3.3 and H3K36me3, a mark of active transcription. Thus, ZMYND11 localizes indeed to transcribed genes but there represses transcription, although in the presence of H3.3 (107). This goes in line with the H3.3 dependent recruitment of the Polycomb Repressive Complex 2 (PRC2) that localizes to the promoters of bivalent genes and is required for the establishment of the heterochromatic PTM H3K27me3 (188). Altogether H3.3's role in transcription is not clear. Various effects of H3.3 suggest that it could function as a transcriptional activator and repressor depending on the context.

Apart from its role in transcription, H3.3 is also responsible for the formation of heterochromatin and maintaining chromatin integrity. In mouse embryos, H3.3 and H3.3K27 are necessary for the initial establishment of heterochromatin. Expression of the H3.3 mutant H3.3K27R leads to increased transcription of pericentric repeats, chromosome segregation defects and developmental arrest (201). Accordingly, mouse embryonic fibroblasts (MEFs) and mESCs derived from H3.3 double knockout mice reveal a more open chromatin at centromeres and telomeres, mitotic defects like anaphase bridges and lagging chromosomes but also increased telomeric sister chromatid exchanges, aneuploidy, and polyploidy, arguing for a role of H3.3 in genome stability (187). Similarly, in mESCs H3.3 has been demonstrated to be critical for telomeric integrity. Depletion of H3.3 leads to the accumulation of telomere dysfunctional induced foci (TIFs), a chromatin structure defined by the presence of DNA damage response factors indicating impaired genome integrity (202).

INTRODUCTION

H3.3 knockout mice die early in embryonic development, however conflicting data exist about the survival of single *H3f3a* or *H3f3b* knockout mice (187, 203-206). Strikingly, H3.3 depleted mice and flies exhibit reduced fertility, suggesting an essential role for H3.3 in germline development (187, 189, 203-206). Indeed, it has been shown that either both, *H3f3a* and *H3f3b* are critical for oocyte development or *H3f3b* alone is essential for spermatogenesis (204, 205). These findings are further supported by the fact, that both genes reveal highest expression in the testes, followed by the ovary, implying again a key function for H3.3 in germ cell development (187).

All in all, rather than functioning in transcription, H3.3 might have an essential role in maintaining genomic integrity and chromosome stability.

Often histone genes are up- or down-regulated in cancer. Also H3.3 was reported to be upregulated in esophagus and lung cancer (207, 208). Furthermore, mutations in H3.3 were the first mutations detected in histones linked to a disease. In 2012, Wu et al. and Schwartzenuber et al. unveiled a somatic heterozygous mutation in *H3f3a*, resulting in an H3.3K27M or H3.3G34R/V mutant in pediatric glioblastoma (209, 210). Additionally, the recurrent mutations H3.3K36M and H3.3G34L/W were found in juvenile bone cancer patients (211). Several studies uncovered the mechanism how these mutations affect chromatin. Normally H3K27 is methylated by the PRC2 complex, resulting in H3K27me₃, an important mark for gene silencing. However, cells expressing the K27M mutant exhibit overall lower levels of H3K27me₃. Noticeably, although the mutant H3.3 contributes only a minor fraction to the total histone pool, the overall levels of H3K27me₂ and H3K27me₃ were dramatically diminished, suggesting that K27M acts as a gain-of-function mutation. The authors could show that the enzymatic activity of the PRC2 subunit EZH2 was inhibited by K27M (212, 213). Moreover, K27M binds PRC2 more tightly than the wildtype equivalent, so that it sequesters PRC2 and it can no longer distribute the repressive K27me₃ mark (214). A cell line derived from a tumor tissue isolated from a glioblastoma patient harboring the H3.3K27M mutation was analyzed by deep sequencing. In addition to globally loosening H3K27me₃, this patient cell line also revealed the differential distribution of the remaining mark. First, the chromatin regions still carrying H3K27me₃ were broader in comparison to human neural stem cells (NSCs) that were used as a control. Secondly, 63% of the remaining peaks were unique, meaning they did not appear in NSCs. This led i.e. to silencing of the tumor suppressor p16INK4A as shown by transcriptome analysis. Moreover, these unique peaks, as well as most of the remaining H3K27me₃ peaks, almost completely overlap with EZH2 peaks, supporting again the idea of H3K27M sequestering PRC2 (213). The oncogenic

INTRODUCTION

potential of H3.3K27M arises probably not only from a general loss of methylation and thereby the activation of potential oncogenes but also from the mislocalization of the remaining H3K27me3 so that tumor suppressor genes get repressed.

A similar scenario can be observed in cells harboring the K36M mutation that occurs in cancers arising from mesenchymal tissues like chondroblastomas. Lysine 36 on H3 lies in the gene body of active genes and is associated with transcriptional elongation. Complementary to K27M inhibiting EZH2 in the PRC2 complex, also the K36M mutation inhibits the catalytic subunits of H3K36 methyltransferases. This inhibition results in reduced H3K36me2 and H3K36me3 levels (215, 216). However, in this case, loss of H3K36 methylation is accompanied by an increase in H3K27me3 at intergenic and a reduction at gene-associated sites. Together with the reallocation of the repressive PRC1 complex that binds to H3K27me3, this results in changes in the transcriptome (215, 217).

How G34 mutations contribute to tumorigenesis is unknown. G34 itself is not posttranslationally modified. Yet it lies in close proximity to lysine 36 and is therefore assumed to influence its accessibility for PTMs. Indeed, a study revealed that H3K36me3 is reduced in H3.3G34R expressing human HEK293T cells, suggesting that it can modulate histone posttranslationally modifications (212). Alternatively, G34 mutations could interfere with the binding of specific H3K36me3 readers and thereby contribute to cancer development.

1.2.4 Histone Variant H3.Y

H3.Y is one of the most recently discovered histone H3 variants. In contrast to the evolutionary conserved H3.3, it is a younger histone variant only present in primates. Alignment of H3.Y with the canonical variants and H3.3 reveals its highest similarity to H3.3, although it shares overall only 80% with H3.3 (Figure 4). Some of the residues prone to posttranslational modification are exchanged in H3.Y such as S10, S28, K14, S31 and K79. Interestingly, acetylation of lysine 18, 23 and 27 was detected on histone H3.Y (218).

INTRODUCTION

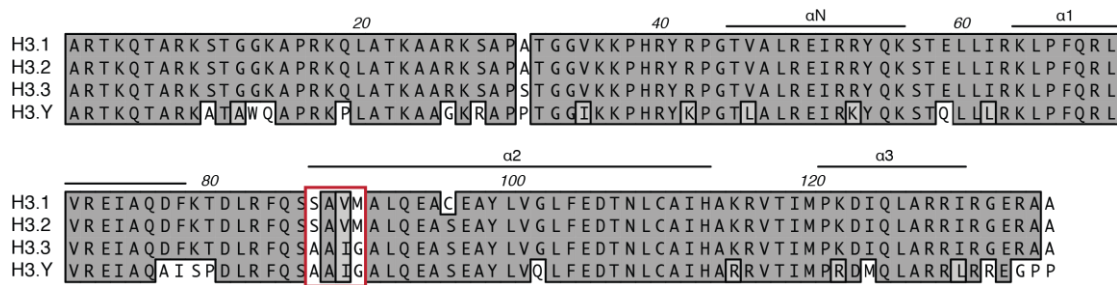


Figure 4: Alignment of human H3 variants. Identical aa are shown in dark gray, similar ones in light gray and aa differences are highlighted with white boxes. The secondary structure of the histones is illustrated with αN , $\alpha 1$, $\alpha 2$ and $\alpha 3$. The canonical variants H3.1 and H3.2 differ only in 4 and 5 aa from H3.3. In contrast, H3.Y shares only 80% similarity with its most similar partner H3.3. The part where H3.3 and the canonical variants differ the most (aa 87-90) is in H3.Y identical to H3.3 (red boxes). Alignment was created using ClustalW Alignment (MacVector 13.5.1).

H3.Y transcripts were detected in some human cell lines but also in primary cells from different human normal and cancer tissues such as lung, bone, breast and ovary tumor tissues as well as in brain and testes. Noticeably, nutritional starvation in combination with overgrowth led to an increase in H3.Y levels in U2OS cells. This osteosarcoma cell line showed minimal H3.Y expression under normal conditions but upregulated its expression during stress. H3.Y is detected in the nucleus, outside of DAPI dense regions, suggesting euchromatic localization and function. Depletion of H3.Y causes transcriptome changes with 293 genes being up- and 974 genes being downregulated, arguing again for a role of H3.Y in euchromatin and gene activation. Moreover, depletion of H3.Y results in diminished cell growth. Classification of downregulated genes uncovered genes belonging to cell cycle control suggesting that this leads to the cell cycle arrest and reduced cell growth (218).

In 2016, the structure of a H3.Y-containing nucleosome was resolved (219). The overall structure was similar to a H3.3-containing nucleosome, however some differences were observed. Residues at the DNA entry/exit site are exchanged in H3.Y suggesting different contacts between the DNA and H3.Y. Indeed, H3.Y nucleosomes had more flexible DNA ends, resulting in a more relaxed chromatin configuration than H3.3-containing nucleosomes. Furthermore, the linker histone H1 that is responsible for chromatin compaction (220) bound less efficiently to H3.Y than H3.3 nucleosomes. Kujirai et al. showed that lysine 42 in H3.Y contributes to the reduced binding of H1. These features of H3.Y are also conserved in heterotypic nucleosomes containing H3.3 and H3.Y: both, DNA end flexibility, as well as binding of H1, are reduced in heterotypic nucleosomes. Finally, the authors stably expressed H3.Y in the cervical carcinoma cell line HeLa and demonstrated its presence at the TSS of actively transcribed genes. Altogether, H3.Y's flexible DNA ends as well as reduced H1 binding might contribute to an open chromatin conformation and

INTRODUCTION

provide better access for the transcription machinery, thereby maintaining active transcription (219).

1.2.5 H3 Specific Chromatin Remodeler & Histone Chaperones

α -thalassaemia/mental retardation X-linked protein (ATRX) is a SWI/SNF remodeler implicated in the deposition of H3.3 to heterochromatic sites such as telomeres, pericentric heterochromatin, and retrotransposons (221, 222). Together with H3.3, ATRX contributes to the establishment and maintenance of H3K9me3 at these regions and transcriptional silencing (190, 197, 223, 224). Moreover, ATRX is implicated in the establishment of a functional telomere and its maintenance (175, 225). Loss of ATRX in human and mouse cell lines is associated with telomere dysfunction, impaired DNA DSB repair and mitotic defects such as chromosome congression defects or chromosome decondensation, leading to genomic instability (225-227). Inactivating mutations and loss of ATRX are associated with a variety of diseases in humans. Initially, ATRX was identified in male patients suffering from mental retardation, α -thalassaemia and facial and genital abnormalities (228). Moreover, ATRX mutations were found in pancreatic neuroendocrine tumors (panNETs) and in glioblastoma where ATRX is often mutated in addition to H3.3 (209, 229-231). Interestingly, tumors associated with ATRX mutations often exhibit an alternative pathway to ensure the maintenance of their telomeres (209, 230). Instead of reactivating telomerase, 10-15% of cancers accomplish immortality by a mechanism based on homologous recombination, so-called alternative lengthening of telomeres (ALT) (232). The high correlation of ATRX mutations and ALT prevalence supports ATRX' known function in telomere maintenance. ATRX loss results in telomere malfunction potentially by impaired deposition of H3.3. This might result in telomere destabilization and lead to the ALT phenotype, emphasizing again the important role of H3.3 and proteins implicated in its deposition for genome integrity.

Histone chaperones are a very diverse group of proteins defined as histone-binders "that influence chromatin dynamics in an ATP-independent manner" (43). Their functions range from nuclear import, providing histone stability, nucleosome assembly, and disassembly to ensuring the right localization in chromatin. From their synthesis to chromatin incorporation histones are permanently bound by histone chaperones. Interestingly, histone chaperones mostly bind either H3-H4 or H2A-H2B (one exception is FACT (facilitates chromatin transcription) (233) and NAP1 (nucleosome assembly protein 1) (234, 235)). In the following, I will elaborate on the diversity of H3-H4 chaperones.

INTRODUCTION

Anti-silencing function 1 (ASF1) is the most conserved chaperone and has been shown to be able to handle the canonical variants as well as the replacement variant H3.3. In humans, two paralogues with non-redundant functions exist: ASF1A and ASF1B. The different isoforms determine the interaction with different downstream chaperones. First, ASF1 is involved in nuclear import of H3-H4 into the nucleus thereby associating with Importin 4, nuclear autoantigenic sperm protein (NASP), retinoblastoma (Rb)-associated protein 46 (RbAp46) and 48 (RbAp48) and histone acetyltransferase 1 (HAT1) (44, 236, 237). After nuclear import, ASF1 functions as a histone donor to downstream chaperones that mediate nucleosome assembly. In complex with ASF1, H3 residues that allow the discrimination between the variants are solvent exposed, meaning different downstream chaperones are able to distinguish between the variants (238). H3.1 and H3.2 are handed over to chromatin assembly factor 1 (CAF1), H3.3 to histone regulatory homolog A (HIRA) and death domain-associated protein DAXX. Evidence exists that HIRA preferentially associates with ASF1A, whereas CAF1 is primarily associated with ASF1B (239-242). Moreover, the binding of CAF1 and HIRA is mutually exclusive, explaining the different deposition modes for the distinct variants (241). All three, CAF1, DAXX and HIRA promote deposition of newly synthesized H3 histones. CAF1 is responsible for the deposition during replication, while HIRA and DAXX mediate H3.3 deposition in a replication-independent manner. ASF1 is not only implicated in *de novo* nucleosome assembly but also aids in the disruption of H3-H4 tetramers and histone eviction at promoters and in coding regions (238, 243-245). A model for the function of ASF1 at the replication fork suggests, that ASF1 associates with the replicative helicase MCM2 during unwinding of the DNA and aids to disrupt tetramers (246). Behind the replication fork, it assists in depositing new histone dimers by handing them over to the CAF1 chaperone complex. This model illustrates the dual function of ASF1 in the deposition of newly synthesized histones and parental tetramer disruption. Thus, ASF1 is implicated in the proper distribution of parental histones on newly synthesized and parental DNA strands, thereby ensuring the proper inheritance of epigenetic information.

Only a few aa differ between the canonical H3 variants and H3.3, however, they are sufficient to cause differential binding to distinct chaperone complexes. Amino acids 87-90 are therefore referred to as chaperone recognition site and determine the association with either replication-coupled deposition pathways, as it is the case for the canonical variants or replication-independent deposition (247, 248).

INTRODUCTION

1.2.5.1 Replication-dependent Deposition of Histone H3

CAF1 is a trimeric complex consisting of the subunits p150, p60, and p48 (also called RbAp48, see above) and is responsible for the deposition of H3.1-H4 and H3.2-H4 during replication and DNA repair (249, 250). The p150 subunit determines CAF1's association with the replication machinery since it directly binds proliferating cell nuclear antigen (PCNA), a protein involved in replication processibility (251). Additionally, CAF1 co-localizes with replication foci in HeLa cells, supporting its role in replication-coupled histone deposition (252). ASF1 directly binds to the p60 subunit, which can be phosphorylated thereby regulating CAF1 localization and activity during the cell cycle and upon DNA damage (253, 254). Only a fraction of total RbAp48 in the cell is present in the CAF1 complex. It is additionally part of histone acetyl- and deacetyltransferase complexes and part of the remodeling complexes NuRD and NURF (42, 255). Depletion of CAF1 or introduction of a dominant negative p150 version in human cells causes tremendously diminished nucleosome assembly, S-phase arrest, DNA replication defects, DNA DSB and even induces cell death in proliferating cells. Thus, CAF1 is essential for chromatin assembly and might also be critical for cell viability (256-258).

Additionally, another chaperone is involved in replication-dependent H3-H4 deposition, namely the FACT complex. It was initially identified as a protein required during transcription and was recently discovered to be involved in H3-H4 deposition during DNA replication in yeast. The FACT complex consists of the two subunits Spt16 (suppressor of Ty16, also called FACT140) and SSRP1 (structure specific recognition protein 1, also called FACT80) (259, 260). Introducing a mutant Spt16 allele into a yeast strain that allows discrimination between FACT functions in transcription and replication revealed its role in replication-coupled nucleosome assembly. The authors suggest a model where FACT cooperates with other chaperones in the deposition of newly synthesized histones (260). It remains to be seen if FACT chaperone function in DNA replication is conserved in humans.

1.2.5.2 H3.3 Chaperones

H3.3 gets deposited replication-independently by two different chaperone complexes, namely the HIRA and DAXX/ATRX complexes. HIRA is responsible for H3.3 deposition in the gene body of actively transcribed genes, regulatory regions like promoters and enhancers and DNA repair sites whereas DAXX/ATRX deposits H3.3 at heterochromatic simple repeat sites often marked by the presence of H3K9me3 (190, 191, 198, 261, 262).

INTRODUCTION

The HIRA complex consists of HIRA, Ubinuclein 1 (UBN1), calcineurin binding protein 1 (CABIN1) and ASF1A (240, 263). HIRA directly binds ASF1A, which does not seem to be a permanent complex member but rather is only transiently bound. This idea is further supported by the fact that H3.3-H4 are still efficiently deposited after ASF1 depletion (264). Recent structural studies revealed that H3.3 specificity is derived from UBN1. It contacts H3.3 around the chaperone recognition site. Especially G90 was identified as the aa that determines UBN1's specificity for H3.3. The mutant H3.3G90M harboring H3.1's methionine instead of glycine at position 90 lost binding to UBN1. In contrast H3.1M90G gained binding, arguing that H3.3G90 mediates the specificity for UBN1 and therefore HIRA (265).

HIRA is recruited to chromatin target sites in multiple ways. The interaction of HIRA with transcriptional regulators, RNA pol II and naked DNA could explain H3.3's presence at regulatory regions and at actively transcribed genes where nucleosomes are displaced and naked DNA occurs (188, 191, 266). Recently, HIRA was shown to build a complex with H3.3 and replication protein A (RPA), a single-stranded DNA binding complex that is involved in DNA replication, repair, and transcription. HIRA, H3.3 and RPA co-localize at gene regulatory regions. Depletion of RPA or HIRA resulted in dramatically reduced H3.3 deposition and association of HIRA at chromatin and altered transcription (262). These data are in conflict with another study. Goldberg et al. observed no changes in H3.3 occupancy at regulatory regions and telomeres after HIRA depletion but demonstrated that gene bodies of actively transcribed genes reveal reduced H3.3 occupancy (190). Moreover, depletion of HIRA leads to reduced CABIN1 expression and vice versa, depletion of CABIN1 results in reduced HIRA abundance. It seems like HIRA and CABIN1 stabilize each other in complex formation (263). Nonetheless, CABIN1 appears to have only a minor effect on H3.3-H4 deposition.

The absence of HIRA and impaired H3.3 deposition is not rescued by CAF1 mediated H3.1 deposition. In contrast, HIRA can compensate for CAF1 loss and deposits H3.3 at replication sites, probably by its DNA binding capability (191). This binding could also explain HIRA's role in DNA repair. Very early after DNA damage HIRA gets recruited to UV-C damaged regions and promotes deposition of H3.3-H4. This H3.3 deposition might serve as a mark for transcription restart after DNA repair (261). It is so far not clear, whether H3.3 deposition by HIRA serves only as a gap-filling mechanism in nucleosome depleted regions thereby ensuring genomic integrity or whether it directly regulates DNA-related processes as suggested by (262).

Additionally, H3.3 deposition at heterochromatic sites is accomplished by the DAXX/ATRX complex (190, 198, 222, 223, 267, 268). Absence of DAXX did not result in a general loss of

INTRODUCTION

H3.3, surprisingly partially due to CAF1's binding to H3.3 (191, 267). On the other hand, DAXX loss affected deposition of H3.3 to pericentric repeats thereby leading to impaired transcription from these repeats, similar to ATRX depletion (267). This result is maybe counterintuitive since H3.3 was shown to be implicated in silencing in these regions and other studies mentioned above showed upregulation of TERRA after ATRX loss (190).

Both DAXX and HIRA knockout mice die during embryonic development. Since DAXX has also crucial roles apart from its functions in nucleosome assembly, these phenotypes can not only be accredited to the loss of H3.3 deposition (269, 270).

The histone-binding domain (HBD) of DAXX was crystallized together with an H3.3-H4 dimer (247, 248). The structure revealed that DAXX occupies an α -helical fold and wraps around an H3.3-H4 dimer (Figure 5). DAXX binding to H3.3-H4 is composed of hydrophobic and electrostatic interactions and hydrogen bonds.

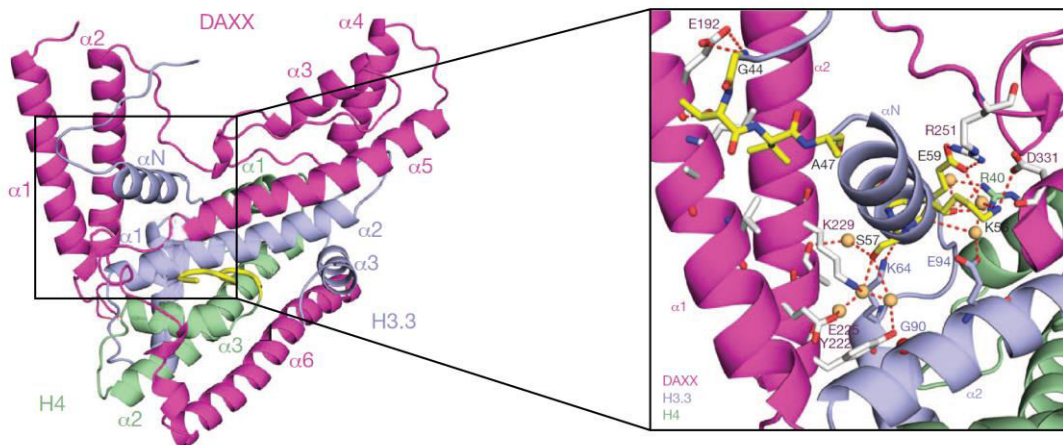


Figure 5: DAXX wraps around an H3.3-H4 dimer. The HBD of DAXX crystallized together with an H3.3-H4 dimer. The crystal structure unveils the overall α -helical fold of DAXX. DAXX is shown in pink, H3.3 in purple and H4 in green. Adapted and reprinted with permission from Nature Publishing Group (247).

DAXX binding competes, such as many other chaperones do, with H3-H4 tetramerization and DNA binding. Moreover, it also competes with ASF1, suggesting that in contrast to HIRA or CAF1 DAXX is not found in one complex with ASF1. Indeed, pull down experiments in HeLa cells revealed that DAXX and ASF1 can not be immunoprecipitated together. Increasing the availability of free H3.3-H4 by depleting ASF1 resulted in an increased association of DAXX-H3.3-H4 ternary complexes. In turn, overexpression of ASF1 led to a diminished abundance of DAXX-H3.3-H4 complexes. DAXX contacts H3.3 at its unique residues A87, I89 and G90. To analyze whether these aa indeed determine DAXX specificity for H3.3, single point mutants exhibiting exchanges with the corresponding H3.1 residues were investigated for DAXX binding. H3.3G90M demonstrated impaired DAXX binding by approximately 50%.

INTRODUCTION

Surprisingly, H3.3G90M pulled down CAF1, suggesting that DAXX loss is partially compensated by CAF1. Conversely, H3.2M90G gained DAXX binding. A closer look identified an extensive hydrogen bond network in the vicinity of Gly90 including H3.3S57 and H3.3E59, whereas the crystal structure of DAXX-H3.3G90M showed a reduced number of hydrogen bonds. These data demonstrate the crucial role of glycine at position 90 in DAXX binding. The α N helix of H3.3 is often disordered in other chaperone complexes. In the DAXX-H3.3-H4 complex, however, it is stabilized (247, 271). Deletion of aa 1-60, including the α N helix, abolishes DAXX binding, highlighting its important role in DAXX binding. DeNizio et al. could also support this by showing that H3.3 α N experienced the highest increase in stability after DAXX binding. In fact, H3.3 changes its conformation from a disordered state in solution to a stable fold when in complex with DAXX. Surprisingly, also DAXX stability itself is highly coupled to H3.3-H4 binding. Both, the chaperone and its substrate achieve a stable conformation by their interaction. The high selectivity for H3.3 can be explained by the stabilized fold that DAXX only achieves when bound to its substrate H3.3 and not by binding to H3.2 (271).

Another function of DAXX was detected in the H3.3 deposition pathway by Delbarre et al. (272). The authors reported a stepwise deposition pathway for H3.3 whereby Promyelocytic leukemia (PML) nuclear bodies (NBs) play a key role as an intermediate triage center for H3.3. PML-NBs are nuclear structures implicated in the storage and PTMs of diverse nuclear proteins (273). Depletion of DAXX results in an accumulation of soluble H3.3, arguing that DAXX is responsible for the recruitment of H3.3 to these structures prior to deposition. In addition to DAXX also ATRX, HIRA, and ASF1A localize to PML-NBs, thus they might function as a triage center for H3.3 to the distinct chaperones (272). Moreover, DAXX or PML loss leads to an impaired incorporation of H3.3 at periCEN. Conversely, overexpression of DAXX results in increased H3.3 levels at PML-NBs and pericentric repeats, arguing for a role for PML-NBs in heterochromatin composition (274). This hypothesis is further supported by a study in mESCs where the depletion of PML results in telomere dysfunction characterized by the increased presence of TIFs (275). Together, these data suggest a function for DAXX in the recruitment of H3.3 to PML-NBs. Thereby they might, on the one hand, serve as a meeting point for H3.3 and its chaperones and/or on the other hand stabilize heterochromatin integrity.

In addition to H3.3 and ATRX, DAXX is also mutated or misregulated in a variety of cancers (166, 229, 231, 276, 277). In line with H3.3 and ATRX DAXX is also mutated in pediatric brain cancer. However, DAXX mutations are less frequently observed than H3.3 or ATRX mutations

INTRODUCTION

(209). In panNETs and leiomyosarcoma DAXX mutations correlate with poor prognosis (278, 279). As mentioned earlier, ATRX and also DAXX mutations are associated with the ALT pathway, an acquired mechanism to escape apoptosis or senescence (229, 230, 232, 277). Notably, DAXX mutations concerning its functions outside of H3.3 deposition pathway also have a high impact on tumorigenesis. In the case of H3.3 deposition, loss of DAXX function can result in diminished association with H3.3, thereby providing an accumulation of soluble H3.3 or a shift towards HIRA-mediated deposition. Simultaneously, H3.3 is missing at heterochromatic sites, impairing heterochromatin integrity and promoting genomic instability.

1.2.6 Nucleosome-free H3.Y Interactome/Chaperones

In order to gain further insight into the function of the new histone H3 variant H3.Y its chaperones responsible for the deposition into chromatin should be identified. H3.Y shows the highest similarity to H3.3 and importantly shares the same chaperone recognition site with H3.3 (aa 87-90, see Figure 4). Due to this similarity it was expected to pull down the same chaperone complexes that are responsible for H3.3 deposition. Clemens Bönisch, a former PhD student in our group, analyzed together with Hans Christian Eberl from the group of Matthias Mann the soluble pool of histone H3 variants concerning their predeposition interaction partners. HeLa Kyoto (HK) cells stably expressing eGFP-H3 variants were SILAC (stable isotope labeling of amino acids in cell culture) labeled. The nuclear fraction was isolated and ultracentrifuged to separate chromatin from the soluble part that was used for immunoprecipitation with GFP-trap magnetic beads to isolate eGFP-tagged H3 variants and their associated binding partners. The associated proteins were identified by mass spectrometry (MS). In Figure 6 the interactome of soluble nuclear eGFP-H3 variants is depicted.

INTRODUCTION

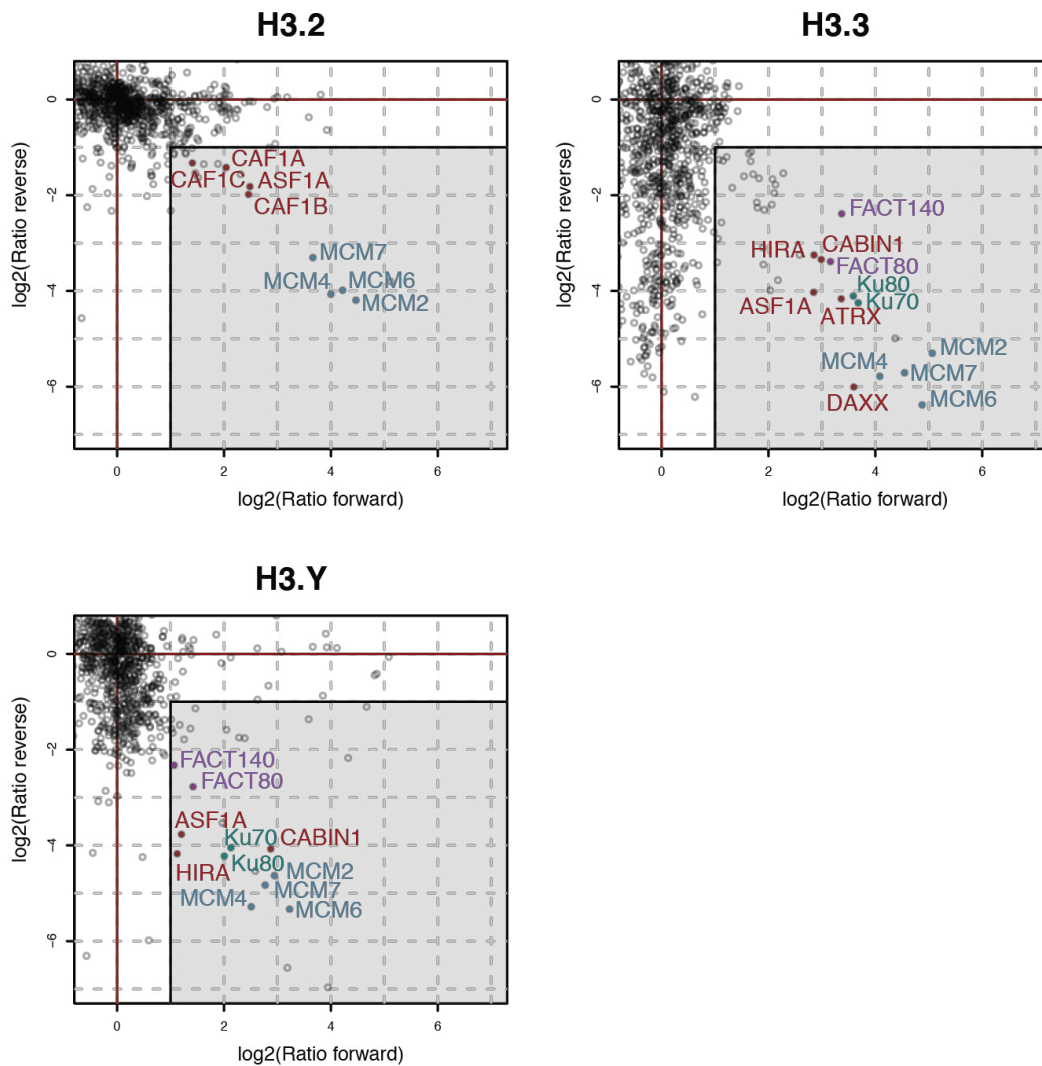


Figure 6: DAXX/ATRX only interacts with H3.3 but not H3.Y. HeLa Kyoto cells expressing eGFP-H3.2, -H3.3 and -H3.Y were SILAC labeled and the soluble nuclear fraction of the H3 variants and their interaction partners were immunoprecipitated via magnetic GFP-trap_M beads. The known chaperone complexes are depicted in red, Ku proteins in green, MCM family members in blue and FACT complex members in purple. Black dots correspond to background binders.

Unsurprisingly, eGFP-H3.2 could pull down chaperone complex members CAF1A, CAF1B and CAF1C in addition to ASF1A, verifying the applicability of the method. Interestingly, eGFP-H3.2 also immunoprecipitated members of the MCM2-7 complex, namely MCM2, MCM4, MCM6 and MCM7. This highlights again the specificity of the approach since these proteins were already identified in a recent study addressing the H3.2 interactome (280).

As expected, DAXX/ATRX and also the HIRA complex members HIRA, CABIN1 and ASF1A were identified in the eGFP-H3.3 pulldown as well as the FACT complex (FACT80 and FACT140). Additionally the Ku proteins Ku70 and Ku80 that are implicated in DNA repair and MCM2, MCM4, MCM6 and MCM7 were pulled down.

INTRODUCTION

eGFP-H3.Y immunoprecipitated as well the FACT complex, Ku70 and Ku80, MCM2, MCM4, MCM6 and MCM7 and HIRA, CABIN1 and ASF1A. Surprisingly, although H3.3 and H3.Y share the same chaperone recognition site, eGFP-H3.Y could not immunoprecipitate the DAXX/ATRX complex, indicating that only H3.3 but not H3.Y interacts with DAXX/ATRX. Despite the fact that both chaperone complexes bind the same region in H3.3 that is identical in H3.Y only the HIRA complex but not DAXX/ATRX binds H3.Y.

1.3 OBJECTIVES

In this thesis I aimed to unravel the function of the novel H3 variant H3.Y. Therefore, I analyzed its localization in chromatin by ChIP-seq and identified its interactome by MS. Although H3.3 and H3.Y share the same chaperone recognition site, H3.Y only interacts with the HIRA complex. Since it is responsible for the deposition into euchromatic sites I evaluated the consequences of this interaction on H3.Y chromatin via ChIP-Seq. Secondly I dissected the H3.Y chromatin composition by label-free interaction proteomics of H3.Y-containing mononucleosomes. Do H3.1, H3.3 and H3.Y interact with different proteins? What can we learn from the different interaction partners about H3.Y's function?

Next, I set out to uncover what residues prevent DAXX-H3.Y interaction or what determines DAXX specificity for H3.3, respectively. Hence, I generated H3.Y mutants that exhibit exchanges with corresponding H3.3 residues. Performing immunoprecipitations of stable HeLa Kyoto cell lines expressing respective H3.Y mutants aims to reveal the residues that determine the DAXX-H3.3 specificity. Furthermore, these mutants that gain DAXX binding should be analyzed regarding their chromatin distribution.

In conclusion, gaining novel insights into H3.Y deposition mechanisms and chromatin localization will allow uncovering unknown aspects of H3.Y function.

2 MATERIALS AND METHODS

2.1 MATERIALS

2.1.1 Technical Devices

Description	Supplier
-20°C freezer	Beko, Liebherr
-80°C freezer	Thermo Scientific
4°C fridge	Liebherr
37°C incubator (bacteria)	Binder
37°C (human cells)	New Brunswick
2100 Bioanalyzer	BioRad
Centrifuges	Beckmann Coulter Optima Max-XP Eppendorf 5424R Heraeus Biofuge pico Roth Rotilabo-mini-centrifuge Thermo Shandon Cytospin 4 Thermo Scientific Multifuge X3R
CASY Cell Counter	Innovatis
Developer machine	AGFA Curix
Dounce homogenizer	Kontes Glass Co
Gel documentation system	BioRad ChemiDoc
Hood	Binder
Incubation shaker (37°C)	Infors, New Brunswick
Microscopes	Leica SP5 II confocal scanning Zeiss Axiovert 200M Epifluorescence Olympus IX71
Nucleofector	Lonza
pH meter	inoLab
Pipetboy	Neolab
Pipettes	Gilson
Protein gel chamber	Novex Mini cell Serva BlueVertical PRiME
Qubit fluorometer	Invitrogen

MATERIALS AND METHODS

Rotating wheel	Neolab
Scales	Sartorius
Sonicator	Covaris S220
Spectrophotometer	Peqlab GFP-trap_M drop ND1000
Thermomixer	Eppendorf 5436
	Thermomixer C
Trans Blot SD semi-dry transfer cell	BioRad
Vortex	Bachofer Genie2

2.1.2 Chemicals and Consumables

Description	Supplier
1.5 ml reaction tubes	Greiner, Sarstedt
2 ml reaction tubes	Greiner, Sarstedt
1.5 ml low binding tubes (DNA and protein)	Sarstedt
15 ml and 50 ml tubes	Sarstedt
16% Formaldehyde Solution (methanol-free)	Thermo Scientific
Acetic acid	Sigma-Aldrich
Agarose	Bio & Sell
Ampicillin	Roth
AMPure XP beads	Beckman Coulter
LB Agar	Serva
BSA 98%	Sigma-Aldrich
Chlorophorm	VWR
Cell culture plates	Sarstedt
Centrifuge tubes (ultracentrifugation)	Beckman Coulter
Combitips plus	Eppendorf
Complete Protease Inhibitor Cocktails Tablets	Roche
Coomassie Brilliant Blue	Sigma-Aldrich
Coverslips	Hecht-Assistant
Cryovials	Roth
DAPI	Invitrogen
Developer	AGFA
DMEM	Sigma-Aldrich
DMSO	Sigma-Aldrich
DNA oligonucleotides	Sigma-Aldrich, Eurofins MWG
dNTP mix	NEB

MATERIALS AND METHODS

DTT	Roth
Dynabeads M-280 sheep anti-rabbit IgG	Invitrogen
ECL Western Blotting detection reagents	Amersham
EDTA	Sigma
EGTA	Sigma
Ethanol, absolute	Roth
Ethidium bromide	Sigma
FCS dialyzed	Sigma
Filter paper Whatman 3MM	Whatman
Filter tips	Biozym, Gilson
Fixer	AGFA
G418-sulfate	Sigma
GFP-trap_M	Chromotek
Glycerol	VWR
Glycine	VWR
HEPES	Serva
IPTG	Roth
Isoamyl alcohol	Merck
KCl	VWR
MaXtract High Density Column	Qiagen
β-mercaptoethanol	Sigma
Methanol	Sigma
MgCl ₂	VWR
Microscope slides SuperFrost	Roth
Mowiol 4-88	Polysciences
Multiply μStripPro with 8 x 0.2 ml tubes	Sarstedt
NaCl	VWR
Na-deoxycholate	Sigma
NP-40	Sigma
Opti-MEM Reduced-Serum Medium	Invitrogen
Penicillin / streptomycin	Sigma
Pipette tips	Biozym, Greiner, Sarstedt
Ponceau S solution	Sigma
Protein gels precast	Invitrogen, Serva
Protran Nitrocellulose Transfer Membrane	Whatman
Proteinase K	life technologies
Qubit assay tubes	Invitrogen
Quick Start Bradford 1x Dye Reagent	Biorad

MATERIALS AND METHODS

RNase A	life technologies
SDS	Serva
TFA	Sigma
TSA	Sigma
Tris	Invitrogen
Triton X-100	Sigma
Trypsin/EDTA (cell culture)	Sigma
Trypsin (MS)	Promega
Tween20	Sigma
Vectashield mounting medium	Vector Laboratories
X-ray films	Fujifilm
X-treme Gene HP Transfection Reagent	Roche

2.1.3 Kits, Enzymes & Markers

Description	Supplier
100 bp ladder	NEB
1 kb ladder	NEB
2-log DNA ladder	NEB
DNA 1000 Kit	Agilent
Gel extraction Kit	Qiagen
Midiprep Kit	Qiagen, Macherey-Nagel
Micronuclease nuclease	Sigma
Microplex Librray Preparation Kit	Diagenode
MinElute PCR Purification Kit	Qiagen
NucleoSpin [®] Plasmid EasyPure Kit	Macherey-Nagel
PCR purification Kit	Qiagen
peqGOLD protein marker IV, V	Peqlab
Phusion High Fidelity DNA polymerase	Biolabs
Pfu Turbo Hotstart DNA Polymerase	Agilent
Qubit dsDNA HS Assay Kit	Invitrogen
Restriction endonucleases	NEB
Taq DNA Polymerase	NEB

MATERIALS AND METHODS

2.1.4 Antibodies

2.1.4.1 Primary Antibodies

Name (product #)	Supplier	Application	Dilution
Rabbit α -DAXX (25C12) (45335)	Cell Signalling	WB	1:1000
Rabbit α -DAXX (M-112) (SC-7152)	Santa Cruz	WB	1:1000
Rabbit α -GFP (ab290)	Abcam	ChIP	5 μ g per IP
Mouse α -GFP (11814460001)	Roche	WB	1:10000
Rabbit α -H3K9me3 (C15410056)	Diagenode	WB	1:1000
mouse α -H3S10ph (ab39636)	Active motif	IF	1:800
Mouse α -PAR	Gift from A. Ladurner, LMU Munich	WB	1:5000
Rabbit α -PML (ab53773)	Abcam	IF	1:100
Mouse α -SUMO-1 (GMP-1) (332400)	Invitrogen	WB	1:1000
Mouse α -Ubiquitin (04-263)	Merck Millipore	WB	1:5000

2.1.4.2 Secondary Antibodies

Name	Supplier	Application	Dilution
α -rabbit HRP	VWR	WB	1:10000
α -mouse HRP	VWR	WB	1:10000
α -rabbit Alexa555	Jackson Laboratories	IF	1:1000
α -rabbit Cy3 conjugated	Jackson Laboratories	IF	1:200

MATERIALS AND METHODS

2.1.5 Plasmids

Name	Source	Description	Marker
pUC57- -N3-Y -NY-3 -3-CY -Y-C3 -H3.Y core GERA -H3.Y K53R core GERA -H3.Y K53R core R122KM124I -H3.Y K53R core C	Genewiz	ordered constructs arrived in pUC57 vector; subcloning	Amp
pIRESneo-eGFP	C. Bönisch	Expression of N-terminally GFP-tagged fusion proteins in mammalian cells	Amp, Neo-mycin (Neo)
pIRESneo-eGFP -H3.Y Q59E	S. Pünzeler	Expression of N-terminally GFP-tagged H3.Y mutant protein in HeLa Kyoto cells	Amp, Neo
pIRESneo-eGFP -H3.Y core -N3-Y -NY-3 -3-CY -Y-C3 -H3.Y core GERA -H3.Y K53R core GERA -H3.Y K53R core R122KM124I -H3.Y K53R core C3 -H3.Y K42R K53R core C3 -H3.Y L46V K53R core C3 -H3.Y K53R L62I core C3 -H3.Y K42R L46V K53R core C3 -H3.Y K42R K53R L62I core C3 -H3.Y L46V K53R L62I core C3	this thesis	Expression of N-terminally GFP-tagged H3.Y mutant proteins in HeLa Kyoto cells	Amp, Neo

2.1.6 Oligonucleotides

2.1.6.1 Oligonucleotides for Cloning

Oligonucleotides were synthesized by Sigma-Aldrich or Eurofins MWG.

Name	Sequence 5' – 3'	Description
gw_H3.3_fwd	GGGGACAAGTTTGTACAAAAAAGCAGGC TTAACTGCCCGAACCAAGCAGAC	Cloning of H3.3, 3-CY and N3-Y into pIRESneo-eGFP

MATERIALS AND METHODS

Name	Sequence 5' – 3'	Description
gw_H3.3_rev	GGGGACCACTTTGTACAAGAAAGCTGGG TCTTAAGCTCTCTCTCCCCGTATCC	Cloning of H3.3, NY-3 and Y-C3 into pIRESneo-eGFP
gw_H3.Y_fwd	GGGGACAAGTTTGTACAAAAAAGCAGGC TTAACTGCGCGACCAAGCAGAC	Cloning of H3.Y mutants into pIRESneo-eGFP
gw_H3.Y_rev	GGGGACCACTTTGTACAAGAAAGCTGGGT CTTAAGGACCCTCTCTGCGGAG	Cloning of H3.Y mutants into pIRESneo-eGFP
gw_H3.Y_GERA_rev	GGGGACCACTTTGTACAAGAAAGCTGGGT CTTAAGCACGCTCTCCGC	Cloning of H3.Y GERA and H3.Y K53R GERA into pIRESneo-eGFP

2.1.6.2 Oligonucleotides for Mutagenesis

Name	Sequence 5' – 3'
H3.Y DFKT_fwd	CGAGATCGCCCAGGATTTCAAACCGACCTGCGCTTCC
H3.Y DFKT_rev	GGAAGCGCAGGTCGGTTTTGAAATCCTGGGCGATCTCG
H3.Y Q102G_fwd	GAGGCCTACCTGGTGGGTCTCTTTGAAGACACC
H3.Y Q102G_rev	GGTGTCTTCAAAGAGACCCACCAGGTAGGCCTC
H3.Y K42R_fwd	GATCAAGAAGCCTCACCGCTACAGGCCTGGCACCTGGCGCTGCGGG
H3.Y K42R_rev	CCCGCAGCGCCAGGGTGCCAGGCCTGTAGCGGTGAGGCTTCTTGATC
H3.Y L46V_fwd	TACAAGCCTGGCACCGTGGCGCTGCGGGAAATC
H3.Y L46V_rev	GATTTCCCGCAGCGCCACGGTGCCAGGCTTGTA
H3.Y L62I_fwd	GAAGTCCACGGAGCTGCTCATTGCAAGCTGCCCTTCCAG
H3.Y L62I_rev	CTGGAAGGGCAGCTTGCGAATGAGCAGCTCCGTGGACTTC
H3.Y K42R_L46V_fwd	GATCAAGAAGCCTCACCGCTACAGGCCTGGCACCTGGCGCTGCGGG
H3.Y K42R_L46V_rev	CCCGCAGCGCCACGGTGCCAGGCCTGTAGCGGTGAGGCTTCTTGATC

2.1.7 Bacterial Strains & Cell Lines

2.1.7.1 Human Cell Lines

Cell line	Origin	Source
HeLa Kyoto (HK)	cervical cancer	H. Leonhardt, LMU Munich
Primary mesenchymal stem cells	bone marrow	P. Collas, University of Oslo

HeLa Kyoto cells were transfected with pIRESneo-eGFP plasmids. Stable human cell lines were derived from G418-sulfate selected cell populations.

MATERIALS AND METHODS

Cell line	Plasmid	Source
HK GFP	pIRESneo-eGFP	this thesis
HK GFP-H3.Y Q59E	pIRESneo-eGFP-H3.Y Q59E	S. Pünzeler
HK GFP-H3.Y core	pIRESneo-eGFP-H3.Y core	this thesis
HK GFP-N3-Y	pIRESneo-eGFP-N3-Y	this thesis
HK GFP-NY-3	pIRESneo-eGFP-NY-3	this thesis
HK GFP-3-CY	pIRESneo-eGFP-eGFP-3-CY	this thesis
HK GFP-Y-C3	pIRESneo-eGFP-Y-C3	this thesis
HK GFP-N3-Y	pIRESneo-eGFP-N3-Y	this thesis
HK GFP-H3.Y core GERA	pIRESneo-eGFP-H3.Y core GERA	this thesis
HK GFP-H3.Y K53R core GERA	pIRESneo-eGFP-H3.Y K53R core GERA	this thesis
HK GFP-H3.Y K53R core R122KM124I	pIRESneo-eGFP-H3.Y K53R core R122KM124I	this thesis
HK GFP-H3.Y K53R core C3	pIRESneo-eGFP-H3.Y K53R core C3	this thesis
HK GFP-H3.Y K42R K53R core C3	pIRESneo-eGFP-H3.Y K42R K53R core C3	this thesis
HK GFP-H3.Y L46V K53R core C3	pIRESneo-eGFP-H3.Y L46V K53R core C3	this thesis
HK GFP-H3.Y K53R L62I core C3	pIRESneo-eGFP-H3.Y K53R L62I core C3	this thesis
HK GFP-H3.Y K42R L46V K53R core C3	pIRESneo-eGFP-H3.Y K42R L46V K53R core C3	this thesis
HK GFP-H3.Y K42R K53R L62I core C3	pIRESneo-eGFP-H3.Y K42R K53R L62I core C3	this thesis
HK GFP-H3.Y L46V K53R L62I core C3	pIRESneo-eGFP-H3.Y L46V K53R L62I core C3	this thesis

2.1.7.2 *E. coli* Strains

Strain	Genotype	Supplier
<i>E. coli</i> DH5a	<i>fhuA2</i> Δ (<i>argF-lacZ</i>)U169 <i>phoA glnV44</i> Φ 80 Δ (<i>lacZ</i>)M15 <i>gyrA96 recA1 relA1 endA1 thi-1 hsdR17</i>	NEB
<i>E. coli</i> Stellar	<i>F</i> ⁻ , <i>endA1, supE44, thi-1, recA1, relA1, gyrA96, phoA, Φ80d lacZ</i> Δ M15, Δ (<i>lacZYA - argF</i>) U169, Δ (<i>mrr - hsdRMS - mcrBC</i>), Δ <i>mcrA</i> , λ ⁻	Clontech

MATERIALS AND METHODS

2.1.8 Software

Application	Software
Image Processing	Adobe Photoshop CS5
	Adobe Illustrator CS5
	Axio Vision (Zeiss)
Primer Design	Primer3 (web-browser based)
qMS	Perseus (1.3.10.0)
	R Studio / R (3.0.2)
Sequencing (ChIP)	BioViz Integrated Genome Browser
	Broad Institute Integrative Genomics Viewer
Sequence Alignment	ClustalW

2.1.9 Standard Buffers & Solutions

Ampicillin stock solution	100 mg/ml Ampicillin (1000x)
Blocking solution	5% milk powder (w/v)
	PBS + 0.1 % Tween20
Coomassie staining solution	10% acetic acid (v/v)
	50% methanol
	0.1% Coomassie Brilliant Blue (w/v)
Coomassie destaining solution	10% acetic acid
	30% methanol
Ethidium bromide stock solution	10 mg/ml Ethidium bromide (20000x)
5x Laemmli loading buffer (adjust pH to 6.8 with HCl)	314 mM Tris
	50% glycerol
	5% SDS
	5% beta-Mercaptoethanol (v/v)
	0.01% Bromphenol blue
Laemmli running buffer	25 mM Tris
	192 mM glycine
	0.1% SDS (w/v)
LB Agar plates	1.5% LB Agar

MATERIALS AND METHODS

LB medium	1.0% Tryptone (w/v) 0.5% yeast extract (w/v) 1.0% NaCl (w/v)
Phosphate buffered saline (PBS)	140 mM NaCl 2.7 mM KCl 10 mM Na ₂ HPO ₄ 1.8 mM KH ₂ PO ₄
TBE	45 mM Tris 45 mM Boric acid 1 mM EDTA
Transfer Buffer (SDS gel electrophoresis)	48 mM Tris 39 mM glycine 0.0375% SDS (w/v) 20% methanol (v/v)
TE	10 mM Tris 1 mM EDTA

2.2 MOLECULAR BIOLOGICAL METHODS

2.2.1 Mutagenesis of H3.Y Constructs

pIRESneo-eGFP-H3.Y plasmids were used for site-directed mutagenesis. Primer pairs carrying the desired mutation were used for PCR amplification with the following conditions (Table 1 and Table 2):

Table 1: Composition of reagents for site-directed mutagenesis.

Template (50 ng/μl)	1 μl
10x Pfu reaction buffer	2 μl
dNTPs	2 μl
Primer fwd (10 μM)	2 μl
Primer rev (10 μM)	2 μl
Pfu Turbo Hotstart DNA Polymerase	0.5 μl
H ₂ O	11.5 μl
Total volume	20 μl

MATERIALS AND METHODS

Table 2: Conditions for site-directed mutagenesis of H3.Y

	Temperature	Time	Cycles
Initial denaturation	95°C	30 s	1
Denaturation	95°C	30 s	20-25
Annealing	55°C	1 min	
Elongation	68°C	6 min	

After PCR, 10 µl of the PCR product were subjected to DpnI digest in order to eliminate the parental template DNA not carrying the mutation. Next, the DpnI digested DNA was transformed into competent *E. coli* cells. Finally, the isolated DNA of several clones was analyzed by sequencing (Eurofins MWG) and the obtained DNA sequence was investigated by the ClustalW sequence alignment program in order to determine whether it contains the desired mutation(s).

2.2.2 Cloning of H3.Y Mutant Constructs into Destination Vector pIRESneo-eGFP

Plasmids that were ordered at Genewiz containing H3.Y mutants arrived in the pUC57 vector. In order to clone the constructs into pIRESneo-eGFP, the vector used for expression in HK cells, the DNA was amplified with primers containing attL overhangs for gateway cloning (see Table 3 and Table 4).

Table 3: Reagents used for PCR to clone H3.Y mutants into destination vector pIRESneo-eGFP.

pUC57 H3.Y mutant (1ng/µl)	1 µl
5x HF buffer	10 µl
dNTPs	1 µl
Primer fwd (10 µM)	0.5 µl
Primer rev (10 µM)	0.5 µl
Polymerase (Phusion)	0.5 µl
H ₂ O	36.5 µl
Total volume	50 µl

Table 4: PCR conditions for amplification of H3.Y mutant constructs.

	Temperature	Time	Cycles
Initial denaturation	95°C	30 s	1
Denaturation	95°C	30 s	30
Annealing	55°C	1 min	
Elongation	72°C	1 min	
Final elongation	72°C	7 min	1

Obtained PCR products were PCR purified and subjected to Gateway Cloning according to the manufacturer's protocol. Briefly, 50-150 ng of the purified PCR product was mixed with 150 ng of pIRESneo-eGFP vector and filled up to 8 µl with TE buffer. 2 µl of LR Clonase II enzyme mix was added to this mixture and incubated at 25°C for 1 hour. Afterwards, 1 µl of Proteinase K was added and

MATERIALS AND METHODS

incubated at 37°C for 10 min. Finally, 2 µl of the final mix were transformed into competent *E. coli* cells. DNA of the received bacterial clones was isolated with the NucleoSpin Plasmid EasyPure Kit and analyzed with the help of the ClustalW sequence alignment program.

2.3 BIOCHEMICAL METHODS

2.3.1 SDS Polyacrylamide Gel Electrophoresis (SDS-PAGE)

Proteins were separated with precast gels from Serva or Invitrogen by SDS-polyacrylamide gel electrophoresis. PeqGOLD protein marker IV and V were used to determine the size of the respective proteins. Before loading samples were boiled 5 min at 95°C in 5x Laemmli buffer and then run for approximately 2 hours at 150 V. Afterwards the gel was either used for Coomassie staining or subsequent immunoblotting.

2.3.2 Coomassie Staining of Polyacrylamide Gels

In order to visualize proteins separated by SDS-PAGE, the polyacrylamide gel was stained for 1 hour in Coomassie staining solution. Subsequently, the gel was destained in destaining solution until the proteins bands became apparent. After washing the destained gel with water, it was scanned in the transparency mode, 300 dpi, 16 bit HDR gray scale.

2.3.3 Immunoblotting

Polyacrylamide gels were blotted onto a nitrocellulose membrane with a semidry blotting device. The polyacrylamide gel, a nitrocellulose membrane and Whatman papers were equilibrated for 5 min in transfer buffer prior to the formation of a blotting sandwich in the following order: 2 Whatmann paper, membrane, gel, two additional Whatman paper. The sandwich was blotted for 1 hour at 250-300 mA. Subsequently, the membrane was blocked for at least 1 hour in blocking solution. Primary antibody was diluted in blocking solution (see 2.1.4.1 for details) and incubated over night at 4°C, followed by three washing steps à 10 min with PBS-T the next day. After washing the membrane was incubated with the secondary antibody diluted in blocking solution (see 2.1.4.2 for details) and incubated for 1 hour at room temperature (RT). Afterwards, the membrane was again washed three times with PBS-T. Next, respective proteins were detected by incubation with ECL detection reagent for 2-10 min. Exposure of X-ray films for a time ranging from 10 sec to 20 min was followed by the

MATERIALS AND METHODS

development of the film with the help of a developing machine. X-ray films were scanned and saved with the settings mentioned in 2.3.2.

2.3.4 Mononucleosome Preparation

The implemented protocol was initially developed by (149). HK cells were harvested, counted with the CASY counter and aliquots of 4×10^7 cells were separated into 15 ml falcon tubes. All following steps were done on ice. The cells were washed with PBS and subsequently lysed for 10 min with 5 ml PBS + 0.3% Triton X-100 + complete protease inhibitors (CPI) at 4°C. Nuclei were pelleted by centrifugation for 5 min at 2000 rpm and washed in 5 ml PBS + CPI. Nuclei were resuspended in 500 μ l EX100 buffer, CaCl_2 was added to a final concentration of 2 mM and the mixture was transferred to a low-binding reaction tube. 1.5 U micrococcal nuclease (MNase) was added to the reaction mix and incubated for 20 min at 26°C. Adding EGTA to a final concentration of 10 mM stopped the reaction. Afterwards, the samples were centrifuged for 30 min at 21130 rcf; the supernatant (S1) was used for subsequent analysis. First, 25 μ l of S1 were boiled for 5 min at 95°C in Laemmli loading buffer to serve as input for immunoprecipitations (2.3.6). Second, 25 μ l of S1 were subjected to DNA extraction (see 2.3.5).

EX100 buffer: 10 mM Hepes pH 7.6
 100 mM NaCl
 1.5 mM MgCl_2
 0.5 mM EGTA
 10% Glycerol
 10 mM β -Glycerol phosphate
prior to use: 1 mM DTT
 1 x CPI

2.3.5 Purification of MNase Digested DNA

In order to determine the MNase digestion degree, DNA was extracted from the S1 fraction obtained after MNase digestion (see 2.3.4). Initially, nucleic acids were isolated by phenol/chloroform/isoamylalcohol extraction, followed by the DNA precipitation by ethanol. First, 175 μ l 5 mM Tris-HCl were added to 25 μ l S1, then 200 μ l phenol and 200 μ l chloroform/isoamylalcohol (ratio 24:1) were added, the mixture was vortexed and transferred to maXtract tubes. Aqueous and organic phase were separated by centrifugation at 7 000 rcf. The aqueous phase containing nucleic acids was used for subsequent DNA precipitation: after addition of glycogen to reach a final concentration of 200 μ g/ml, sodium acetate (final concentration 0.3 M) and

MATERIALS AND METHODS

500 μ l 100% ethanol the DNA was precipitated for at least 20 min at -20°C . Centrifugation for 20 min at 20000 rcf at 4°C pelleted the DNA. The pellet was washed twice with 500 μ l 70% ethanol and dried at RT for 10 min. After drying, the DNA pellet was resuspended in 30 μ l double distilled water (ddH_2O). The DNA concentration was analyzed by the Nanodrop ND1000 spectrophotometer (Peqlab). 500 ng DNA were analyzed regarding the digestion degree on a 2% agarose gel.

2.3.6 Mononucleosome-Immunoprecipitation (MNase-IP)

Mononucleosomes from HK cells were prepared as described in 2.3.4 and then subjected to immunoprecipitation. All following steps were done on ice or at 4°C . 4×10^7 cells were used for immunoprecipitation with 25 μ l slurry GFP-trap magnetic beads (GFP-trap_M, Chromotek). First, 25 μ l of GFP-trap_M beads were equilibrated in EX100 buffer. Next, the S1 fraction containing the mononucleosomes was added to the GFP-trap_M and incubated for 2.5 hours at 4°C . The mixture was then magnetically separated and the supernatant kept as "nonbound". The beads were washed twice in 1 ml wash buffer 1 for 5 min and twice in 1 ml wash buffer 2. After washing beads were magnetically separated, the supernatant was removed and the beads were boiled in 25 μ l 1x Laemmli loading buffer. The obtained immunoprecipitated fractions (IP) were analyzed by immunoblotting.

Wash buffer 1: 10 mM Tris pH 7.5
150 mM NaCl
0.1% NP-40

prior to use: 1 mM DTT
1 x CPI

Wash buffer 2: 10 mM Tris pH 7.5
150 mM NaCl

prior to use: 1 mM DTT
1 x CPI

2.3.7 MNase-IP followed by Quantitative MS (MNase-IP-qMS)

Mononucleosomes were generated and immunoprecipitated as described in 2.3.4 and 2.3.6 with the following variations: instead of 4×10^7 cells only 3.5×10^7 cells were used for immunoprecipitations. IPs were done in technical triplicates ($3 \times 3.5 \times 10^7$ cells). The S1 fractions of the three replicates were combined after MNase digestion and 50 μ l S1 was kept as input for DNA extraction. The rest of the combined samples was equally distributed and subjected to three IP reactions with GFP-trap_M magnetic beads. IP and washing were done as described before (2.3.6).

MATERIALS AND METHODS

2.3.7.1 On-bead Tryptic Digest

Immunoprecipitated proteins were subjected to an on-bead tryptic digestion. To do so, wash buffer 2 was removed after washing and the beads were incubated for 20 min at 25°C in buffer E1 (mild shaking) followed by magnetic separation. The supernatant was then transferred to a new low-binding tube before adding 2-chloroacetamide (CAA) to reach a final concentration of 5 mM. The remaining beads were resuspended in buffer E2, incubated for 5 min (mild shaking) before adding trypsin (final concentration 5 µg/ml). The resulting reaction was then incubated for 1 hour at 25°C while shaking. After magnetic separation both supernatants were combined and incubated overnight at RT. The next morning 1 µl concentrated trifluoroacetic acid (TFA) was added to the reaction to stop the tryptic digest. The beads were boiled in Laemmli buffer to check whether protein elution from the beads was completed by SDS-PAGE and Coomassie staining.

2.3.7.2 StageTips

StageTips were supplied by our collaboration partner Eva Keilhauer from the group of Matthias Mann (MPI of Biochemistry) (281). After activation of the tips with 100 µl methanol, they were centrifuged for 1 min at 1500 rcf followed by two washing steps with 100 µl 0.5% acetic acid. The trypsin digested samples (see 2.3.7.1) were split in two halves (50 µl each) and loaded on the tips to serve as working and backup sets. The tips were washed with 50 µl 0.5% acetic acid and dried by centrifugation. Finally, they were stored at 4°C until LC-MS/MS analysis.

2.3.7.3 LC-MS/MS Analysis

Our collaboration partner Eva Keilhauer eluted the peptides from the StageTips according to the standard protocol (281) and analyzed them by reversed-phase liquid chromatography on an EASY-nLC 1000 system (Thermo Fisher Scientific, Odense, Denmark) coupled to a Q-Exactive mass spectrometer (Thermo Fisher Scientific) with the help of a nanoelectrospray source (Thermo Fisher Scientific). High-performance liquid chromatography (HPLC) columns with 20 cm length and an inner diameter of 75 µm were in-house packed with ReproSil-Pur 120 C18-AQ 1.9 µm particles (Dr. Maisch GmbH). Peptides were analyzed using a linear gradient (buffer A++: 0.1% FA, buffer B++: 80% ACN, 0.1% FA) with a flowrate of 250 µL/min and a retention time of 140 min at 50°C in a column oven (Sonation GmbH). The mobile phase was directly applied to the mass spectrometer. The spray voltage was adjusted to 2.4 kV and the capillary temperature to 250°C. Data acquisition was performed in 'data-dependent mode'. Precursor ion scan acquired data at 70,000 resolution with an AGC target of 3E06 and an injection time of 20 ms. Top10 ion spectra were selected for fragmentation with an isolation window of 2 m/z and fragmented by HCD (higher energy collisional dissociation) with a normalized collision energy of 25. MS2 spectra were acquired at 17,500 resolution with an AGC target value of 1E05 ions and 120 ms injection time. Dynamic exclusion was enabled at 20 sec time window.

MATERIALS AND METHODS

2.3.7.4 Raw Data Analysis

Raw data analysis was performed by our collaboration partner Eva Keilhauer: RAW data files were searched against the UniProtKB human proteome database (Swissprot May 2013) and a database containing frequently detected contaminants, using the MaxQuant software (282) (vers. 1.3.9.20). Two missed cleavages and a protein false discovery rate of 1 % were set as analysis parameters. Carbamidomethylation of cysteine residues was defined as fixed modification and methionine oxidation and N-terminal acetylation as variable modifications. Label-free quantification (LFQ) was set to a minimum ratio count of 1 and Raw files of the same baits were analyzed using the match-between-runs option.

2.3.8 Chromatin Immunoprecipitation (ChIP) of Crosslinked & Sonicated HK Cells

2.3.8.1 Fixation of HK Cells

HK cells were harvested, counted and cross-linked for 10 min at RT in 12.5 ml DMEM + 1% formaldehyde (methanol free (Thermo Fisher Scientific) at a density of 2×10^6 cells/ml (results in 2.5×10^7 cells per fixation reaction). The reaction was stopped by adding glycine to a final concentration of 0.125 M. After incubating the mixture 5 min at RT, the cells were pelleted by a 5 min centrifugation step at 1600 rcf. Now the cells were washed twice with 10 ml PBS + 10% fetal calf serum (FCS) and flash frozen in liquid nitrogen. The fixed cells were stored at -80°C .

2.3.8.2 Chromatin Shearing

The cross-linked HK cells were thawed on ice and resuspended in 5 ml lysis buffer 1 (LB 1). All the following steps were conducted on ice or at 4°C . The samples were rotated for 10 min and centrifuged for 5 min at 1350 rcf. Afterwards the cell pellets were resuspended and incubated for 10 min in LB 2 before pelleting the nuclei by a 5 min centrifugation at 1350 rcf. Now 1 ml buffer B was added and the samples were sheared for 35 min using a Covaris S220 (PP 120; DF 20, CB 200) in 1 ml 12x12 tubes with AFA fiber) to obtain chromatin fragments of 150 bp in average. After chromatin shearing, the samples were transferred into low binding tubes and centrifuged for 1 min at 20000 rcf. The soluble chromatin containing supernatant was again transferred into a new low binding tube and diluted to 2.5×10^6 cells/ml by the addition of 9 ml buffer A. This mixture was now divided into 1 ml aliquots and subjected to immunoprecipitation (see 2.3.8.3).

Lysis buffer 1 (LB 1): 50 mM Hepes KOH, pH 7.5
 140 mM NaCl
 1 mM EDTA
 10% glycerol
 0.5% NP-40

MATERIALS AND METHODS

	0.25% Triton X-100
prior to use:	1 x CPI
<u>Lysis buffer 2 (LB 2):</u>	10 mM Tris-HCl, pH 8.0
	200 mM NaCl
	1 mM EDTA
	0.5 mM EGTA
prior to use:	1 x CPI
<u>Buffer B:</u>	50 mM Tris-HCl, pH 8.0
	10 mM EDTA
	0.5% SDS
prior to use:	1 x CPI
<u>Buffer A:</u>	10 mM Tris-HCl, pH 7.5
	1 mM EDTA
	0.5 mM EGTA
	1% Triton x-200
	0.1% SDS
	0.1% Na-deoxycholate
	140 mM NaCl
prior to use:	1 x CPI

2.3.8.3 Chromatin Immunoprecipitation of Sheared Chromatin

First 30 μ l of Dynabeads M-280 sheep anti rabbit IgG were washed twice in 500 μ l PBS + 0.1% Tween20 in low binding tubes. After washing, 5 μ g GFP antibody was coupled to the beads for at least 2 hours in 500 μ l PBS + 0.1% Tween20 while rotating at 4°C. Additionally, one mock sample was prepared without the addition of antibody. The beads were then washed twice with PBS + 0.1% Tween20 and 1 ml of sheared chromatin (see 2.3.8.2) was added to the pre-coupled beads. Now the beads were incubated over night at 4°C while rotating at 7 rpm. The next day 50 μ l supernatant of the mock sample was saved as input and the beads were washed four times with 900 μ l buffer A and one time buffer C, each time rotating the samples for 10 min. Subsequently 100 μ l elution buffer was added to the beads and incubated at 65°C over night to elute and reverse crosslink the immunoprecipitated material. The following day the supernatant was transferred into a new tube and 100 μ l TE and 4 μ l RNase A (10 mg/ml DNase-free) was added and the reactions were incubated at 37°C for 1 hour. Afterwards 4 μ l Proteinase K (10 mg/ml DNase-free) was added and the samples were incubated for 2 hours at 56°C. Finally, the DNA was purified with the MinElute PCR purification Kit (Qiagen). The DNA was eluted in 30 μ l elution buffer and DNA size was analyzed on a 1000 DNA

MATERIALS AND METHODS

BioAnalyzer chip (Agilent). Additionally the DNA concentration was measured with the Qubit Assay (life technologies).

Buffer C: 10 mM Tris-HCl, pH 8.0
10 mM EDTA

Elution buffer: 50 mM Tris-HCl, pH 8.0
10 mM EDTA
1% SDS

2.3.8.4 Library Preparation

Illumina sequencing libraries were prepared according to the manufacturer's protocol (MicroPlex Library Preparation kit v2, Diagenode) with the following variations. 10 ng of purified DNA was subjected to library preparation. The number of amplification cycles was adjusted until a concentration of 5 ng/ μ l of the library was obtained. After library purification, the DNA was eluted in 20 μ l 0.1 x TE and analyzed on a 1000 DNA BioAnalyzer chip (Agilent). 10 μ l of the purified library DNA were sent for Illumina sequencing.

2.3.9 Illumina Sequencing

Next-generation sequencing was performed at the Laboratory of Functional Genome Analysis (LAFUGA) in the Gene Center (Munich) by Dr. Stefan Krebs. Libraries were sequenced on an Illumina HiSeq 2000 using V3 clustering and sequencing reagents (50 bp read length, single end) according to the manufacturer's instructions.

2.4 CELL BIOLOGICAL METHODS

2.4.1 Maintenance of Human HK & Mesenchymal Stem Cell Lines

HK wildtype cells were cultivated in Dulbecco's modified Eagle medium (DMEM) plus 10% FCS and 1% penicillin/streptomycin (P/S) at 37°C and 5% CO₂. Transfected HK cells and stable HK cell lines were kept in DMEM plus FCS, P/S and G418-sulfate at a concentration of 600 μ g/ml. Normally, cells were kept in 10 cm dishes with 10 ml growth medium until they reached confluency. In this case, old medium was removed, cells were washed with sterile PBS to remove the remaining medium and incubated for 5 min at 37°C with 1 ml Trypsin/EDTA (diluted 1:10 in PBS). Subsequently, cells were detached by resuspending them in 9 ml medium. 1 ml of this cell suspension was then further

MATERIALS AND METHODS

cultivated (corresponds to the usual splitting ratio of 1:10) and the rest was either discarded or transferred to 15 cm dishes to expand the cells for further experiments. For storage, cells were frozen at regular intervals. To do so, trypsinized cells were resuspended in FCS + 10% DMSO. Usually, 1×10^7 cells were resuspended in 3 ml FCS + 10% DMSO and separated into three 1 ml aliquots, transferred to cryovials and frozen at -80°C . For long term storage, cells were relocated to liquid nitrogen. In the case of thawing, the frozen cells were put into a 37°C waterbath for quick melting, transferred to a 10 cm dish and 9 ml DMEM + FCS + P/S was added.

Mesenchymal stem cells were cultured by our collaboration partner Erwan Delbarre (University of Oslo) in GlutaMAX (Gibco) containing 20% FCS (272). Cells were passaged 1:3 and passages 5-15 used for transfection (see 2.4.3 and (272)).

2.4.2 Generation of Stable eGFP-H3.Y Mutant HK Cell Lines

To establish HK cell lines stably expressing eGFP-tagged histone proteins, 4×10^5 cells were seeded into 6-well plates. The following day, the cells should have reached a confluency of approximately 90%. 1 μg plasmid DNA was mixed with 100 μl Opti-MEM before adding 3 μl X-tremeGENE transfection reagent. Additionally, one negative control HK sample that was not transfected was set up. All plasmids were transfected in triplicates. The reaction mixture was incubated for 15 – 30 min at RT and then drop-wise added to the cells. The plates were mildly shaken to distribute the transfection mix into the cell medium. Cells were then incubated for 48 hours before analyzing the transfection efficiency by flow cytometry (see 2.4.5) and transferring them to cell plates of 10 cm diameter. 12-24 hours after the transfer cells were subjected to selection medium containing 600 $\mu\text{g}/\text{ml}$ G418-sulfate until the non-transfected control cells were dead. The transfected surviving cells were again analyzed by flow cytometry when they reached again a confluency of at least ca. 50%. Stable cell lines containing 50-100% green cells (except the eGFP-Y-C3 cell line, see Figure 24) were used for further experiments.

2.4.3 Transfection of Human Mesenchymal Stem Cells

Cells were transfected by our collaboration partner Erwan Delbarre as described in (272).

2.4.4 Immunofluorescence (IF) of HK Cells & Mesenchymal Stem Cells

2.4.4.1 IF Staining

1×10^5 HK cells were seeded onto a round coverslip with a diameter of 12mm in a 24-well plate. The

MATERIALS AND METHODS

next day, cells were washed with 400 µl PBS and fixed for 15 min at RT with 400 µl 1% formaldehyde in PBS. After fixation, cells were washed with 400 µl PBS + 0.1% Triton X-100 (PBS-Tr). Now, cells were blocked in 400 µl PBS-Tr+ 1% BSA (PBS-Tr-B) for at least 20 min at RT before incubating them for at least 30 min at RT with the primary antibody in 100 – 200 µl PBS-Tr-B while slowly shaking. The cells were then washed three times with 400 µl PBS-Tr for 5 min each and incubated with the secondary antibody in 100 – 200 µl PBS-Tr-B for 30 min. Again, the cells were washed three times with 400 µl PBS-Tr. Afterwards, the DNA was stained with 200 µl DAPI (200 ng/ml) in PBS for 5 min. Subsequently, cells were washed once with 400 µl PBS, the coverslips were dipped into ddH₂O and mounted using Vectashield mounting medium (Vector laboratories).

Mesenchymal stem cells were prepared for immunofluorescence by our collaboration partner Erwan Delbarre according to (272).

2.4.4.2 Preparation of Metaphase Chromosome Spreads

A 10 cm cell culture plate 100 % confluent with HK cells expressing eGFP-tagged H3 variants were transferred onto a 15 cm cell culture dish and incubated over night with DMEM + Nocodazole (200 ng/ml). The following day metaphase-arrested cells were harvested by mitotic shake off and diluted to a concentration of 800.000 cells/ml. For lysis 3 volumes of prewarmed RBS buffer was added and incubated for 15 min at 37°C. After 15 min cells were transferred on ice and the slides were prepared for cytopinning. 100 µl cell suspension were spread on microscope slides by the Shandon cytospin 4 for 10 min at 2000 rpm with low acceleration. After centrifugation cells were fixed for 10 min with 50 µl 2% formaldehyde in PBS. Now the cells were washed twice for 5 min with KCM + 0.1% Triton X-100. Metaphase chromosomes were then extracted with KCM + 0.1% Tween + 0.5% Triton X-100 (20 min incubation) and washed with KCM + 0.1% Tween20. Now, DNA was stained with DAPI (400 ng/ml) for 5 min. Afterwards slides were washed with PBS and mounted with Vectashield mounting medium (Vector laboratories). Chromosome spreads were analyzed by confocal imaging (see 2.4.4.3).

RBS buffer: 10 mM Tris-HCl, pH 7.5
 10 mM NaCl
 5 mM MgCl₂

KCM buffer: 120 mM KCl
 20 mM NaCl
 10 mM Tris pH 8.0
 0.5 mM EDTA

MATERIALS AND METHODS

2.4.4.3 IF Microscopy

Fixed HK cells on coverslips were analyzed with the Zeiss Axiovert 200 epifluorescence microscope LSM200 and pictures were taken with a CDD camera (AxioCamMR, Zeiss). Images were edited in Adobe Photoshop CS5 and Adobe Illustrator CS5.

Mesenchymal stem cells were analyzed by our collaborator Erwan Delbarre (272).

Metaphase chromosome spreads were analyzed and recorded on the confocal microscope Leica SP5 II. For the Confocal images the Argon laser (488 nm) for GFP and the UV-diode (405 nm) for DAPI was used. Further settings are summarized below:

Laserlines	Argon (488 nm, 15%); UV-diode (405 nm, 100%)
Acousto-optical tunable filters (AOTF)	488 nm: 25%; 405 nm: 10%
Photomultiplier tubes (PMTs)	PMT1: DAPI 415-470 nm; PMT2: GFP: 498 – 570 nm
Frame averaging	4 frames per channel
Objective	PL APO CS 63x 1.3 Gly 21°C UV
Pinhole	default
Scanning speed	400 Hz
Image depth	16 bit
Image size	1024 x 1024 pixel
Zoom	6x
Pixel size	40 x 40 nm

2.4.5 Flow Cytometry Analysis of Transfected Human Cell Lines

Flow cytometry analysis was performed with the FACSCanto machine (BDI Biosciences), the FACS Diva software and FlowJo (8.8.7). HK cells were harvested and 200 – 1000 µl of the cell suspension were subjected to flow cytometry analysis. First, forward (FSC) and sideward scatter (SSC) were applied to gate for living single cells. GFP fluorescence was then visualized by a histogram.

2.4.6 Preparation of Chromatin-free Extracts

HK cells were seeded onto 5 cell culture plates (or 10 in the case of Y-C3) with a diameter of 15 cm to reach a confluence of approximately 90-100%. Cells were harvested, centrifuged 5 min at 400 rcf, washed twice with PBS and incubated on ice for 10 min in five volumes buffer A. All following steps were carried out on ice or at 4°C. After incubation, cells were centrifuged for 5 min. Due to the osmotic uptake of liquid, cell volume increased. Now the cells were resuspended in 2 volumes of buffer A + 0.2% NP-40 + CPI and transferred to a Dounce homogenizer. Cells were lysed with 30 – 40 strokes with a type B pestle and centrifuged for 15 min at 3550 rcf. The supernatant contains the

MATERIALS AND METHODS

cytoplasmic extract and was removed; the nuclear pellet was washed twice with 10 volumes PBS, transferred into a 1.5 ml reaction tube suitable for ultracentrifugation and incubated in 500 μ l buffer C for 1 hour. The nuclear suspension was then ultracentrifuged for 1 hour at 186 000 rcf. The supernatant contains the chromatin-free extract and was flash frozen in liquid nitrogen and stored at -80°C. Small aliquots from 1-10 μ l were used for the determination of the total protein concentration by Bradford protein assay according to manufacturer's protocol (Biorad).

Buffer A: 10 mM Hepes KOH, pH 7.9
 1.5 mM MgCl₂
 10 mM KCl

Buffer C: 420 mM NaCl
 20 mM Hepes KOH pH 7.9
 20% glycerol
 2 mM MgCl₂
 0.2 mM EDTA

prior to use: 0.1% NP-40
 CPI
 0.5mM DTT

2.4.7 Immunoprecipitation of eGFP-H3 Variants in Chromatin-Free Extracts

400 – 1500 μ g of total protein of nuclear extracts according to the eGFP expression determined by flow cytometry analysis (see 2.4.5) was subjected to immunoprecipitation. Nuclear extracts were diluted with buffer C to obtain the same concentration of all extracts utilized in the experiment and with dilution buffer to reach a final NaCl concentration of 210 mM. After GFP-trap_M equilibration (three times with equilibration buffer), diluted nuclear extracts were added to the beads and incubated for 2 hours at 4°C. After the incubation, beads were magnetically separated from the supernatant (referred to as nonbound and stored for further immunoblot analysis) and washed 5 times with wash buffer. Finally, samples were boiled 10 min in 20 μ l 2x SDS loading buffer and subjected to immunoblot analysis (see 2.3.1 and 2.3.3). 20 μ g chromatin-free extracts were boiled in SDS loading buffer and used as input.

Dilution buffer: 50 mM Tris HCl, pH 7.5
prior to use: CPI
 0.01% NP-40
 0.5 mM DTT

Equilibration buffer: mix dilution buffer and buffer C (see 2.4.6) in a 1:1 ratio

MATERIALS AND METHODS

<u>Wash buffer:</u>	50 mM Tris HCl, pH 7.5
	150 mM NaCl
prior to use:	CPI
	0.01% NP-40
	0.5 mM DTT

2.5 BIOINFORMATICS

2.5.1 MNase-IP-qMS Analysis

MNase-IP-qMS analysis was performed by our collaborator Eva Keilhauer. Protein intensities obtained by the software suite MaxQuant of 3 biological replicates were extracted, merged by protein name and analyzed in Perseus (283, 284) (vers. 1.5.3.0). Proteins detected in a single replicate were eliminated as well as hits to the reverse database, contaminants, proteins with one or less razor. Unique peptides and single peptide identifications present in at least 1 triplicate were included. LFQ intensities were normalized to the peptide count and log₂-transformed. Missing values in the data matrix were assigned to values representing a normal distribution close to the detection limit of the mass spectrometer. Protein abundances in the 12 histone pulldowns were averaged, and the significance of their fold-changes (FC) to the 3 eGFP control was assessed by a two-sample t-test. Protein identifications were identified as true if their enrichment to the negative control was at least two-fold. Subsequent t-tests were performed using the filtered databases comparing H3.2 vs. H3.1, H3.3 vs. H3.1, H3.Y vs. H3.1, and H3.Y vs. H3.3. Significant outliers were dissected by permutation-based FDR. Number of permutations was set to 250 and 50, FDR parameters were modified for each experiment. Respective p-values were plotted against their t-test differences in volcano plots using R (vers. 2.15.3). Also, the average ratios of interactor to bait intensities were calculated and displayed by a heatmap. Therefore, the log-FC of averaged LFQ intensities from triplicates of histone H3 mononucleosome pull-downs were plotted using Perseus and displayed by a color scale.

2.5.2 ChIP-seq Analysis

ChIP-seq analysis was executed by our collaborator Marek Bartkuhn (JLU Gießen). First, quality control of FASTQ files was done without additional trimming or filtering using *fastqc* (<http://www.bioinformatics.babraham.ac.uk/projects/fastqc/>). Additional publicly available ChIP-seq data were downloaded from NCBI's Gene Expression Omnibus (GEO). Raw reads were downloaded as SRA archives and were extracted into FASTQ files using the *fastq-dump* program of the NCBI SRA Toolkit (<https://trace.ncbi.nlm.nih.gov/Traces/sra/>).

MATERIALS AND METHODS

Publicly available data used in this study: H3K9me3 ChIP-seq data from HeLa cells (sample GSM2308949 from GSE86811) and H3K4me3 ChIP-seq coverage data from HeLa cells (ENCODE data downloaded through the UCSC genome browser portal (<http://hgdownload.cse.ucsc.edu/goldenpath/hg19/encodeDCC/wgEncodeBroadHistone/wgEncodeBroadHistoneHelas3H3k4me3StdSig.bigWig>)).

Reads were aligned with Bowtie 2 (285) as previously described (286). Parameter settings were *bowtie2-align -p 6 -D 15 -R 2 -N 0 -L 32 -i S,1,0.75 -M 10000*. Repeat information was downloaded through the hg19 table browser of the UCSC genome browser. Peaks were called using MACS version 2 (287) with default settings. If not indicated differently, all downstream analyses were done in R/BioConductor (288). Neighboring peaks were stitched together when lying within 2 kb. When available, the overlap between two replicates was then selected as the actual set of binding sites for downstream analysis. Hg19 RefSeq annotations were downloaded from Illumina's iGenome repository. In order to identify H3.3 sites bound differentially for H3.Y, extended reads (200 bp) were counted across these intervals. DESeq2 was used for normalization of read counts as well as for inference of regions with relevant binding differences between H3.3 and H3.Y (289). DESeq2-normalized read counts were further normalized for peak width and then used in order to visualize differential binding efficiencies between individual H3.Y-mutants. Observed differences were statistically tested with Wilcoxon-signed-rank test. De novo discovery of enriched motifs within sites with reduced H3.Y binding was done with MEME-ChIP (290). Coverage vectors were produced using deepTools bamCoverage function. Similarly, deepTools was used for the representation of ChIP-seq coverage across peak intervals as heat maps (291). Bigwig files were used for visualization via the R/BioC-package Gviz (292).

3 RESULTS

3.1 H3.Y ONLY INTERACTS WITH THE HIRA COMPLEX BUT NOT DAXX/ATRX

Although sharing the same chaperone recognition site (see alignment Figure 4), only H3.3, but not H3.Y, was able to interact with DAXX (Figure 6). As the results obtained in the SILAC approach previously performed by Hans Christian Eberl (group of Matthias Mann, MPI Munich) and Clemens Boenisch (former PhD student in the Hake group) were surprising in regard to DAXX interaction, they should first be confirmed. To verify this result soluble nuclear proteins were extracted from HeLa Kyoto cell lines stably expressing eGFP as a negative control or eGFP-tagged H3.1, H3.3 or H3.Y. eGFP-tagged proteins were precipitated with GFP trap_M beads and the interaction with DAXX was analyzed by immunoblot (Figure 7). The SILAC results could be confirmed: whereas H3.3 was able to bind DAXX, H3.Y was not.

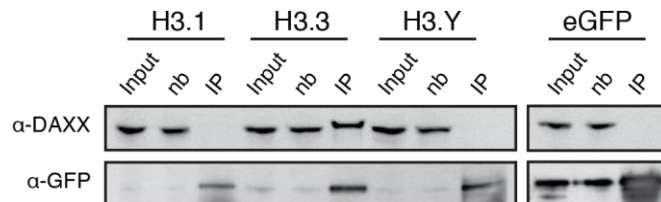


Figure 7: DAXX interacts with H3.3 but not H3.Y. Soluble nuclear proteins were isolated from stable HeLa Kyoto cell lines expressing eGFP-H3 variants in addition to eGFP as a negative control. Respective Input was subjected to immunoprecipitations (IP) and analyzed by immunoblotting with a DAXX antibody. Anti-GFP antibody served to control for successful precipitation. nb = nonbound fraction.

Interestingly, I observed a higher molecular weight of DAXX when bound to H3.3 (Figure 7). DAXX is known to be differentially modified. First, the attachment of SUMO (small ubiquitin-like modifier) is reported to have an effect on DAXX localization, the regulation of transcription mediated by DAXX and its recruitment to PML nuclear bodies (293-295). Second, DAXX has been shown to be hyperphosphorylated (293, 296-298) with distinct outcomes for the diverse roles of DAXX. To complicate the situation a crosstalk between different modifications of DAXX exists: phosphorylation of DAXX modulates its function by enhancing the association with SUMO and this, in turn, increases DAXX-PML interaction and

RESULTS

its localization to PML-NBs (293). Third, DAXX was also reported to be ubiquitinated, marking DAXX for proteasomal degradation (299, 300). Finally, poly (ADP-ribose) polymerase 1 (PARP1) is an enzyme catalyzing poly ADP-ribosylation (301). Since an interaction of DAXX and PARP1 was detected in an interactome screen in HeLa cells (302), I speculated whether this interaction could result in the poly ADP-ribosylation of DAXX.

I was wondering whether the higher molecular mass reflects any of these modifications, hence I tested this by using specific antibodies against several modifications. GFP-tagged H3 variants were immunoprecipitated with the GFP-trap_M beads, the IP was split into two halves and subjected to immunoblotting with a DAXX antibody on the one hand and the modification specific antibodies on the other hand. This way I could directly compare the heights of the two bands and conclude whether immunoprecipitated DAXX is modified in the H3.3-bound fraction (Figure 8).

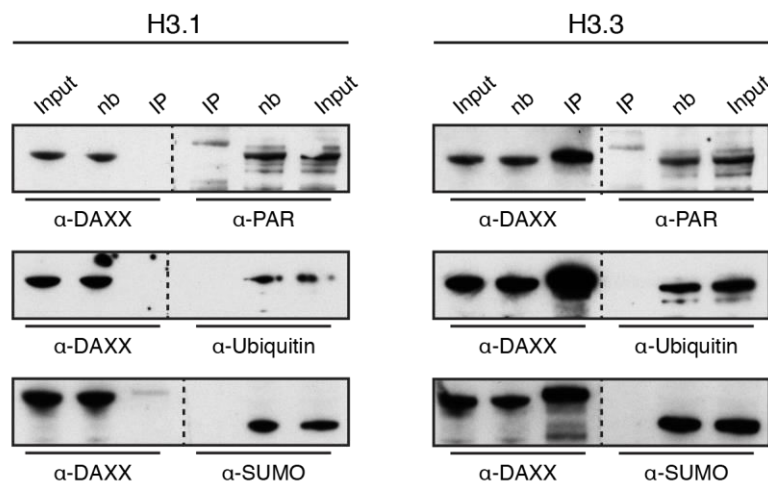


Figure 8: DAXX is neither sumoylated (SUMO), polyadenoribosylated (PAR), nor ubiquitinated. Stable HeLa Kyoto cell lines expressing GFP-tagged H3 variants were employed for isolation of soluble nuclear proteins (Input). These were subjected to immunoprecipitation (IP) via the GFP-tag of H3 variants and immunoblotting using DAXX- and indicated modification-specific antibodies. The IP was split into two halves to directly compare the DAXX band and the potential band of the different modification antibodies. On the left, H3.1 immunoprecipitations were used as a negative control. Nb = non-bound fraction after immunoprecipitation.

H3.3-bound DAXX did not seem to be sumoylated, polyadenoribosylated or ubiquitinated. Bands for these modifications occurred in H3 variant pulldowns but they were neither H3.3-specific nor did they show the same molecular weight than DAXX. Additionally, a potential hyperphosphorylation of DAXX was analyzed by treating the immunoprecipitated material with λ -phosphatase. Unfortunately, this did not show a clear result. It is therefore still possible, that phosphorylation corresponds to the shift in the DAXX band.

RESULTS

As mentioned earlier, the intermediate localization of H3.3 to PML-NBs prior to deposition into chromatin is DAXX-dependent (272). Since H3.Y does not interact with DAXX, no localization of H3.Y to PML-NBs is expected. In order to further confirm our obtained results, a collaborative work with Erwan Delbarre from the group of Philippe Collas at the University of Oslo was set up. Mesenchymal stem cells were transiently transfected with H3.3-GFP or eGFP-H3.Y and PML body localization was analyzed 24h after transfection (Figure 9).

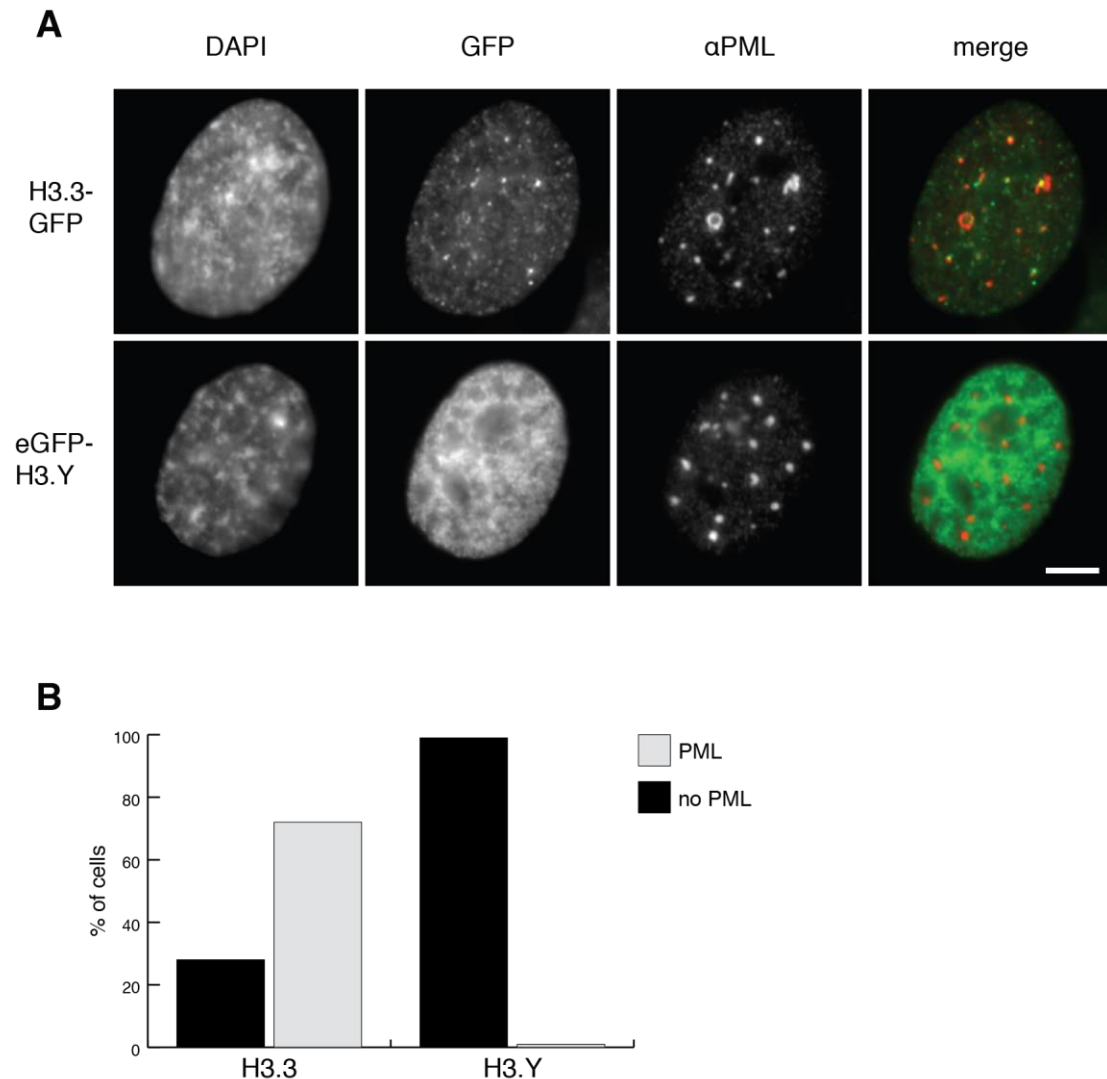


Figure 9: eGFP-H3.Y does not localize to PML nuclear bodies. (A) Human primary mesenchymal stem cells were transiently transfected with H3.3-GFP or eGFP-H3.Y, respectively and analyzed for PML body recruitment. DNA is stained with DAPI (left panel), GFP-tagged H3 variants are shown in green (second left panel) and PML-NBs are visualized with a commercially available antibody (red, second right panel). Scale bar is 5 μ m. (B) >100 cells were quantified regarding H3.3's or H3.Y's localization to PML-NBs (gray) or not (black).

While H3.3-GFP was recruited to PML-NBs, H3.Y was depleted from PML structures and only localized to chromatin, again confirming that H3.Y does not interact with DAXX and is therefore not found in PML-NBs.

3.2 H3.Y NUCLEOSOMES ARE DEPLETED FROM H3K9ME3 ENRICHED SIMPLE REPEAT SITES

The HIRA chaperone complex was described to be responsible for the deposition at open chromatin sites like transcribed genes and sites of DNA repair (190, 191, 261, 266). DAXX/ATRX on the other hand deposits H3.3 at heterochromatic sites like telomeres and pericentric heterochromatin (190, 198, 222, 267, 268). Since H3.Y only interacts with the HIRA complex but not with DAXX/ATRX I was wondering whether this impacts H3.Y localization in chromatin. In order to investigate the chromatin localization of H3.3- and H3.Y-containing nucleosomes, stably expressing eGFP (as a negative control), eGFP-H3.3, and -H3.Y HeLa Kyoto cell lines were employed for a genome-wide chromatin immunoprecipitation combined with high-throughput sequencing (ChIP-seq) analysis of two independent biological replicates. To do so, cells were fixed with formaldehyde and chromatin mechanically sheared into 150 bp fragments on average. Using a GFP-antibody, fragments were immunoprecipitated. Input DNA and immunoprecipitated DNA were purified and subjected to sequencing libraries preparation. Illumina sequencing was carried out by the LAFUGA lab at the Gene Center Munich and bioinformatic analyses performed by Marek Bartkuhn (JLU Giessen).

To first test the feasibility of our method we analyzed the co-localization of H3.3 and H3.Y with H3K4me3. H3K4me3 serves as a mark for euchromatin and is found at the promoters of active genes (303, 304). Since H3.3 and H3.Y are both deposited by the HIRA complex we were wondering whether this interaction is also reflected by the presence at open chromatin and thus co-localization with H3K4me3. Indeed, both, H3.3 and H3.Y were enriched at genic regions, especially at the TSS and underrepresented at intergenic regions (Figure 10A). Moreover, H3.3 and H3.Y shared the majority of peaks (Figure 10B).

RESULTS

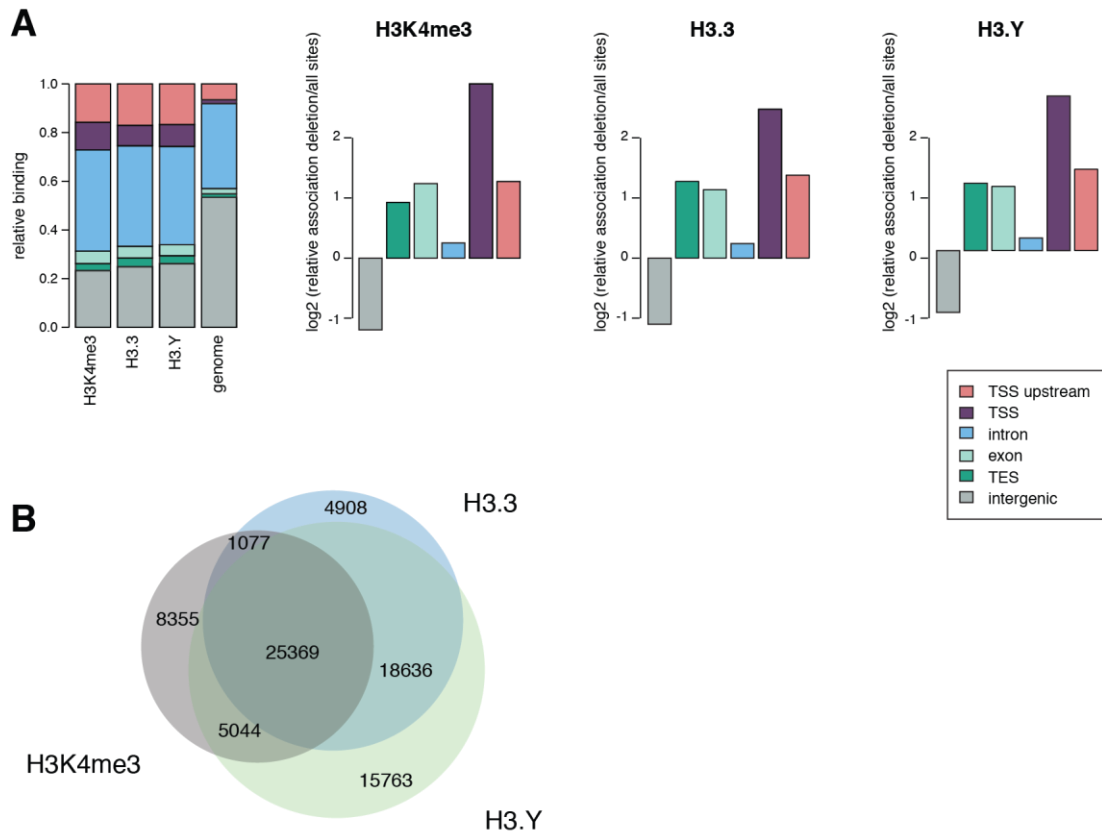


Figure 10: Both H3.3 and H3.Y mainly localize to genic, euchromatic H3K4me3-positive sites in the human genome. (A) Annotation of H3.3, H3.Y and HK4me3 to different genomic regions compared to the total human genome obtained by ChIP-seq. Data for H3K4me3 downloaded from ENCODE. (B) Venn diagram illustrating the overlap of H3.3, H3.Y and H3K4me3 peaks. Depicted are the numbers of peaks. Most peaks overlap, indicating H3.3's and H3.Y's presence at euchromatic sites.

Correspondingly to the presence of the active PTM H3K4me3, H3K9me3 as a heterochromatic mark was absent from H3.3 and H3.Y enriched sites (Figure 11). These results, so far, suggested that most of H3.3 is incorporated by the HIRA complex. To identify DAXX/ATRX deposition sites we were searching for regions where only H3.3 but not H3.Y is localized and called them “H3.Y-reduced sites” (Figure 11B).

RESULTS

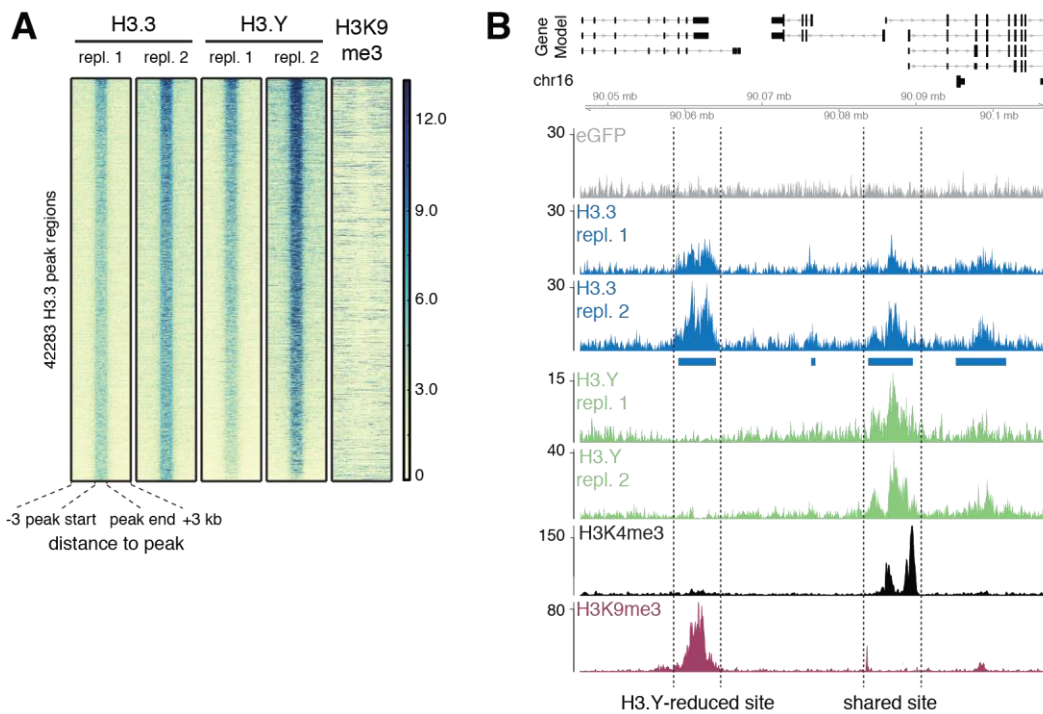


Figure 11: H3.Y and most of H3.3 are depleted from H3K9me3-positive sites. (A) ChIP-seq density heatmap of peaks identified in H3.3 replicate 1, correlated to H3.3 replicate 2, both H3.Y replicates and H3K9me3 (H3K9me3 data from (305)). Color intensity represents normalized and globally scaled tag counts. (B) Snapshot from Genome browser of a representative region on chromosome 16 depicting eGFP (gray) as a negative control, H3.3 (blue) and H3.Y (green) in two replicates, H3K4me3 (black) and H3K9me3 (ruby). Annotated gene features are shown above. Blue boxes illustrate assigned peaks by MACS 2 peak calling method. “H3.Y-reduced site” refers to sites in the genome where only H3.3 but not H3.Y is present, whereas “shared site” describes sites where both, H3.3 and H3.Y, are enriched.

In total we found 359 (at fold change <2 and adjusted p-value <0.05) of these H3.Y-reduced sites that were overlapping with H3K9me3 (Figure 12).

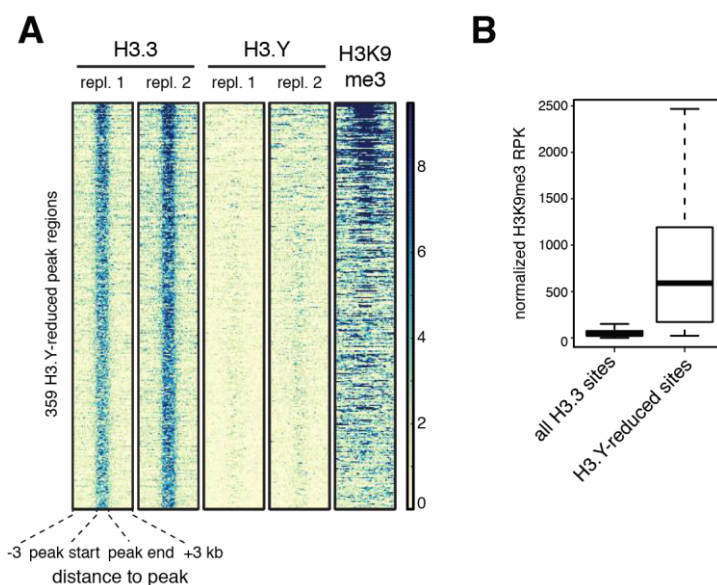


Figure 12: H3.Y-reduced sites are enriched with H3K9me3. (A) ChIP-seq density heat map of H3.3 H3.Y-reduced sites (replicate 1 and 2), H3.Y (in both replicates) correlated to H3K9me3. Color

RESULTS

< 0.05). Repeats were ranked according to the observed/expected ratio. Simple repeats are highlighted in red.

Notably, guanosines and thymidines and GT repeats were enriched in both, the newly identified motifs and in the top hits of the repeats. Among the top 20 repeats were 12 simple repeats (Figure 13B, marked in red).

All in all, we could show that H3.3 and H3.Y were mainly found in euchromatic sites, likely as a result of HIRA-mediated deposition. H3.Y-reduced H3.3 incorporation sites were enriched in simple repeat sequences and might accordingly represent DAXX/ATRX deposition sites.

3.3 CHROMATIN INTERACTOME OF H3.Y-CONTAINING NUCLEOSOMES

Since H3.Y indeed associated with active chromatin and was depleted from heterochromatic, repetitive sequences, I wondered whether this feature is also reflected by differential interaction partners of H3.3- or H3.Y-containing mononucleosomes. Considering H3.Y's localization to H3K4me3-positive, likely euchromatic sites (see Figure 10), it is tempting to speculate that H3.Y is enriched in interaction partners that are associated with active chromatin and depleted in interaction partners, that are linked to repressive chromatin states. To test this hypothesis, nuclei from different stable HeLa Kyoto cells lines expressing eGFP-tagged H3.1, H3.2, H3.3, H3.Y and eGFP as a negative control were isolated, and chromatin was digested with MNase in triplicates (see Figure 14).

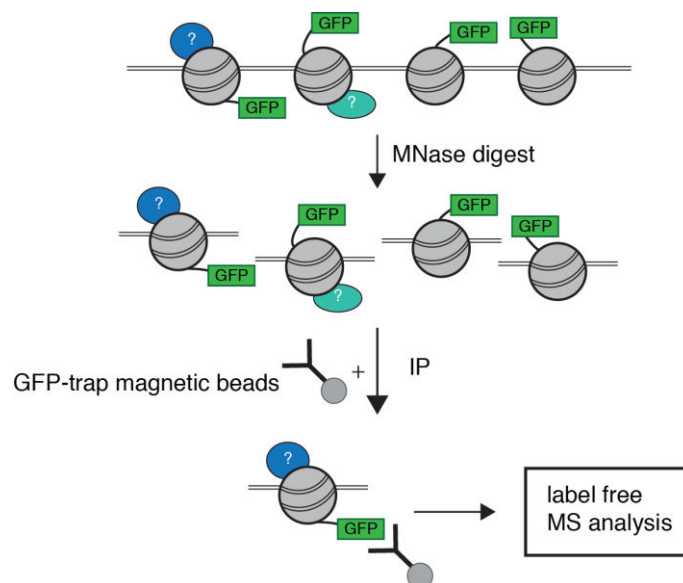


Figure 14: Schematic overview of isolation of mononucleosomes. Nuclei isolated from different HeLa Kyoto cell lines stably expressing eGFP-tagged H3.1, H3.2, H3.3 or H3.Y and eGFP as a negative control

RESULTS

were isolated and subjected to MNase digestion. The resulting mononucleosomes were immunoprecipitated using GFP-trap_M beads. The immunoprecipitated material was then analyzed by label-free quantitative mass spectrometry.

Chromatin that was digested to almost 100% mononucleosome purity (Figure 15A) was used for immunoprecipitation. Mononucleosomes containing eGFP-tagged H3 variants and bound complexes were precipitated with GFP trap_M beads and afterwards subjected to on-bead-tryptic digestion. Our collaborator Eva Keilhauer, a PhD student from the group of Matthias Mann, analyzed the samples by label-free quantitative mass spectrometry: Precipitated peptides were identified and quantified using MaxQuant software version 1.3.9.20 (306, 307). Further analysis was performed with Perseus software, version 1.5.3.0. First, specific H3 variant binders were determined by comparing H3 variant pulldowns to GFP pulldowns (see Figure A.1 in appendix). Next, two sample t-tests comparing eGFP-H3.1 with eGFP-H3.2, eGFP-H3.3 or eGFP-H3.Y, as well as comparing eGFP-H3.3 with eGFP-H3.Y provided *p*-values and t-test differences which were subsequently plotted against each other in volcano plots using R 2.15.3. This way the nucleosome interactome of the different H3 variants could be compared and the distinct binding partners were analyzed (Figure 15B-E). First, the interacting proteins of the canonical variant H3.1 on the left were plotted against the interacting proteins of H3.2 on the right (Figure 15B). Only minor differences in the interactome could be detected.

Comparison of the eGFP-H3.1 and the -H3.3 interactome, revealed more differences (Figure 15C): whereas the canonical variant H3.1 on the left showed enrichment of known chaperone complex members CAF1A and CAF1B, H3.3 on the right was enriched in DAXX and H3.3, suggesting homotypic nucleosomes, that contain only H3.3 and no other H3 variant.

The biggest difference in enriched interacting proteins, however, was observed between eGFP-H3.1 and -H3.Y (Figure 15D). The H3.1 nucleosome interactome (Figure 15D, left) contained members of the CAF1 complex, CAF1A and -B (shown in light green) and of the PRC1 complex (displayed in orange) like Chromobox protein homolog 8 (CBX8), E3 ubiquitin-protein ligase RING2 (RNF2) and RING1, Polyhomeotic-like protein 2 and 3 (PHC2 and PHC3) and Polycomb Ring Finger BMI1. In addition, H3.1 nucleosomes were enriched in SUV39H (suppressor of variegation 3-9) proteins (shown in pink), which are responsible for setting the trimethylation on lysine 9 of histone H3 (308, 309), a well-established mark for heterochromatin. Moreover, H3.1 nucleosomes also pulled down all HP1 proteins, Chromobox protein homolog 1, 3 and 5 (CBX1, 3 and 5, shown in blue), which are known to

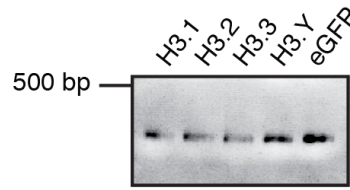
RESULTS

recognize trimethylated H3K9 and are implicated in further repression of chromatin (310, 311). While H3.1-containing nucleosomes precipitated members of heterochromatin-associated complexes, H3.Y (Figure 15D, right) was enriched in FACT complex members that have been implicated in chromatin recovery during transcription (312) and DAXX.

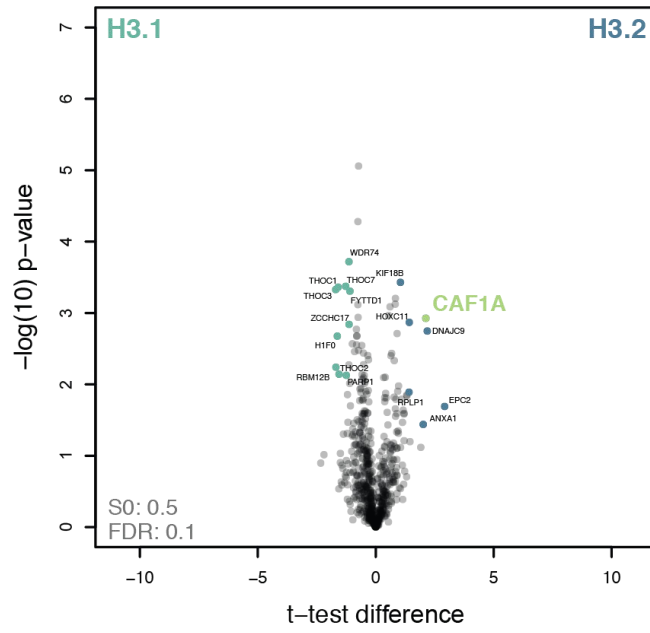
While H3.3 and H3.Y shared most of their deposition sites (Figure 10), they revealed differences in their associated proteins (Figure 15E). H3.3 nucleosomes specifically interacted with CAF1B (light green), members of the PRC1 complex (PHC3 and BMI1 in orange) and all HP1 proteins CBX1, 3 and 5 (shown in blue), whereas H3.Y nucleosomes (Figure 15E, right) were associated with FACT complex members FACT140 and FACT80 (Figure 15E, left, petrol blue).

RESULTS

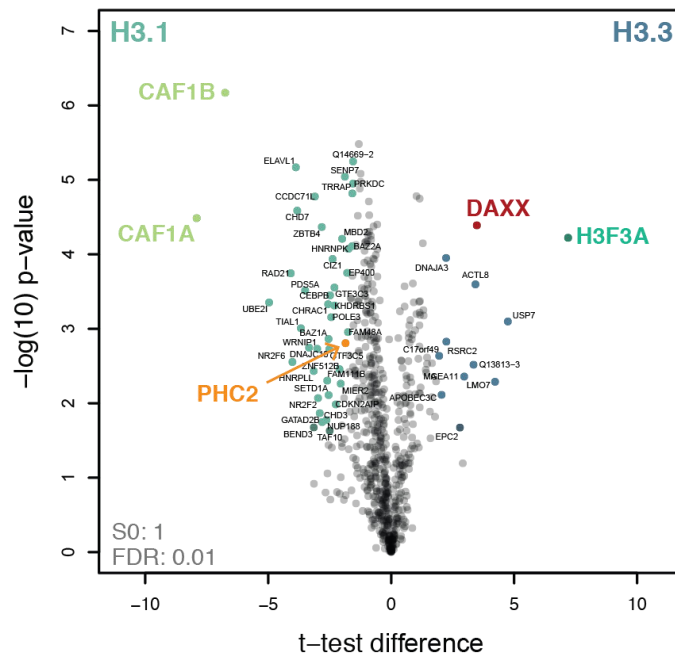
A



B



C



RESULTS

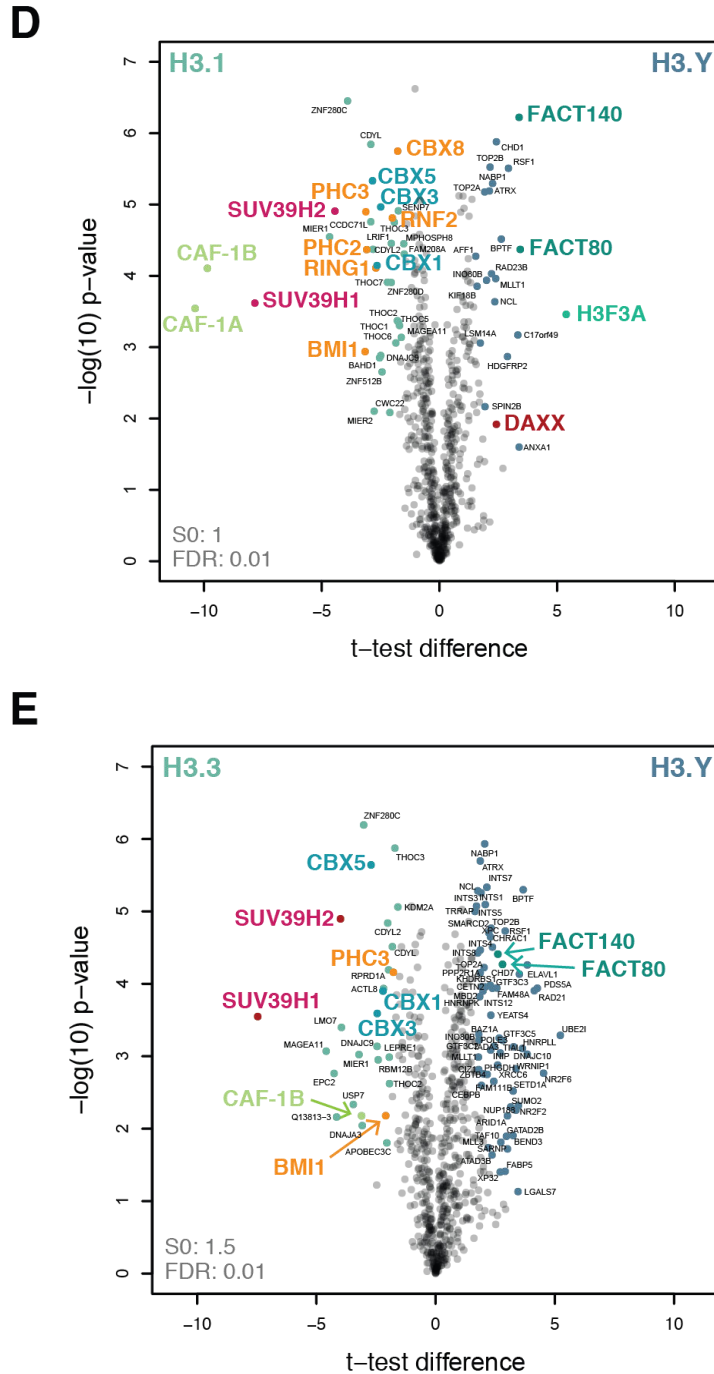


Figure 15: Nucleosome interactome of different H3 variants. Chromatin from different HeLa Kyoto cell lines stably expressing eGFP or eGFP-tagged H3 variants was successfully digested to mononucleosomes. (A) The agarose gel indicates a DNA size of 150 bp that reflects the corresponding DNA size of mononucleosomes. (B-E) Volcano plots visualize the specific enrichment of different H3 variant interactors. After performing two sample t-tests, obtained p -values and t -test differences were plotted against each other in volcano plots using R. Permutation-based FDR cutoff was applied to identify specifically enriched candidate proteins, indicated with colored dots in green and blue, respectively. Interesting candidates were written in enlarged, colored letters. PRC1 complex members are shown in orange, CAF1 complex members in light green, SUV39H members in pink, CBX1 proteins in blue, DAXX in red, H3.3 in mint green and FACT complex members in petrol blue.

RESULTS

In conclusion, all H3 variant-containing nucleosomes except H3.Y demonstrated an enrichment in heterochromatic proteins such as members of the PRC1 complex, SUV39H proteins and HP1. In contrast, H3.Y mononucleosomes were enriched in the transcription associated FACT complex.

To illustrate the enrichment of interesting candidate proteins, a heatmap was created using Perseus showing log₂-fold changes of various interaction partners immunoprecipitated with H3 variant mononucleosomes (Figure 16A). Since SUV39H1 and 2 are responsible for the trimethylation of lysine 9 on histone H3 (308, 309) I wondered whether the depletion on H3.Y nucleosomes is also reflected by reduced levels of H3K9me₃. To test this hypothesis, I isolated chromatin from HeLa Kyoto cells stably expressing eGFP and eGFP-H3.1, -H3.3 and -H3.Y and performed an MNase digest. Resulting eGFP-H3 variant-containing mononucleosomes were immunoprecipitated with GFP-trap_M, followed by immunoblotting using a commercially available H3K9me₃ antibody (Figure 16B).

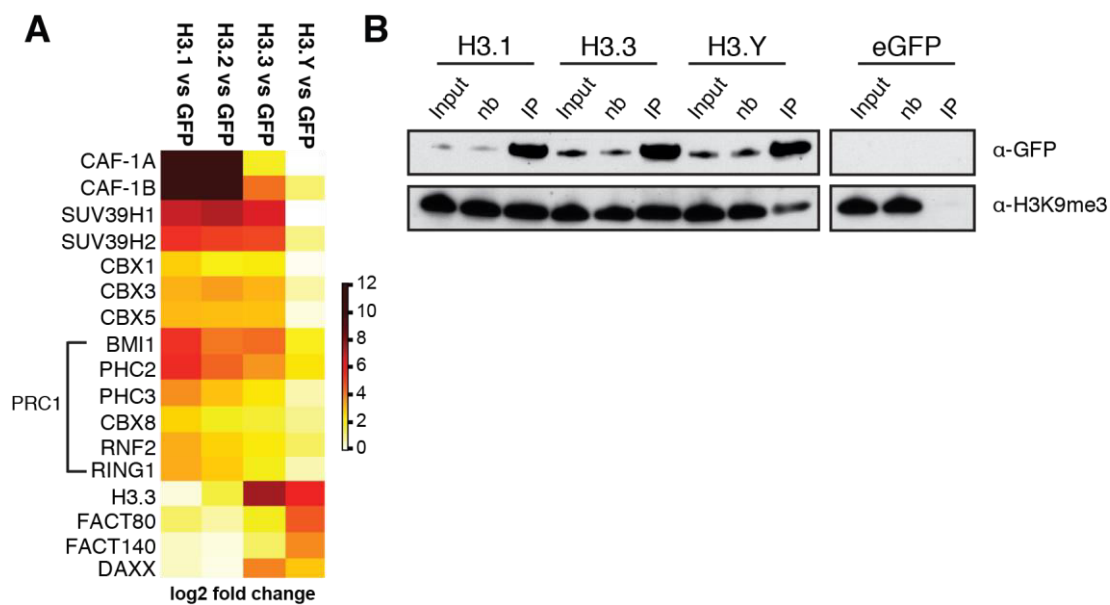


Figure 16: Enrichment of heterochromatic proteins on H3 variant-containing nucleosomes is also reflected by distinct H3K9me₃ levels. (A) Heatmap visualizing enrichment of different candidate proteins for distinct H3 variant-containing nucleosomes (see Figure 15B-E). H3.1- and H3.2-containing nucleosomes are highly enriched in CAF1A and B. Besides, both the canonical variants H3.1 and H3.2 and the replacement variant H3.3 are associated with heterochromatic proteins. In contrast, H3.Y nucleosomes are enriched in the FACT complex and DAXX. (B) Depletion of SUV39H on H3.Y nucleosomes is also reflected in reduced H3K9me₃ levels, as seen by immunoblot.

Indeed, a depletion of H3K9me₃ could be noticed on immunoprecipitated H3.Y nucleosomes, whereas eGFP-H3.1 and -H3.3 revealed similar levels of trimethylated H3K9,

RESULTS

again confirming H3.Y's localization to euchromatic HIRA dependent sites (see also Figure 10 and 11).

3.4 RESIDUES IN THE H3.Y CORE & C-TERMINUS ARE NECESSARY FOR DAXX INTERACTION

3.4.1 Mutation of the Single Q59E Residue in H3.Y is not Sufficient for DAXX Binding

Since the structure of the HBD of DAXX together with an H3.3-H4 dimer has been crystalized (247, 313), we were able to further examine the interaction of DAXX HBD and H3.3. Glutamic acid in H3.3 at position 59 is directly binding DAXX arginine 251 and participates in a hydrogen bond network together with H3.3 serine 57 and DAXX tyrosine 222, glutamic acid 225, and Lysine 229 (247). As Q59 is replaced in H3.Y by glutamine (see Figure 4) I speculated whether this replacement could be responsible for the missing interaction of H3.Y and DAXX. To check this hypothesis Sebastian Pünzeler, a former PhD student from our lab, generated a stable mutant eGFP-H3.Y cell line called eGFP-H3.Y Q59E where he exchanged H3.YQ59 with the corresponding H3.3E59. eGFP expression was determined in G418-sulfate selected cells by flow cytometry analysis (Figure 17A). To confirm the nuclear localization of the H3.Y Q59E mutant and to exclude the possibility of a localization or incorporation defect into chromatin, I analyzed these HeLa Kyoto cells expressing eGFP-H3.Y Q59E by immunofluorescence. The cells showed nuclear localization in interphase cells as well as localization to condensed chromatin indicated by co-localization with H3S10 phosphorylation signal (Figure 17B). Phosphorylation of H3 serine 10 is a posttranslational modification that occurs during mitosis and indicates condensed chromatin (116, 118). Since most chromatin components that are not stably associated, dissociate from condensed chromatin during mitosis co-staining with H3S10 phosphorylation serves as an indicator for stable chromatin incorporation.

RESULTS

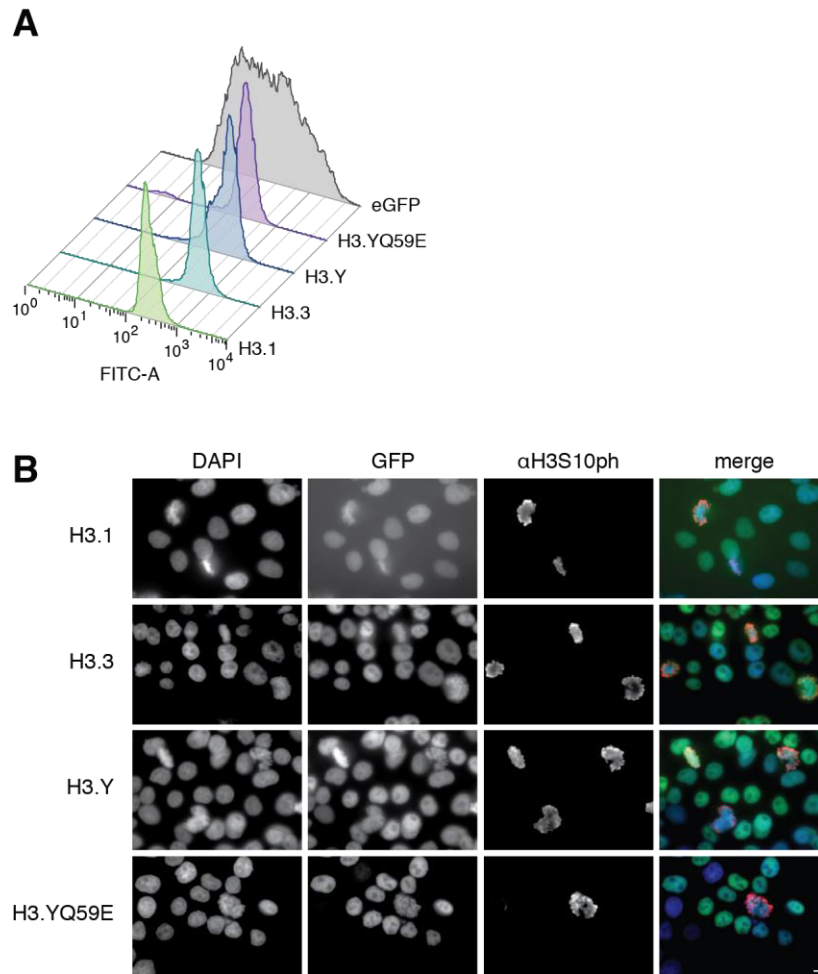


Figure 17: All H3 variant cell lines reveal stable GFP expression and are stably incorporated into chromatin. (A) Flow cytometry analysis of stable HeLa Kyoto cell lines expressing eGFP (gray histogram) or eGFP-H3.1 (light green), -H3.3 (turquoise), -H3.Y (blue) and -H3.Y Q59E (purple). eGFP serves as positive control. GFP intensity was detected in the FITC-A channel and plotted in a histogram. (B) Immunofluorescence imaging of stable H3 variant cell lines. HeLa Kyoto cells stably expressing eGFP-H3 variants and mutant -H3.Y Q59E were fixed; DNA was stained with DAPI (blue, left panel), H3 variants are shown in green (GFP, second left panel) and H3S10 phosphorylation was probed using a commercially available antibody to visualize mitotic cells (red, second right panel). The overlay is depicted on the right. Scale bar: 5 μ m.

In addition, all variants including eGFP-H3.Y Q59E were visible on metaphase chromosome spreads (Figure 18), suggesting that they are stable parts of the nucleosome core.

RESULTS

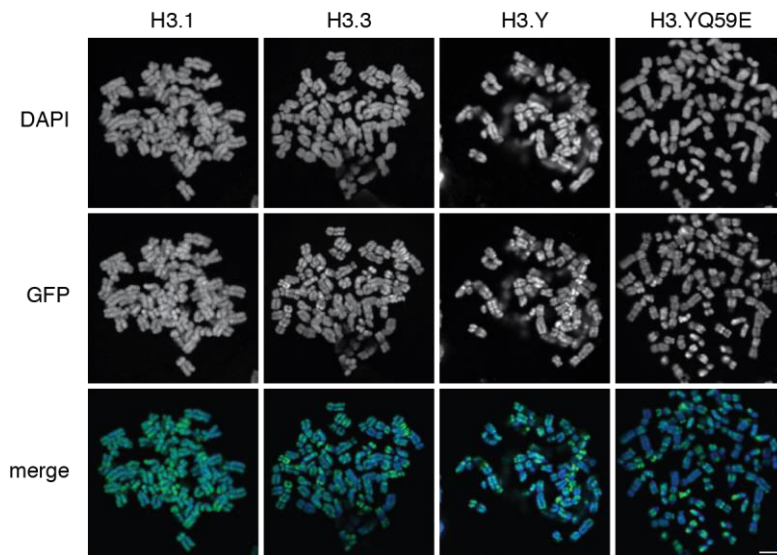


Figure 18: Chromosomal localization of eGFP-H3 variants. HeLa Kyoto cells stably expressing eGFP-H3.1 (left), -H3.3 (second left), -H3.Y (second right) and mutant -H3.Y Q59E (right) were metaphase-arrested and chromosomes spread on microscope slides. The distinct H3 variants appear in different patterns along the chromosome. DNA was stained with DAPI (blue, upper panel), eGFP-H3 variants shown in green (middle lane) and overlay is depicted in the lower panel. Scale bar is 5 μ m.

Whereas eGFP-H3.1 was distributed uniformly along the chromosome, the other variants showed a more defined pattern, supporting the barcode hypothesis suggested by (314).

In order to analyze the importance of the E59 residue in H3.3 for DAXX binding, I again isolated soluble nuclear proteins from the different eGFP-H3 variant expressing cell lines and immunoprecipitated them using GFP trap_M beads. As before, the samples were analyzed by immunoblotting with a commercially available DAXX antibody (Figure 19).

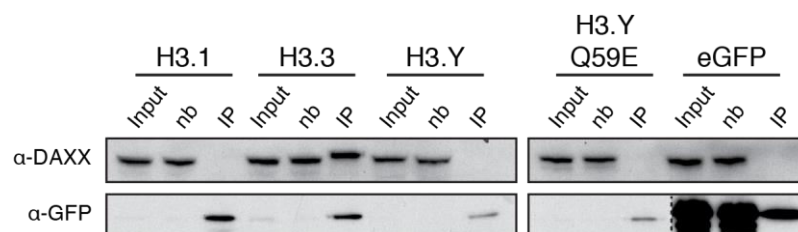


Figure 19: Mutation of Q59E in H3.Y is not sufficient for DAXX binding. GFP-H3 variant cell lines and the H3.Y mutant H3.Y Q59E were tested regarding their DAXX binding ability. For details see Figure 7.

The exchange of the single residue Q59 to the corresponding H3.3's glutamic acid did not allow a stable DAXX interaction. Although this amino acid plays a crucial role in an extensive hydrogen bonding network with DAXX, its sole replacement was not sufficient to gain DAXX binding.

RESULTS

3.4.2 Replacing Core Residues in H3.Y does not Enable DAXX Interaction

Obviously, replacing glutamine at position 59 with the corresponding glutamic acid from H3.3 did not enable DAXX interaction. Next, I decided to further mutate H3.Y at core residues: a stretch from residue 77-80 is completely replaced in H3.Y. Additionally, H3.3 glycine 102 is exchanged to glutamine in H3.Y. Both, the stretch 77-80 and G102 are flanking the chaperone recognition site. Thus I speculated, whether these amino acids could perturb the recognition or binding of H3.Y to DAXX. To test this hypothesis, I mutated the referred residues and finally obtained a so-called “H3.Y core” mutant (Figure 20), which comprises a combination of the replacement of glutamine 59 to glutamic acid, the stretch from position 77-80 and glutamine 102 to glycine.



Figure 20: Alignment of H3.3, H3.Y and the “H3.Y core” mutant. In the mutant H3.Y’s amino acids 59, 77-80 and 102 are replaced by the corresponding H3.3 residues. H3.3 residues are depicted in blue, H3.Y residues in green. The chaperone recognition site is highlighted in purple.

A new stable cell line, called eGFP-H3.Y core was established. GFP expression was confirmed by flow cytometry analysis (Figure 21A) and chromatin incorporation was again investigated by immunofluorescence (Figure 21B). eGFP-H3.Y core mutant showed an exclusive nuclear staining. H3S10 phosphorylation was once more used for the visualization of mitotic cells and co-localization indicated a stable chromatin incorporation of the mutant.

RESULTS

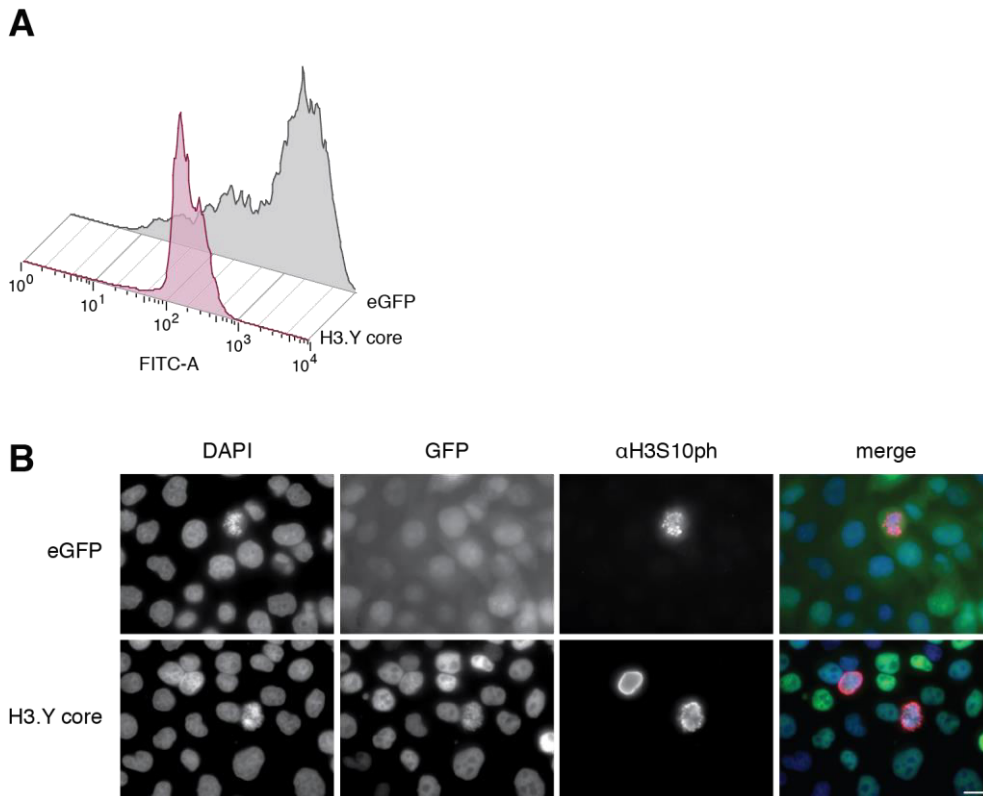


Figure 21: H3.Y core mutant is stably expressed in HeLa Kyoto cells and localizes to chromatin. (A) Flow cytometry analysis of eGFP as a positive control (gray) and eGFP-H3.Y core (red) indicates a stable expression of the GFP-tagged construct. (B) eGFP as a control and the H3.Y mutant eGFP-H3.Y core were analyzed for their localization by immunofluorescence microscopy. eGFP is found in cytoplasm and nucleus, whereas eGFP-H3.Y core shows only nuclear staining. For details see Figure 17.

Also this new H3.Y mutant cell line was investigated for DAXX interaction. Therefore, chromatin-free extracts of eGFP-tagged H3 variants, including this new eGFP-H3.Y core mutant were prepared and subjected to immunoprecipitation, followed by immunoblotting (Figure 22).

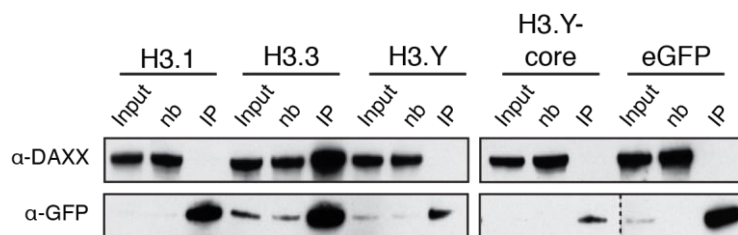


Figure 22: eGFP-H3.Y core mutant does not pull down DAXX. GFP-H3 variant cell lines, the mutant cell line H3.Y core and eGFP as a negative control were analyzed in respect to DAXX binding. For details see Figure 7.

Surprisingly, also this H3.Y mutant, although being nearly identical to H3.3 in core residues, is not able to pull down DAXX.

RESULTS

3.4.3 H3.3 & H3.Y Tail Swap Mutant Consisting of N-terminal H3.Y & H3.3 Core/C-Terminus Allows Stable DAXX Interaction

As a next step we decided to examine larger regions of the histone variant proteins to identify their important sites for DAXX interaction. Therefore I designed several swap mutants, which are either exchanged at the N- or C-terminus with the corresponding H3.3 or H3.Y part (Figure 23).

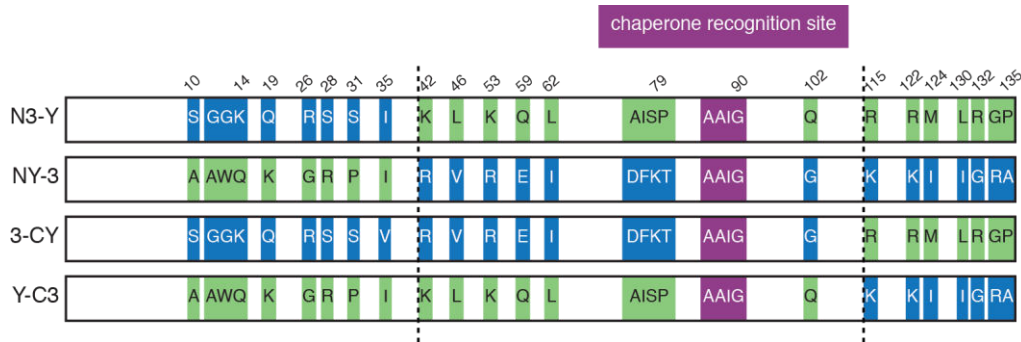


Figure 23: Alignment of H3.3 and H3.Y swap mutants. H3.3 residues shown in blue and H3.Y residues in green are either exchanged at their N-termini (N3-Y and NY-3, left) or C-termini (3-CY and Y-C3, right) to study DAXX interaction. The dotted line indicates sites of swaps: N-terminal at aa position 42, C-terminal at residue 115.

The N3-Y mutant consists of the H3.3 N-terminus from aa 1 to 35 and of H3.Y from aa 36 to aa 135. NY-3 is composed of an H3.Y N-terminus (aa 1-35) fused to an H3.3 core (aa 36-135). The C-terminal swap mutants consist of either H3.3 (aa 1-114) combined with an H3.Y C-terminus (aa 115-135) or H3.Y fused to an H3.3 C-terminal tail. These four different constructs were ordered at *Genewiz* and arrived in a pUC57 vector. To allow expression in HeLa Kyoto cells, the different mutants were then cloned into the pIRESneo-eGFP vector via gateway cloning. Subsequently, HK cells were transfected with the constructs fused to an N-terminal GFP-tag and selected with G418-sulfate to obtain stable cell lines. The stable GFP expression was determined by flow cytometry analysis (Figure 24A) and nuclear localization was analyzed by immunofluorescence (Figure 24B). The flow cytometry profile of the eGFP-Y-C3 cell line (Figure 24A, orange) revealed that only a fraction of approximately 20% stably expresses the GFP-tagged construct. Several attempts failed to stably express this construct, thus following experiments were performed with appropriate higher cell numbers to ensure the same cell number of eGFP expressing cells and thus the same amount of eGFP tagged protein. To determine their subcellular localization, the different H3.3/H3.Y swap mutants were analyzed by immunofluorescence. All four swap mutants revealed exclusive nuclear staining. Co-localization with H3S10 phosphorylation indicated stable chromatin incorporation.

RESULTS

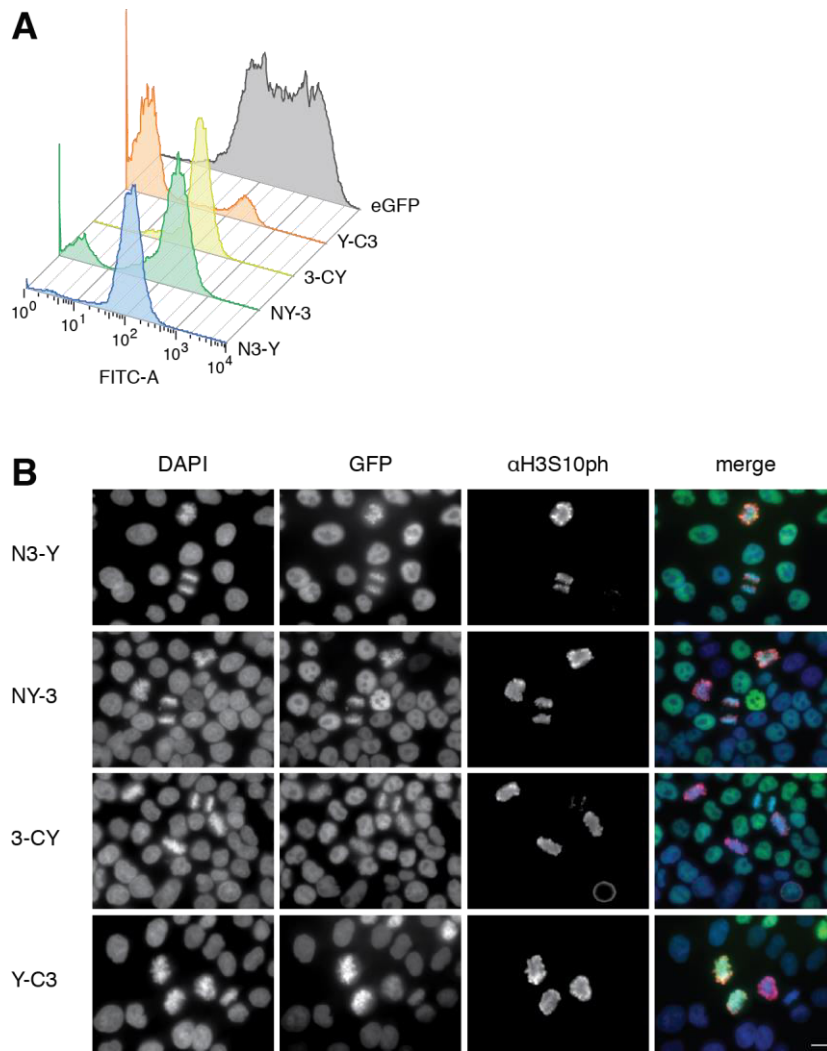


Figure 24: N-terminal GFP-tagged H3.3 and H3.Y swap mutants are stably expressed in HeLa Kyoto cells and show localization to chromatin. (A) Flow cytometry analysis of four different mutant swap HeLa Kyoto cell lines (see Figure 23) indicates a stable GFP expression of the eGFP-N3-Y (blue), eGFP-NY-3 (green) and eGFP-3-CY constructs (yellow), whereas only a minor fraction of the eGFP-Y-C3 cell line (orange) expresses the GFP-tagged construct. EGFP (gray) served as positive control. (B) For details see Figure 17.

In order to examine the potential DAXX interaction capability of the H3.3/H3.Y swap mutants I isolated soluble nuclear proteins from the respective stable HeLa Kyoto cell lines and performed pull-down experiments, again using the GFP-trap_M. Afterwards, interaction with DAXX was analyzed by immunoblotting (Figure 25).

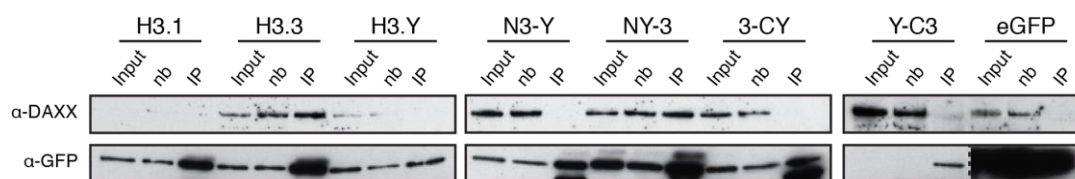


Figure 25: eGFP NY-3 interacts with DAXX. Stable GFP-H3 variant cell lines and H3.3/H3.Y swap mutants were investigated regarding DAXX binding ability. For details see Figure 7.

RESULTS

The positive control eGFP-H3.3 and the swap construct eGFP-NY-3 interacted with DAXX. This H3.3-H3.Y chimera is composed of the N-terminal H3.Y tail and the H3.3 core. In contrast, all other swap mutants did not bind DAXX. Apparently, the H3.Y C-terminus prevented the interaction (eGFP-3-CY), whereas the N-terminal tail did not (eGFP-NY-3). Moreover, exchanges in the core of H3.Y were necessary for DAXX binding as eGFP-Y-C3, which consists of H3.Y and the H3.3 C-terminus, did not pull down DAXX. In conclusion a combination of residues in the core and C-terminus was necessary to determine DAXX interaction and only the construct eGFP-NY-3 was able to pull down DAXX.

To test whether the interaction of eGFP-NY-3 with DAXX also results in its localization to PML bodies, our collaboration partner Erwan Delbarre transiently transfected mesenchymal stem cells and analyzed the potential co-localization with PML-NBs and the different swap chimeras (Figure 26A). To ensure a representative result, 200 cells were counted and swap mutants analyzed for their differential distribution in chromatin or PML structures (Figure 26B). Since the recruitment to PML-NBs was DAXX-dependent we assumed a localization of eGFP-NY-3 to these structures, whereas, as already shown in Figure 9, eGFP-H3.Y is restricted to chromatin. As expected, eGFP-NY-3 is enriched in PML-NBs (Figure 26A and B). Surprisingly, also eGFP-3-CY localized there. This swap construct consists of H3.3 and an H3.Y C-terminus. Although this mutant did not reveal a stable DAXX interaction in immunoprecipitation experiments followed by western blot, it did localize to PML-NBs.

RESULTS

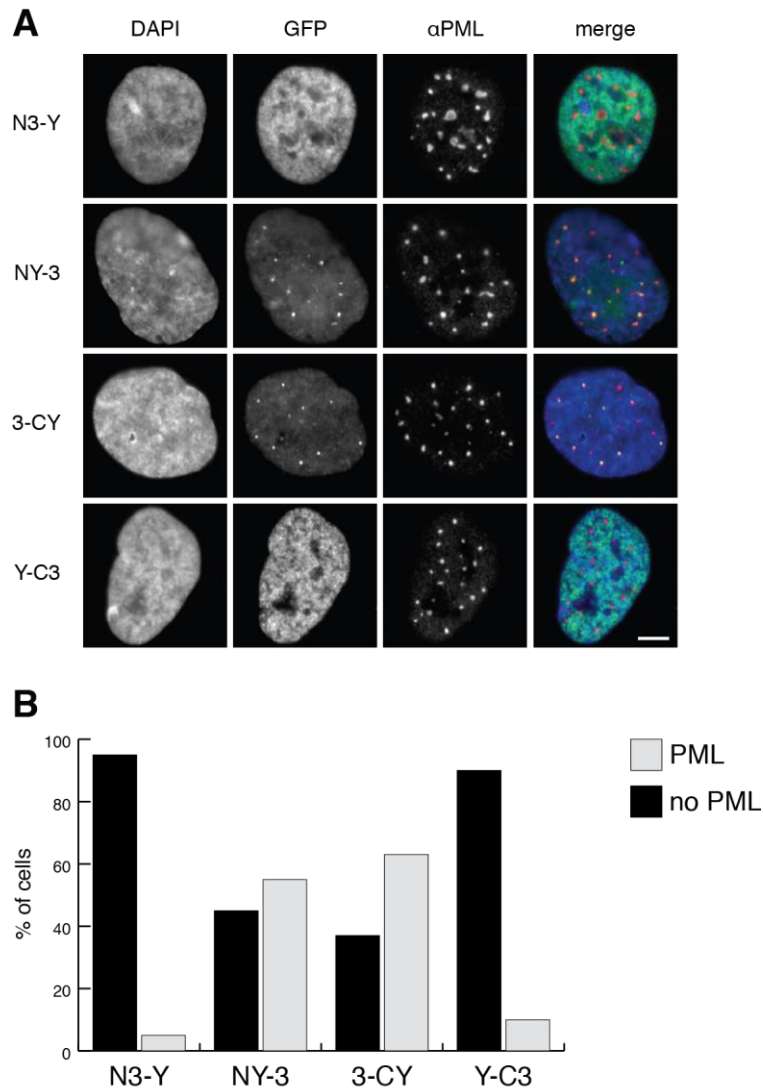


Figure 26: eGFP-NY-3 and -3-CY localize to PML-NBs. (A) eGFP-N3-Y, -NY-3, -3-CY, and -Y-C3 were transiently transfected into mesenchymal stem cells and localization to PML-NBs was analyzed by fluorescence microscopy. DNA was stained with DAPI (left column, blue), histones are depicted in green (GFP, second left panel) and PML-NBs are stained with an antibody (red, second right panel). Overlay image is displayed on the right; scale bar is 5 μ m. (B) 200 cells were counted and the percentage of cells that display either a chromatin distribution (black) of the constructs or an enrichment in PML-NBs (gray) was depicted in a bar chart. Notably, not only eGFP-NY-3 but also eGFP-3-CY are found in PML-NBs.

Since not only eGFP-NY-3 but also 3-CY got recruited to PML-NBs it is tempting to speculate, that this localization is due to a transient interaction of DAXX and 3-CY. This association, not stable enough to be detected in immunoblot might be sufficient for PML-NB localization. Hence, for a transient interaction, DAXX could tolerate both, the N-terminus (present in NY-3) and the C-terminus (present in 3-CY) of H3.Y, meaning the replacement of H3.Y core residues might be sufficient for PML-NB recruitment.

RESULTS

3.5 H3.3-DAXX INTERACTION: A DEFINED COMBINATION OF AMINO ACIDS MATTERS

Both NY-3 and 3-CY were localizing to PML-NBs, indicating that the sole replacement of H3.Y core residues might be sufficient for transient DAXX interaction. However, the C-terminus of H3.Y seems to prevent a stable DAXX-association and thus 3-CY could not be detected in immunoprecipitation experiments. Aiming for the identification of the exact residues that determine strong DAXX interaction, I used the H3.Y core mutant and further mutated several amino acids in the C-terminus to investigate which H3.Y-residues prevent stable DAXX interaction. Depending on the different mutants, distinct parts of the C-terminus in the H3.Y core mutant were exchanged with H3.3 residues (Figure 27). First, I designed the H3.Y core GERA mutant by replacing the last three exchanged amino acids of H3.Y with H3.3's residues. Additionally, arginine at position 53 was replaced with the corresponding lysine from H3.3 resulting in another mutant called H3.Y K53R core GERA. R53 is in close proximity to lysine 56 which is known to be posttranslationally modified (95, 96, 109, 315) and was shown to play a role as a predeposition mark to regulate the association with distinct chaperone complexes in yeast (316). As arginine 53 lays close to K56 the exchanged residue might perturb the acetylation of K56 so I decided to further exchange this residue. Similarly, in H3.Y core R122K M124I amino acid 122 and 124 were exchanged in the background of H3.Y core. DeNizio et al. demonstrated that DAXX directly binds lysine 122, thus I speculated that an arginine in H3.Y might influence DAXX interaction (271). Furthermore, I also decided to replace amino acid 124, as it is in close proximity and might, therefore, perturb the binding to R122. Lastly, H3.Y K53R core C3 was generated to serve as a positive control since it only differs in the three residues 42, 46 and 62 from NY-3 that was already demonstrated to bind DAXX.



Figure 27: Alignment of H3.3 and mutant H3.Y. Different H3.Y mutants were designed to further define the residues important for DAXX interaction. All mutants have the H3.Y core background and in the case of H3.Y core GERA the last four amino acids were exchanged to H3.3 residues, in H3.Y K53R core GERA the additional arginine 53 was exchanged. In H3.Y core R122K M124I arginine at position 122 and methionine at position 124 were exchanged with the corresponding H3.3 lysine and isoleucine, respectively. Details see Figure 20.

RESULTS

As before, HeLa Kyoto cells were transfected with the different mutant H3.Y constructs and stable cell lines were established by selection with G418-sulfate. Stable GFP expression was determined by flow cytometry analysis (Figure 28A) and immunofluorescence microscopy revealed nuclear localization of these new mutant constructs. Co-staining with an antibody recognizing H3 serine 10 phosphorylation indicated again stable incorporation into chromatin (Figure 28B).

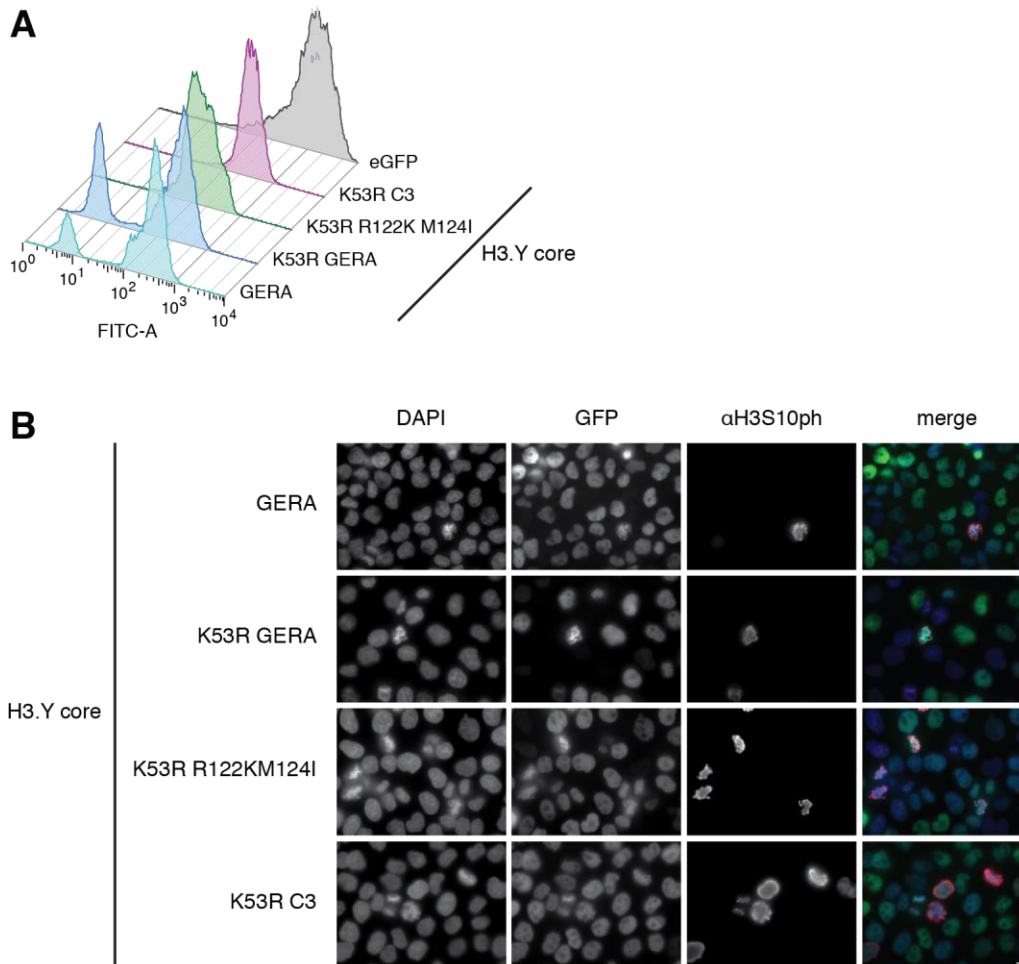


Figure 28: GFP-tagged H3.Y mutants are stably expressed in HeLa Kyoto cells and show nuclear localization. (A) GFP expression of stable HeLa Kyoto cells expressing eGFP-H3.Y core GERA (light blue), -H3.Y K53R core GERA (dark blue), -H3.Y K53R core R122K M124I (green), and -H3.Y K53R core C3 (purple), was determined by flow cytometry analysis. HeLa Kyoto cells expressing eGFP were used as a negative control (gray). (B) For details see Figure 17.

To investigate the interaction with DAXX, soluble nuclear proteins were isolated from the stable HeLa Kyoto cell lines and eGFP-tagged histone mutants were immunoprecipitated via their GFP-tag. Finally, DAXX binding was analyzed by immunoblotting (Figure 29).

RESULTS

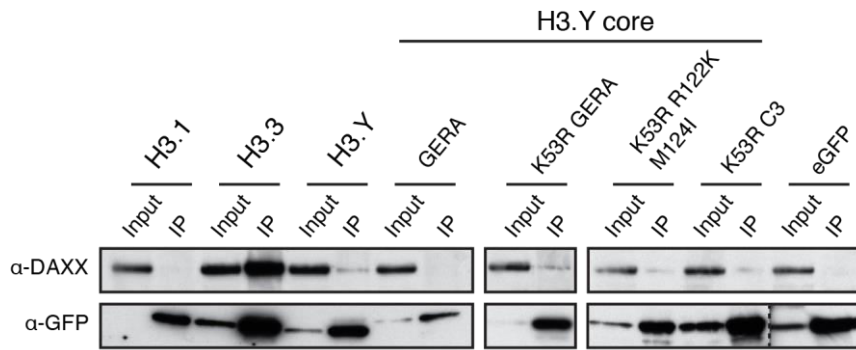


Figure 29: New C-terminal H3.Y core mutants do not interact with DAXX. The H3.Y core mutant was further mutated in the C-terminus, giving rise to H3.Y core GERA, H3.Y core K53R GERA, H3.Y core K53R R122K M124I and H3.Y core K53R C3. These new H3.Y mutants were investigated regarding DAXX binding. For details see Figure 7.

Surprisingly, none of the newly established mutants could stably bind DAXX. Replacement of the last three exchanged residues, with or without the additional K53R mutation, was not sufficient for DAXX binding. Likewise, neither H3.Y K53R core R122K M124I nor the putative positive control H3.Y K53R core C3 were able to bind DAXX.

To test the ability of the new C-terminal mutants to weakly associate with DAXX and consequently localize to PML-NBs, our collaboration partner Erwan Delbarre also analyzed the recruitment of these mutants to PML-NBs. He again transfected mesenchymal stem cells and analyzed >200 cells after 24h regarding their subcellular localization (Figure 30).

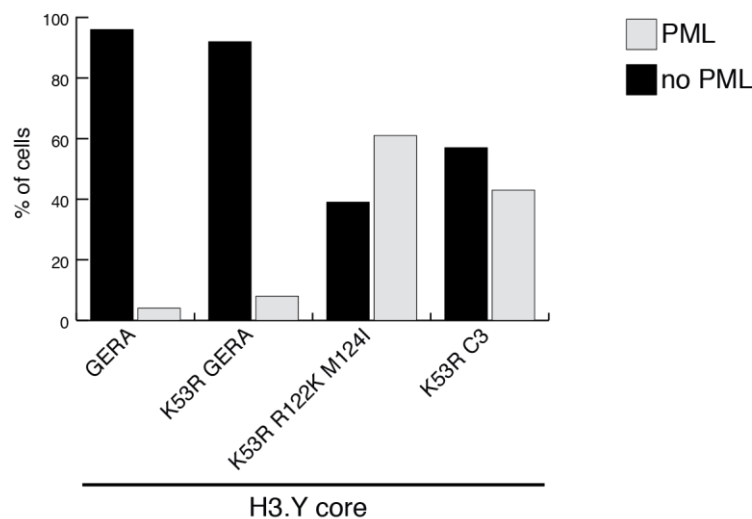


Figure 30: eGFP-H3.Y K53R core R122K M124I and -H3.Y K53R core C3 localize to PML-NBs. Mesenchymal stem cells were transfected with the eGFP-tagged constructs H3.Y core GERA, H3.Y K53R core GERA, H3.Y K53R core R122K M124I and H3.Y K53R core C3. After 24h, >200 cells per construct were investigated regarding their PML-NB localization (gray: found in PML-NBs, black: not in PML-NBs).

RESULTS

As expected, H3.Y K53R core R122K M124I and H3.Y K53R core C3 were localized in PML-NBs. Contrary and surprisingly, neither H3.Y core GERA, nor H3.Y K53R core GERA could be found in PML-NBs. Although 3-CY which possesses the whole C-terminus of H3.Y localized to PML-NBs, the new GERA mutant with the last 4 residues identical to H3.3 could not.

The missing stable interaction of H3.Y K53R core C3 and DAXX was surprising as this mutant differs only in 3 amino acids from the swap mutant construct NY-3 that was shown to bind DAXX (Figure 25). Therefore I further analyzed which of the remaining three residues that are different between H3.YK53R core C3 and NY-3 matter for the differential outcomes regarding DAXX interaction. To do so, I mutated the residues K42, L46 and L62 of H3.Y singly and in combination to the corresponding H3.3 residues, so that I ended up with six more constructs (Figure 31): first H3.Y K42R K53R core C3, second H3.Y L46V K53R core C3, third H3.Y K53R L62I core C3, fourth H3.Y K42R L46V K53R core C3, fifth H3.Y K42R K53R L62I core C3 and sixth H3.Y L46V K53R L62I core C3.

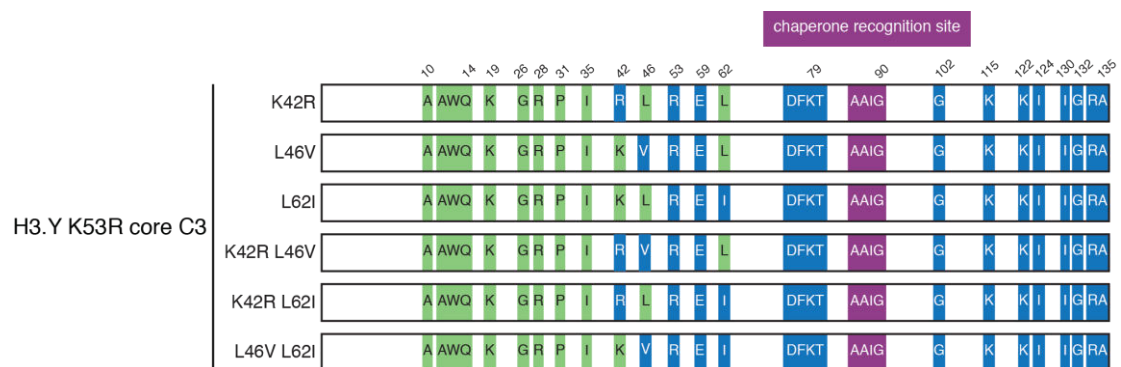


Figure 31: Alignment illustrating amino acid differences between additional H3.Y core mutants. H3.Y R53K core C3 was further mutated in its remaining three residues that are different from NY-3 that was shown to interact with DAXX. H3.Y's residues lysine 42, leucine 46 or leucine 62 were mutated singly or in combinations to the corresponding H3.3 amino acids. Details see Figure 20.

Again, we established stable cell lines with eGFP-tagged constructs, determined the stable expression by flow cytometry analysis and checked nuclear localization by immunofluorescence (Figure 32).

RESULTS

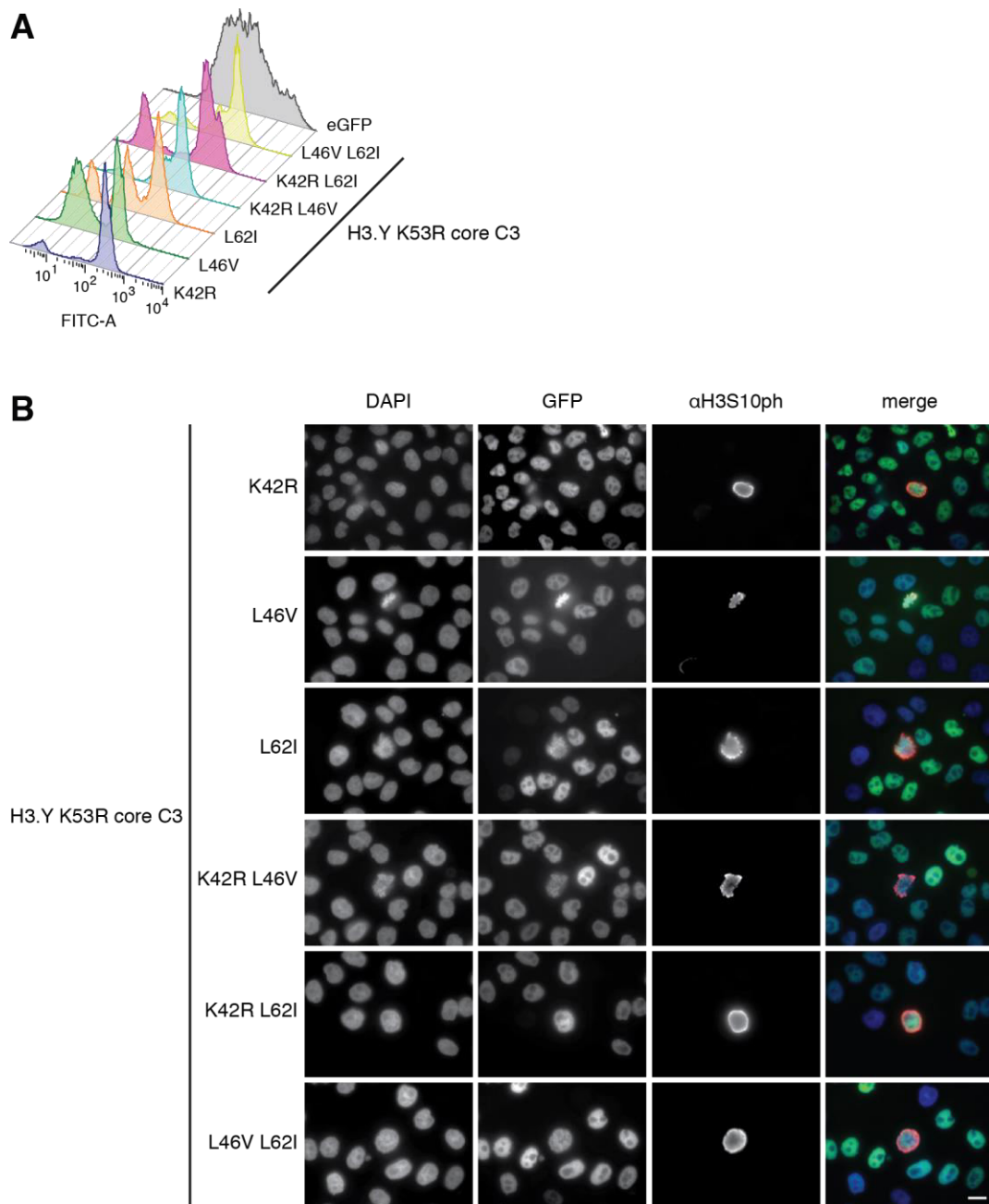


Figure 32: eGFP-H3.Y K53R core C3 mutants are stably expressed in HeLa Kyoto cells and incorporated into chromatin. (A) eGFP-H3.Y K42R K53R core C3 (dark blue), -H3.Y L46V K53R core C3 (green), -H3.Y K53R L62I core C3 (orange), -H3.Y K42R L46V K53R core C3 (light blue), -H3.Y K42R K53R L62I core C3 (fuchsia) and -H3.Y L46V K53R L62I core C3 (yellow) expression was analyzed by flow cytometry. eGFP cells were used as a positive control (gray). (B) For details see Figure 17.

After confirming the mutant's stable chromatin incorporation I again prepared nuclear extracts, followed by immunoprecipitations with GFP-trap_M. Extracts and immunoprecipitates were analyzed for DAXX binding by immunoblotting (Figure 33).

RESULTS

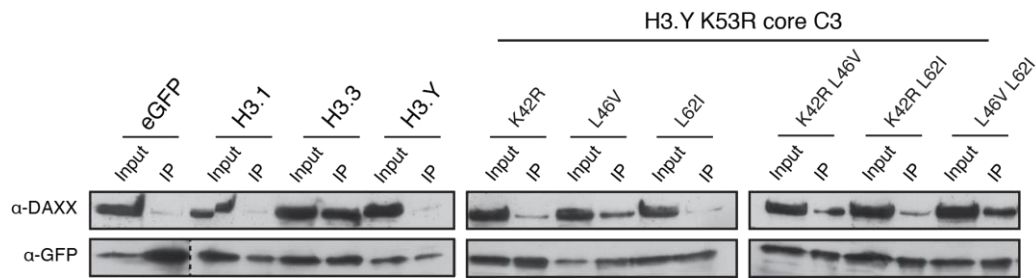


Figure 33: Leucine 46 in H3.Y K53R core C3 prevents DAXX binding. For details see Figure 7. Exchanges of K42, L46, L62, singly or in combinations, with the corresponding H3.3 residues were investigated for their contribution to DAXX binding. Notably, the exchange of leucine 46 in H3.Y to H3.3's valine has the biggest effect on DAXX binding, whereas the exchanges of K42R and L62I have only minor effects. Replacing L46V in combination with K42R or L62I could nearly fully restore DAXX binding.

Particularly replacing leucine at position 46 with valine affected DAXX binding. Here, the biggest increase in DAXX binding could be detected when exchanging a single residue. Accordingly, exchanging L46 in combination with K42R and especially L62I re-established DAXX binding to nearly H3.3 binding levels. However, also H3.Y K42R K53R L62I core C3 showed DAXX binding, although to a minor extent.

3.6 DAXX BINDING TO H3.Y MUTANTS INFLUENCES CHROMATIN INCORPORATION SITES

In 3.2 the difference between H3.3 and H3.Y in binding DAXX could also be observed by different genomic localization sites of H3.3 and H3.Y, respectively. Both variants mostly overlapped in their chromatin incorporation sites, however, a discrepancy was detected in putative DAXX-dependent, H3K9me3-positive simple repeat sites: whereas H3.3 was deposited to these sites, H3.Y was completely absent. Thus, we were wondering whether the mutants that are now able to bind DAXX could localize to these sites and thereby share H3.3 deposition sites. In order to investigate this, we used the eGFP-expressing H3.3 and H3.Y mutant cell lines N3-Y, NY-3, 3-CY, Y-C3, H3.Y L46V K53R L62I core C3 and eGFP, H3.3 and H3.Y as controls. The procedure was done as described in 3.2. Crosslinked chromatin fragments were immunoprecipitated with a GFP-antibody, sequenced by the LAFUGA lab at the gene center Munich and results bioinformatically analyzed by Marek Bartkuhn (JLU Giessen).

RESULTS

Initially, the chromatin incorporation ability of all constructs was tested (Figure 34). As expected, peak regions of all constructs overlapped with those of H3.3, consistent with H3.3's predominant localization to HIRA-dependent H3K4me3-positive sites (compare to Figure 10).

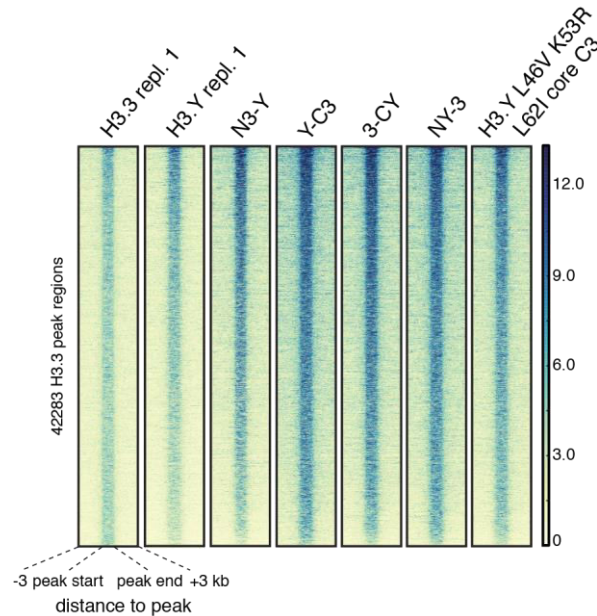


Figure 34: H3.Y mutants incorporate into shared chromatin regions where H3.3 and H3.Y are present. CHIP-seq density heat maps of peaks for the mutants N3-Y, NY-3, 3-CY, Y-C3, H3.Y L46V K53R L62I core C3 and H3.3 and H3.Y (H3.3 and H3.Y replicate 1, compare to Figure 11). Mutants co-localize with the controls H3.3 and H3.Y. Color intensity represents normalized and globally scaled tag counts.

Next, we were checking whether gained DAXX binding of the mutants is also reflected by their presence at H3.Y-reduced incorporation sites in chromatin. The tail-swap mutants N3-Y and Y-C3, which could neither immunoprecipitate DAXX nor localize to PML-NBs were found at shared sites where both H3.3 and H3.Y are present (Figure 35A). 3-CY however, which was not stably associated with DAXX in immunoblot but localized to PML-NBs revealed an intermediate phenotype regarding its incorporation sites: some H3.Y-reduced sites showed a slight enrichment of 3-CY, while others did not. Notably, both NY-3 and H3.Y L46V K53R L62I core C3 which gained stable DAXX binding, also localized to H3.Y-reduced H3.3 deposition sites, again overlapping with H3K9me3 (Figure 35).

RESULTS

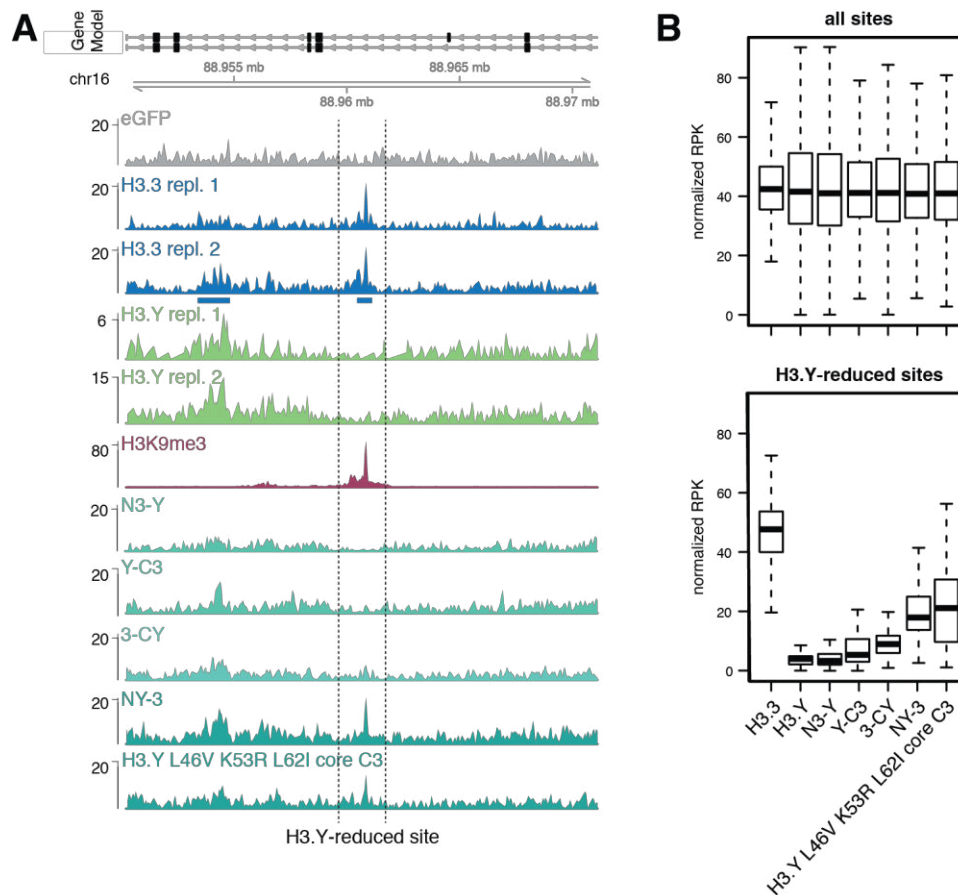


Figure 35: NY-3 and H3.Y L46V R53K L62I core C3 localize to H3.Y-reduced H3K9me3-positive sites. (A) Genome browser snapshot of H3.3 (blue), H3.Y (green), H3.3/H3.Y swap mutants and H3.Y L46V R53K L62I core C3 (different shades of turquoise), H3K4me3 (black) and H3K9me3 (ruby, (305)). Annotated gene features are depicted above. Blue boxes illustrate assigned peaks by MACS 2 peak calling method. Compare to Figure 11B. (B) Boxplot illustrating peak intensities of H3.3/H3.Y swap mutants and H3.Y L46V R53K L62I core C3 at all H3.3 sites versus H3.Y-reduced sites. RPK = reads per kilobase. Mean signal intensities for two H3.3 and H3.Y replicates are shown. Statistical significance was determined using Wilcoxon signed rank test.

In conclusion, we could demonstrate that DAXX binding to H3.Y mutants enabled their deposition at H3K9me3 sites.

Summary

All in all, I demonstrated that H3.Y in contrast to H3.3, although sharing the same chaperone recognition site, was not able to bind DAXX. An H3.Y mutant that is identical to H3.3 in the core region failed to interact with DAXX. Only the H3.3-H3.Y chimera NY-3, which consists of an H3.Y N-terminal tail fused to H3.3, was able to stably bind DAXX. This suggests that the H3.3 N-terminus alone is dispensable, whereas a combination of residues in the core and the C-terminus are necessary for the interaction. Aiming for the identification of exact amino acid residues that determine DAXX binding, I dissected NY-3 into further mutants. These H3.Y mutants carry H3.3 residues in the core and in addition different substitutions in the C-

RESULTS

terminus. None of the new H3.Y constructs, including the supposed positive control H3.Y R53K core C3 was able to bind DAXX. H3.Y R53K core C3 shares all amino acids except three with NY-3, thus I further mutated these remaining residues singly or in combination. We finally identified H3.Y L46V R53K L62I core C3 as the mutant enabling strong DAXX binding. Apparently, for the stable interaction of H3.3 and DAXX, a defined combination of aa matters and only the H3.3 N-terminal tail is dispensable. The localization to PML-NBs, however, was achieved by several H3 variant constructs, suggesting a weak DAXX binding that is sufficient to for PML-NB localization. In Figure 36 DAXX binding ability and PML-NB localization of all mutants generated in this study are summarized.

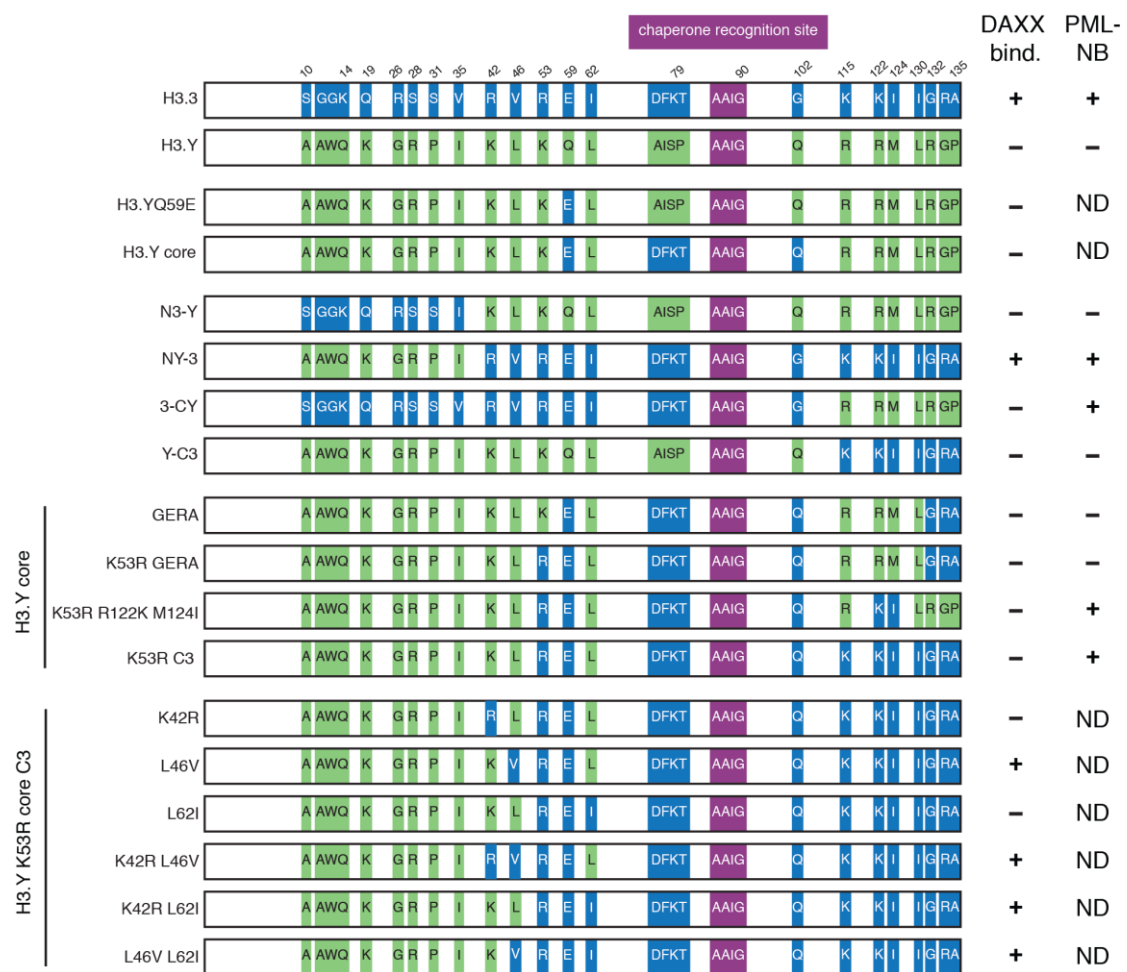


Figure 36: Alignment of H3.3, H3.Y and their mutants summarized with their binding ability towards DAXX and their localization to PML-NBs. Only the H3.3/H3.Y chimera NY-3 and H3.Y L46V R53K core C3 as well as H3.Y K42R L46V R53K core C3, H3.Y L46V L62I R53K core C3 and H3.Y K42R R53K L62I core C3 stably interact with DAXX. Details see Figure 20.

DAXX is the chaperone needed for deposition of H3.3 into heterochromatic sites, whereas HIRA is responsible for deposition into euchromatic sites. The fact that H3.Y only interacts

RESULTS

with HIRA was also reflected by its chromatin incorporation sites and its nucleosomal interactome. We have demonstrated by CHIP-seq analysis that H3.3 and H3.Y mainly localize to euchromatic H3K4me3-positive sites. However, a fraction of H3.3 was incorporated into so-called H3.Y-reduced sites, where no H3.Y was present. Instead, these sites were H3K9me3-positive and enriched with simple repeats.

In comparison to eGFP-H3.1, -H3.2 and -H3.3, eGFP-H3.Y associated with the transcription associated FACT complex and was depleted in heterochromatic factors like PRC1, HP1 proteins, and SUV39H. Accordingly, H3.Y revealed reduced levels of H3K9me3, again confirming the CHIP-seq results where H3.Y was absent from H3K9me3 sites.

Mutants that gained DAXX binding got incorporated into H3.Y-reduced H3K9me3-positive simple repeat sites, suggesting that H3 variant-DAXX interaction is necessary and sufficient for deposition into human heterochromatic sites.

4 DISCUSSION

H3.Y is a novel primate-specific H3 variant expressed mainly in testis and brain but also in ovary, breast or lung cancer tissues (218). It shares the highest similarity with H3.3, especially the so-called chaperone recognition site that is thought to determine the interaction with distinct chaperone complexes mediating the localization of H3 variants to diverse genomic loci. H3.3 gets deposited by two chaperone complexes, namely the HIRA complex and DAXX/ATRX (190, 191, 198, 222, 266-268). The HIRA complex is responsible for H3.3's localization to euchromatic sites, such as gene bodies of actively transcribed genes or promoters. In contrast, DAXX/ATRX promotes the deposition of H3.3 to heterochromatic sites, such as telomeres, periCEN or retrotransposons.

Generally, H3.Y localizes outside of DAPI dense regions as seen in super-resolution 3D-SIM microscopy (218). The combination of starvation and overgrowth stress leads to an increase in cells expressing H3.Y. Moreover, H3.Y has been implicated in the regulation of cell cycle genes since its depletion results in diminished cell growth and transcriptome analysis revealed deregulated expression of cell cycle-associated genes (218). Aiming to unravel H3.Y's functions, first the chaperone complexes responsible for its deposition were analyzed. To do so, the interactome of H3 variants including H3.Y was identified in the chromatin-free fraction by SILAC-MS of immunoprecipitated H3 variants and the interacting proteins. H3.3 and H3.Y are expected to interact with the same chaperone complexes due to their high sequence similarity. Surprisingly, the two variants seem to have differences in their binding partners. H3.Y only interacts with the HIRA complex but not DAXX/ATRX (Figure 6).

4.1 H3.Y ONLY INTERACTS WITH THE HIRA COMPLEX & LOCALIZES TO EUCHROMATIC SITES

In order to verify whether indeed only H3.3 but not H3.Y can pull down DAXX I started to immunoprecipitate eGFP-H3 variants from stably expressing HeLa Kyoto cells. Instead of MS I now performed immunoblotting using an anti-DAXX antibody (Figure 7). Indeed, I could verify the results obtained by MS and only observed an interaction between H3.3 and DAXX but not between H3.Y and DAXX.

Notably, DAXX exhibits a higher molecular weight when immunoprecipitated with H3.3. Thus, I was wondering whether DAXX modifications cause this shift and analyzed diverse reported DAXX PTMs. However, DAXX was neither sumoylated, ubiquitinated nor poly ADP-ribosylated (Figure 8). Analysis of the phosphorylation status of DAXX did not reveal a clear result due to technical problems. Phosphorylation of DAXX was already observed to have an impact on H3.3 loading in neurons (296). The authors observed a correlation between DAXX-dependent H3.3 deposition and the phosphorylation status of DAXX. However, in neurons H3.3 preferentially interacts with hypophosphorylated DAXX. Expressing a phosphomimetic version of DAXX (S669E) or a version that can not be phosphorylated in DAXX knockout cells (S669A) revealed that H3.3 loading is impaired in cells expressing the S669E mutant (296). The model suggests that upon neuronal activation, DAXX gets dephosphorylated and promotes H3.3 deposition and transcription of particular loci. Thus, DAXX function in H3.3 deposition seems indeed to be regulated by its phosphorylation status. It remains to be seen if this is a cell type-specific phenomenon or affects only a subclass of H3.3 deposition sites. Nonetheless, in HeLa Kyoto cells H3.3 immunoprecipitates DAXX of higher molecular weight, hence potentially hyperphosphorylated instead of hypophosphorylated DAXX. Notably, the distinct running behavior of DAXX can only be observed in the first immunoblots (Figure 7, 19 and 22) and is not present in further pulldowns. Although I can not exclude that DAXX is posttranslationally modified, my results show so far no evidence that a potential modification influences its function. Moreover, it could well be that technical influences like different charges of polyacrylamide gradient gels affect the running behavior of DAXX and are causing the observed shift.

The association of H3.Y with the HIRA complex, but not DAXX/ATRX is further confirmed by the absence of H3.Y in PML-NBs. This localization is DAXX-dependent and therefore the absence of H3.Y reflects the lacking interaction of DAXX and H3.Y. PML-NBs are thought to serve as a triage centers for a fraction of H3.3, where H3.3 and its chaperones “meet” to

DISCUSSION

form stable interactions before getting deposited into chromatin (272). Several chaperones, including ASF1A, HIRA, and ATRX are also found in PML-NBs arguing for a role as a meeting point for diverse chaperone complexes. Although - at least in HeLa cells - most of newly synthesized H3.3 associates with HIRA (191), a fraction of H3.3 might also be recruited to PML-NBs for further distribution to distinct chaperone complexes. Since H3.Y can interact with the HIRA complex, it is present in chromatin albeit absent from PML-NBs.

DAXX/ATRX is responsible for the deposition of H3.3 at heterochromatic simple repeat sites, characterized by the presence of H3K9me3 (175, 190, 197, 198, 268). HIRA complex mediated deposition sites are, in contrast, characterized by open chromatin (190, 191, 266), a state that is often defined by the presence of H3K4me3. In order to find out whether the lack of DAXX in H3.Y immunoprecipitates also determines its deposition sites I performed a ChIP-seq analysis of H3.3 and H3.Y together with Marek Bartkuhn from the University of Gießen. Both H3.3 and H3.Y are highly enriched at TSS, marked by H3K4me3. Moreover, they are enriched at exons, sites upstream of the TSS, TES and only mildly enriched on introns (Figure 10A). In contrast, H3.3 and H3.Y, as well as H3K4me3, are depleted in intergenic regions. This result is in contrast to ChIP-seq data from mESCs and MEFs where H3.3 was highly enriched in intergenic regions and introns (181, 190). It might well be that this difference is due to different organisms, differences in differentiation states, in experimental procedure or bioinformatic analysis. Nonetheless, H3.3 and H3.Y share the majority of peaks that overlap with H3K4me3 (Figure 10B) but are depleted in H3K9me3 (Figure 11) indicating that either the majority of H3.3 is incorporated by HIRA or our method reaches its technical limits at heterochromatic, often repetitive regions. All in all, our results are in agreement with previous data for H3.Y function. H3.Y is indeed located to euchromatic regions, confirming the finding obtained in high-resolution microscopy that depicted H3.Y outside of DAPI dense regions. Furthermore, depletion of H3.Y resulted overall in a higher number of downregulated genes, again supporting H3.Y's role in euchromatic regions like TSS, potentially promoting transcription. The unique H3.3-specific, H3.Y-depleted incorporation sites are characterized by the presence of H3K9me3 (Figure 11 and Figure 12). This enrichment is typical for DAXX/ATRX-dependent deposition sites (197, 198, 223) and further supports the absence of H3.Y from these regions. In mESCs DAXX/ATRX are responsible for the deposition of H3.3 into telomeres, pericentric heterochromatin, differentially methylated imprinted loci, and retroviral elements (198, 223, 224). Interestingly, here DAXX/ATRX are even required for the maintenance of H3K9me3.

DISCUSSION

Depletion of DAXX or ATRX results in the loss of H3K9me3 at differentially methylated regions, endogenous retroviral elements and telomeres (197, 223, 224). Two studies demonstrate that H3K9me3 is indeed directly dependent on H3.3 since its loss led to reduced H3K9me3 levels at telomeres and retroviral elements in mESCs (197, 198, 224).

Remarkably, our results indicate that HIRA-independent deposition of H3.3 happens exclusively at simple repeat sites, whereas in mouse cells H3.3 gets deposited to various repeat types. A recent study performing ChIP-seq with DAXX and ATRX antibodies in mESCs reported an enrichment of simple repeats (224). These data support our hypothesis that in human cells H3.3 enrichment at simple repeats is DAXX-dependent whereby H3.Y is absent from these sites. Generally, repeat sequences are often hypomethylated in cancer cells (317, 318). Since our studies are carried out in the cervical cancer cell line HeLa Kyoto this might also be true in our experiments. Low methylation levels of some simple repeats were even observed in human embryonic stem cells (319). In the case of DNA hypomethylation, Su et al. reported high levels of DAXX/ATRX and H3K9me3 to prevent aberrant transcription of repeats (319). DAXX might play a central role in targeting ATRX and SUV39H since DNA methyltransferase triple knockout cells showed loss of H3K9me3 at these sites when DAXX is depleted (224). It seems that low levels of DNA methylation coincide with high levels of DAXX/ATRX and H3K9me3 at respective repeat sites to ensure a silent state. It is tempting to speculate that also in humans the low methylation levels that were observed for some (simple) repeat types reflect sites of high DAXX occupancy and might thus be enriched with H3.3 and depleted in H3.Y.

It might well be that technical or experimental variation led to the enriched detection of H3.Y-depleted H3.3 deposition sites at simple repeat sites. However, it is still possible that this discrepancy is a biological feature stressing the difference between organisms (mouse and human) or their distinct development stages.

Interestingly, in human HeLa cells, DAXX depletion does not affect global H3.3 deposition (191) arguing again, that DAXX deposits H3.3 only to a limited number of sites in humans, supporting our data showing that the majority of H3.3 is incorporated by HIRA.

All in all, our data reveal that H3.Y is exclusively deposited by the HIRA complex. H3.3, on the other hand, gets deposited by both the HIRA complex and DAXX/ATRX leading to the localization of H3.3 but not H3.Y to simple repeat sites. If both H3.3 and H3.Y get deposited by the HIRA complex to the same euchromatic regions the presence of heterotypic nucleosomes consisting of both H3.3 and H3.Y should be observed. Indeed, immunoprecipitated mononucleosomes containing GFP-H3.Y also have H3.3 incorporated as

DISCUSSION

Figure 15D suggests. Furthermore, Kujirai et al. demonstrated that H3.3/H3.Y-containing heterotypic nucleosomes exist *in vitro* (219). These heterotypic nucleosomes also retained the characteristics of H3.Y nucleosomes. They were more responsive to MNase digestion and showed reduced H1 binding, suggesting that also these nucleosomes might be a part of open and relaxed chromatin.

4.2 H3.Y NUCLEOSOMES ARE ENRICHED IN TRANSCRIPTION-ASSOCIATED INTERACTION PARTNERS

In order to analyze the interactome of the distinct H3 variant associated interaction partners I performed MNase-IP-qMS. The applicability of our method was confirmed by the enrichment of the CAF1 complex on canonical H3.1 (Figure 15C, D). The immunoprecipitation and/or identification of CAF1A and CAF1B but not CAF1C has already been observed in a study focusing on the identification of the H3.2 interactome and is therefore not surprising (280). Obviously the CAF1 complex is not only responsible for the deposition of the canonical histones but remains also stably bound to chromatin. This was also noticed by Latreille et al.: the authors detected the p150 subunit of the CAF1 complex not only in the soluble nuclear fraction but also in the chromatin fraction (280). In the course of this, yeast CAF1 has been demonstrated to bind DNA (320, 321). Moreover, mouse and human CAF1A binds to DNA *in vitro* and mouse CAF1A localizes to DAPI dense foci in fibroblast cells supporting our result that CAF1 is not only a transient interactor but stays stably bound to mononucleosomes (320).

The PRC1 complex is enriched on H3.1 and H3.3 containing mononucleosomes. It comprises of four core subunits: polycomb group finger (PCGF), Polyhomeotic-like protein (PHC), E3 ubiquitin-protein ligase RING1 and chromobox protein (CBX) (322, 323). In humans all of these subunits exist in multiple homologs, enabling the existence of various PRC1 complexes with distinct subunit compositions. In fact, 180 different PRC1 complexes can occur in humans including canonical and non-canonical complexes that do not contain CBX and PHC (322). Although it seems unlikely, it is so far unclear whether all of these potential complexes exist and what functions these distinct complexes fulfill. However, it is speculated that different PCGF homologs define different PRC1 complexes in humans. Gao et al. observed six major PRC1 complexes, all of them containing distinct PCGF homologs but with

DISCUSSION

only PGC4 (BMI1) and PCGF2 (MEL18) giving rise to canonical complexes that contain CBX and PHC (324). These six major complexes can in turn associate with various other proteins, making the PRC1 composition even more complex. In our results, only BMI1 is detected indicating the presence of one canonical PRC1 complex (Figure 15D, E and Figure 16A). Indeed, the E3 ubiquitin ligases RNF2 and RING1, PHC2 and 3 and CBX8 are identified, giving rise to a canonical PRC1 complex consisting of all core members. Interestingly, RNF2 has only been shown to bind H3K27me3 whereas all other detected proteins are known to bind H3K27me3 as well as H3K9me3 (325). Conversely, CBX1, 3 and 5, that bind H3K9me3 (310, 311), are enriched on eGFP-H3.1- or -H3.3-containing mononucleosomes, respectively (Figure 15D, E and Figure 16A). Moreover, SUV39H1 and 2 are enriched on H3.1- and H3.3-containing mononucleosomes (Figure 15D, E and Figure 16A) connecting the presence of H3K9me3 and CBX proteins on H3.1 and H3.3.

H3.Y's presence in open euchromatic regions is further confirmed by the enrichment of the FACT complex on H3.Y-containing mononucleosomes (Figure 15D, E and Figure 16A). The FACT complex is involved in nucleosome reorganization during transcription, DNA repair, and replication (326). As the name implies it facilitates transcription by disrupting nucleosomes, thereby generating an accessible DNA template for RNA polymerase II. Moreover, it promotes nucleosome recovery following transcription. Hence, the presence of FACT indicates active transcription and H3.Y's implication in transcription. Whereas the HIRA complex may be responsible for the deposition of newly synthesized H3.Y into euchromatic sites, the FACT complex might deposit H3.Y to regions of active transcription where nucleosomes are displaced. FACT is a rather promiscuous chaperone since it is also involved in the deposition of CENP-A, it binds H3-H4 tetramers and H2A-H2B dimers arguing that it could also bind H3.Y (233, 327).

H3.Y's euchromatic distribution is further stressed by the absence of heterochromatin-associated proteins SUV39H1 and 2. SUV39H is responsible for the trimethylation of H3K9 (308, 309), a PTM that marks chromatin repression at the telomeres and pericEN. Depletion of both genes, *Suvar39h1* and *Suvar39h2*, results in diminished H3K9me3 levels and elevated transcription (197). DAXX and ATRX were reported to interact with SUV39H, underlining the association of DAXX/ATRX and heterochromatin (197, 224). Thus, the absence of SUV39H and the reduced levels of H3K9me3 on eGFP-H3.Y-containing immunoprecipitated mononucleosomes (Figure 15D,E and Figure 16B) support our view on H3.Y as a marker for open euchromatin. Moreover, I observed H3K9me3 on the fraction of H3.3 that is reduced in H3.Y (Figure 11 and Figure 12).

DISCUSSION

Furthermore, I observed an enrichment of various subunits of distinct remodeling complexes on H3.Y-containing mononucleosomes (Figure 15D, E). CHD1 is a remodeler associated with open, transcriptionally active chromatin and has accordingly been reported to bind H3K4me3 (328, 329). It localizes to the 5' end of actively transcribed genes and might there function in the disassembly of nucleosomes (329). Moreover, CHD1 seems to be a potential candidate for the deposition of H3.3 at actively transcribed regions (330). Apart from CHD1 also bromodomain plant homeodomain (PHD) finger transcription factor (BPTF) has been demonstrated to bind H3K4me3. BPTF is the largest and histone-binding subunit of the NURF complex that is generally associated with transcriptional activation (331, 332). Chromatin accessibility complex 1 (CHRAC1) was also enriched on H3.Y-containing mononucleosomes. CHRAC1 can directly bind ATP-dependent chromatin assembly factor1 (ACF1) and builds together with CHRAC17 and the ATPase subunit SNF2H the CHRAC complex (333). CHRAC has been shown to enhance nucleosome sliding and assembly (333). Moreover, the remodeling and spacing factor 1 (RSF1) has been detected as an interaction partner of H3.Y-mononucleosomes. It is part of the RSF complex that consists of the ATPase SNF2H and the accessory protein RSF1 (334). Recent studies revealed RSF1's function in the DSB repair. RSF1 is necessary for both repair pathways, in non-homologous end joining as well as in homologous recombination (335).

In line with H3.Y's proposed function in euchromatin transformation/transcription associated protein (TRRAP) was identified on H3.Y-containing mononucleosomes (Figure 15E). TRRAP is part of various histone acetyltransferase complexes and was suggested to be responsible for the recruitment of HATs to promoters by binding to the respective TF (336, 337). As mentioned in 1.2.1 acetylation is generally associated with transcriptionally active chromatin, thereby the presence of TRRAP on H3.Y mononucleosomes links again H3.Y to transcription. Interestingly, TRRAP is also part of an SWI2/SNF2 remodeling complex the so-called p400 complex, characterized by the E1A binding protein p400 (EP400) that harbors ATPase activity (338, 339). P400 is responsible for the deposition of H2A.Z and has recently been identified to also co-deposit H3.3 into enhancer and promoter regions of active genes (339). Its depletion resulted in diminished levels of H3.3 and H2A.Z deposition and reduced transcription levels. Since others (219) and I already speculated about the existence of heterotypic H3.3/H3.Y nucleosomes it could well be that TRRAP together with p400 deposits H3.3 to active sites where H3.Y is present. Its enrichment on H3.Y nucleosomes versus H3.3-containing nucleosomes highlights H3.Y's sole localization to euchromatin whereas H3.3 is also found in heterochromatin where TRRAP does not play a role. Interestingly, albeit the

DISCUSSION

accessory subunits of remodeling complexes were enriched on H3.Y nucleosomes, the ATPase subunits SNF2H and EP400 did not appear as enriched proteins. They could actually be detected but are not enriched on H3.Y nucleosomes. It might be possible that the catalytically active subunits were more equally distributed between H3.1 or H3.3 and H3.Y. Indeed, the ATPase subunits are common to different complexes and solely the composition of different accessory subunits gives rise to distinct subcomplexes thereby enhancing or shaping their function (340-343). It is tempting to speculate that H3.Y's localization to transcriptionally active regions requires the presence of diverse chromatin remodeling complexes since these are sites of high nucleosome turnover.

Noticeably, apart from remodeling complexes the SET (Su(var)3-9, Enhancer of Zeste, Trithorax) domain containing methyltransferases mixed-lineage leukemia 3 (MLL3) and SETD1A (SET domain containing 1A) are enriched on H3.Y-containing mononucleosomes. Both proteins are implicated in H3K4 methylation (344, 345). Whereas MLL3 is responsible for the monomethylation at enhancers, SETD1A promotes H3K4 di- and trimethylation at the TSS of active promoters (90, 346, 347). Thus, both proteins are implicated in euchromatic regions, supporting H3.Y's role in open H3K4me3 marked chromatin (see also Figure 10).

The absence of HIRA complex members on mononucleosomes was surprising since HIRA has been shown to be able to bind free DNA. However, the data are in agreement with a previous study reporting that HIRA, in contrast to DAXX, is not a stable interaction partner of H3.3 (268).

DAXX' presence on H3.Y-containing mononucleosomes might at first glance be surprising. However new ChIP-seq studies in mESCs revealed that only a fraction of DAXX associates with ATRX. Both proteins are co-enriched at repetitive elements, arguing for a role in H3.3 deposition at these sites as we and others demonstrated (Figure 13 and (197, 198, 222)). Yet, 66% of DAXX peaks are not overlapping with ATRX, demonstrating DAXX functions apart from H3.3 deposition. Notably, DAXX independently localizes preferentially to promoter regions (224). Additionally, DAXX has been shown to bind TFs, again indicating a distinct role apart from H3.3 deposition for DAXX in euchromatin explaining its appearance on H3.Y mononucleosomes (296).

Figure 37 summarizes the interaction partners of the different H3 variants in the chromatin-free fraction and on chromatin as well as the chromatin features that determine the distinct deposition sites in the genome.

DISCUSSION

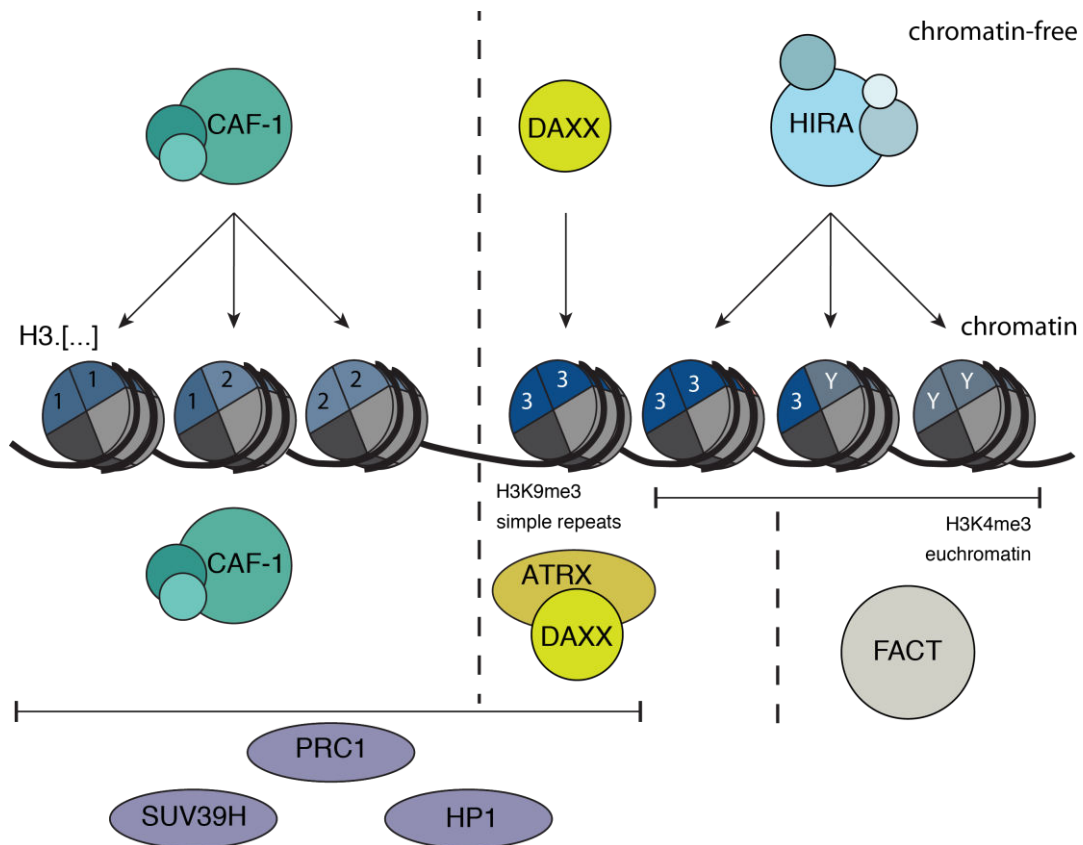


Figure 37: Interactome of human H3 variants and chromatin features of the respective H3 variant deposition sites. The canonical variants H3.1 and H3.2 get deposited by the CAF1 complex, that stays stably associated on chromatin. H3.3 gets deposited by two distinct chaperone complexes: DAXX/ATRX that determines H3.3's localization to H3K9me3-positive and simple repeat-enriched sites and the HIRA complex. H3.Y gets deposited only by the HIRA complex that is responsible for its deposition to euchromatic, H3K4me3-positive sites. On chromatin the heterochromatic factors SUV39H, PRC1 and HP1 are enriched on canonical and H3.3-containing nucleosomes, whereas H3.Y-containing nucleosomes are enriched in the transcription-associated FACT complex.

4.3 A COMBINATION OF CORE & C-TERMINAL H3.3 RESIDUES DETERMINES DAXX INTERACTION

Strikingly, although H3.3 and H3.Y share the same chaperone recognition site (aa 87-90) they show distinct associations with chaperone remodeling complexes. So far, studies focused on the difference between the chaperone recognition sites of canonical H3 variants and H3.3. Displacing single residues in the stretch ranging from aa 87 to aa 90 was sufficient to lose DAXX binding partially (247). Especially G90 seems to play a crucial role in DAXX binding. Yet, in H3.Y aa 87-90 are identical to H3.3 raising the question which residues in

DISCUSSION

H3.Y prevent DAXX binding. Overall, H3.Y and H3.3 differ in 26 aa. Thus, H3.Y represents an endogenous H3.3 “mutant” allowing the analysis of DAXX interaction prerequisites. Noticeably, all our established mutants show stable chromatin association, arguing that H3.3-H3.Y hybrids form stable nucleosomes than can be incorporated into chromatin (Figures 17, 18, 21, 24, 28, 32).

Although H3.3E59 participates in a hydrogen network that is crucial for DAXX interaction, I could show that this residue alone is not sufficient for DAXX interaction (Figure 19). Likewise, the replacement of the whole aa stretch from aa 77-80 and the exchange of H3.YQ102 with the respective glutamine in the H3.Y Q59E mutant background (H3.Y core, see Figure 20) did not result in H3.Y-DAXX interaction (Figure 22). The structure of the HBD of DAXX revealed also the importance of the α N helix for the interaction: a reported H3.3 Δ N mutant, that lacks aa 1-60 abrogated DAXX binding (247). In contrast, an H3.3 mutant with a deletion from aa 1-43 still immunoprecipitated DAXX, arguing that aa 44-60 are critical but the H3.3 N-terminus is dispensable for DAXX interaction (247). Accordingly, the swap mutants with either exchanged N- or C-termini (see Figure 23) supported this observation. Solely NY-3, a mutant of H3.3 that carries the H3.Y N-terminus is able to interact with DAXX (Figure 25). Once more the results revealed that the H3.3 tail is dispensable for DAXX binding. Moreover, our data are in agreement with a hydrogen/deuterium exchange mass spectrometry (H/DX-MS) study that highlighted the importance of C-terminal residues for a stable H3.3-DAXX complex formation (271). H3.3D105, R116, R122 and R128 are contacting DAXX residues and might be crucial for DAXX binding (Figure 38).

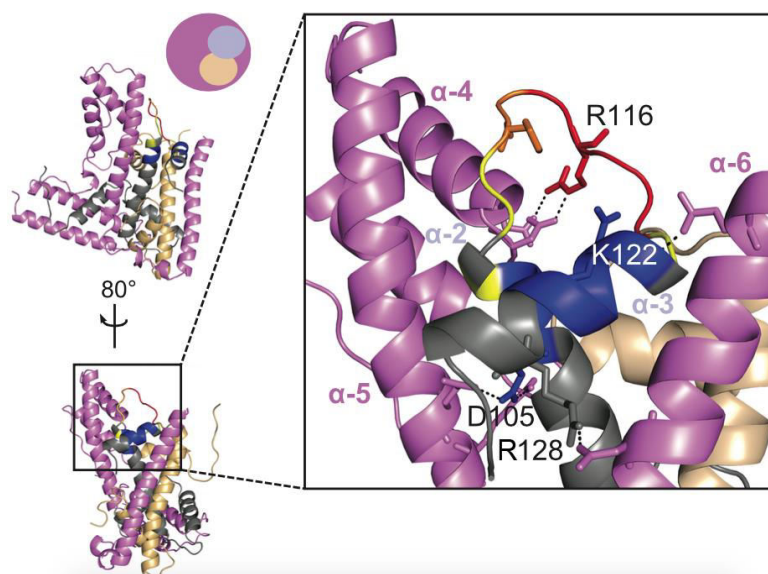


Figure 38: H3.3 C-terminal residues might be necessary for DAXX interaction. The HBD domain of DAXX is depicted together with an H3.3-H4 dimer. H3.3 D105, R116, K122 and R128 are directly

DISCUSSION

binding DAXX. H3.3 is shown in blue, crucial residues that are directly contacting DAXX in gray, H4 in beige and DAXX in magenta. Adapted and reprinted with permission from Oxford Journals (271).

DeNizio et al. observed a coupled binding-folding mechanism of DAXX and its substrate H3.3-H4 (271). Initially, both DAXX and H3.3-H4 are in an unfolded state. After DAXX builds first contacts to the H3.3 chaperone recognition site, it scans the remaining part of H3.3 and a stable heterotrimeric complex forms. Since this new study illustrated the importance of the C-terminus and I could show that the H3.3 N-terminus is not necessary for DAXX binding I focused on H3.Y's C-terminal residues to establish new H3.Y mutants in the background of H3.Y core. One exchanged residue, H3.3R53, is in close proximity to H3.3K56, a residue shown to be posttranslationally modified (96, 109, 315). In *S. cerevisiae* H3K56 acetylation is important for the increased affinity of the H3 chaperone Rtt106 for H3 (316). Since DAXX has a Rtt106-like domain (267, 348) I speculated whether this modification might also be important for DAXX affinity. However, meanwhile it became clear that H3K56ac is only present on 1% of newly synthesized H3 and therefore not a predeposition mark in humans (349). Additionally, as mentioned earlier, H3.3K122 was demonstrated to directly contact DAXX and might therefore be necessary for DAXX recognition. The closeness of M124 to K122 prompted me to also exchange this residue. Interestingly, H3.YM124 was identified as the aa that contributes to H3.Y's stable association in the nucleosome (350). Replacing M124 by isoleucine reduced the stability of the nucleosome. However, I could not detect any differences in nucleosome incorporation (Figure 28). Finally, as a supposed positive control, H3.Y K53R core C3 was established. This H3.Y mutant highly resembled NY-3, the swap mutant that was able to immunoprecipitate DAXX, with only 3 differences at position 42, 46 and 62 (Figure 27). Surprisingly, none of these mutants including the putative positive control H3.Y K53R core C3 was able to interact with DAXX (Figure 29). Although the substitutions at position 42, 46 and 62 from lysine to arginine or from leucine to valine or isoleucine, respectively, are conserved and happen within one group of amino acids (charged aa in the case of lysine and arginine and hydrophobic aa in the case of leucine, isoleucine, and valine) they are sufficient to prevent DAXX binding to H3.Y. Figure 39 illustrates the location of H3.3R42, V46 and I62 in the DAXX-H3.3-H4 crystal structure.

DISCUSSION

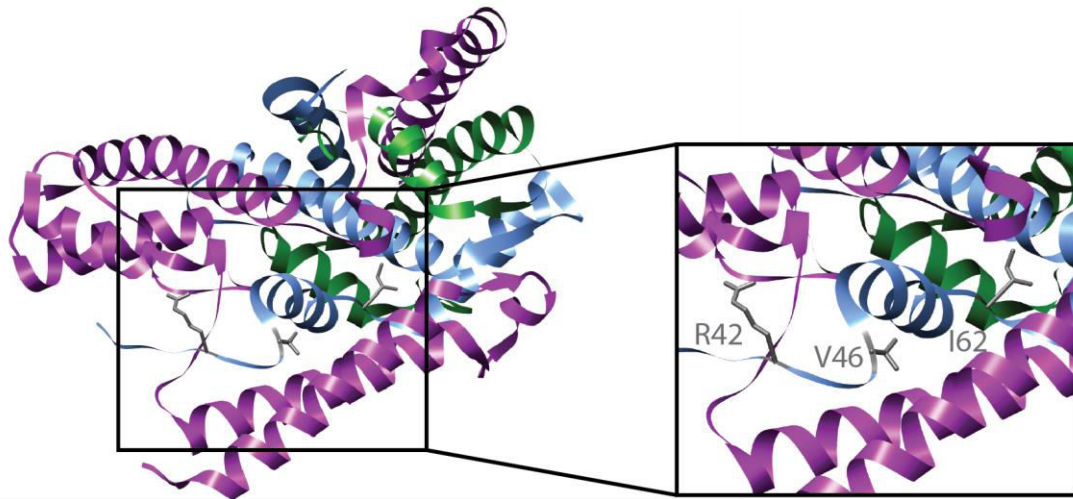


Figure 39: HBD of DAXX together with an H3.3-H4 dimer illustrating the position of R42, V46 and I62 in H3.3. DAXX HBD is depicted in purple, H4 in green and H3.3 in blue. Highlighted in gray are the remaining H3.3 residues that distinguish NY-3 and H3.Y R53K core C3. Crystal structure downloaded and adapted from UCSF Chimera (PDB no. 4H9N).

Two scenarios seem possible. First, one or a combination of the residues 42, 46 and 62 in H3.3 are necessary for H3.3 recognition by DAXX, meaning H3.Y R53K core C3 is not recognized as a substrate. DeNizio et al. suggested a model whereby unfolded DAXX and H3.3-H4 couple their own folding to the mutual binding (271). This binding happens in a stepwise manner with initial contacts being formed at the chaperone recognition site followed by DAXX sampling the remaining H3.3 residues. Thus, if the remaining H3.Y residues are not recognized by DAXX during the “scanning” of H3.Y R53K core C3, this mutant is not able to bind DAXX. In a second scenario, the H3.Y residues could prevent a stable complex formation of DAXX-H3.Y R53K core C3-H4. It was shown that also the non-optimal DAXX substrate H3.2-H4 can bind DAXX, however, the complex does not achieve a stable conformation (247, 271). It might be possible that H3.YK42, L46 and/or L62 as well prevent the formation of a stable complex thereby hindering DAXX immunoprecipitation. To investigate whether the exchange of a single aa or the combination of all three of the remaining ones allows DAXX binding I further mutated the remaining residues that distinguish H3.Y R53K core C3 from NY-3 singly or in combinations (Figure 31). Noticeably, H3.YL46 seems to prevent DAXX recognition and/or binding. Replacing L46 in H3.Y R53K core C3 is sufficient to gain back DAXX binding, albeit not to H3.3 levels (Figure 33). Lysine 42 and leucine 62 have only mild effects on DAXX interaction, even though H3.Y L46V R53K L62I core C3 reveals DAXX binding comparable to H3.3 levels. In summary, H3.Y L46V appears to have the biggest impact on the interaction of H3.Y and DAXX, and a combination of H3.3 C-terminal and core residues seems to be necessary for H3.Y-DAXX interaction.

DISCUSSION

Interestingly, PML-NB localization revealed other prerequisites in H3.Y sequence. Although PML-NB localization is dependent on DAXX interaction also the mutants 3-CY, H3.Y R53K core R122K M124I and H3.Y R53K core C3 that did not immunoprecipitate DAXX were detected in PML-NBs (Figure 36). It might be possible that the localization of these mutant proteins to PML-NBs happens DAXX independent or that only a transient interaction between DAXX and the respective mutants occurs and is sufficient to determine their localization to these nuclear structures. This transient binding, however, would not be sufficient to immunoprecipitate DAXX explaining its absence in immunoblots.

Noticeably, it seems unlikely that DAXX is not responsible for PML-NB localization since 3-CY is mildly enriched at H3.Y-reduced sites in chromatin (Figure 35). This enrichment is most likely DAXX dependent and the transient interaction can account for the presence of 3-CY at some but not all H3.Y-reduced sites. Considering DeNizio et al.'s model (271) it seems likely that 3-CY can indeed transiently bind DAXX (such as H3.2-DAXX), however a stable complex is not formed. This transient binding is demonstrated by the localization at some DAXX-dependent genomic sites and at PML-NBs. In contrast, both NY-3, as well as H3.Y L46V R53K L62I core C3, can be found at the same genomic sites like H3.3 including H3.Y-reduced sites, arguing again that these mutants are able to interact with DAXX.

In the future it would be interesting to analyze the identified residues responsible for DAXX interaction also in H3.3. So far all studies focused on the importance of the chaperone recognition site, but clearly this aa stretch is not sufficient to determine DAXX binding. Thus, which residues would inhibit DAXX-H3.3-H4 complex formation? Are even single residues sufficient to prevent H3.3-DAXX interaction? Can, therefore, a hierarchy of importance of H3.3 aa for DAXX recognition/binding be established? Although it seems like single aa substitutions of H3.Y can not establish DAXX interaction, it could well be that the binding to H3.3 is disrupted more easily. Knowing the responsible residues in H3.3, it could be used to mutate these aa in the endogenous background via CRISPR. This way an endogenous H3.3 mutant is generated that is able to interact with the HIRA complex but not DAXX/ATRX. Although the H3.3 knockout mouse indicated its importance in heterochromatin formation and genome stability, the effect of H3.3 loss on transcription is not clear. So far only general H3.3 depletions could be analyzed, however, by uncoupling HIRA-mediated deposition from DAXX-mediated deposition the implications on different sites and functions in the genome can be studied. Since DAXX has additional functions apart from H3.3 deposition, effects of its

DISCUSSION

depletion can not only be ascribed to the loss of DAXX in H3.3 deposition. Additionally, loss of DAXX mediated deposition can be studied in various cell types. Whereas in mESCs DAXX is responsible for the deposition at various heterochromatic sites like telomeres, periCEN or endogenous retroviral elements, in humans we only detected DAXX-dependent H3.3 deposition into simple repeat sites. It would be interesting to see whether loss of H3.3 in human simple repeat sites also affects genome stability. Thus by analyzing H3.3's roles in heterochromatin of human cells like HeLa Kyoto or in mouse cells like mESCs we could gain further insights into H3.3 function in distinct cell types or organisms. Moreover, by further differentiating mESCs one could investigate the role of H3.3 in DAXX-dependent sites in development.

Apart from shared H3.3/H3.Y sites H3.Y also localizes to some few H3.3-independent sites where only H3.Y can be detected. It is tempting to speculate that new chaperone complexes mediate this deposition, independent from H3.3. Although we did not detect any known chaperone complexes in our SILAC approach, it could be possible that proteins with other known functions take over this task. It could as well be that additional factors associate with the HIRA complex and thus mediate the deposition of H3.Y. Recently, RPA has been identified to be involved in HIRA-mediated H3.3 deposition to regulatory genomic sites. This protein has initially been implicated in DNA replication and repair and is known to bind ssDNA. Hence it does not seem unlikely that H3.Y binders will be identified as new members of chaperone complexes that regulate the deposition of H3.Y.

I now gained some insights about H3.Y's function. However, the usage of HK cells as a model system has its limitations since these cells do not express endogenous H3.Y. Thus it would be interesting to also investigate endogenous H3.Y protein in other cell types. Recently, all attempts to identify in detail those cell types in the human brain that express H3.Y failed. In the meanwhile, new techniques developed that might be able to help to identify H3.Y expressing cell types or brain regions in human brain sections. Imaging MS (IMS) allows the identification of proteins by MS while sustaining the spatial information that a tissue section provides (351, 352). Potential crossreactions of the antibody are inapplicable. Moreover, the trigger causing enhanced H3.Y abundance after stress stimuli in U2OS cells is not known. Stressing U2OS cells and performing IMS might also enable the characterization of other proteins that increase their expression after stress and thus could be implicated in triggering H3.Y expression.

DISCUSSION

Furthermore, it would be interesting to investigate the H3.Y expression pattern in cancer patients. Unlike H3.3, no mutation in H3.Y is known that is associated with cancer. However, several cancer tissues displayed H3.Y expression in contrast to their healthy counterparts as analyzed by quantitative PCR (218). It is tempting to speculate that cancer patients reveal altered H3.Y levels in their cancer tissues that might cause alterations in the transcriptome and thus be implicated in cancer progression.

In conclusion I could show that H3.Y interacts with the H3.3-specific chaperone HIRA and is deposited to euchromatic H3K4me3-positive, H3K9me3-depleted genomic regions. It can however not interact with the second H3.3-specific chaperone DAXX, explaining its absence from heterochromatic H3K9me3-enriched simple repeat sites. Accordingly, immunoprecipitations of mononucleosomes followed by MS revealed the association of mainly euchromatic factors on H3.Y and concurrently the depletion of heterochromatic factors like SUV39H. Furthermore, I could demonstrate that a combination of H3.Y C-terminal and core residues prevents stable H3.Y-DAXX complex formation. In contrast, a transient interaction between H3.Y mutants and DAXX is sufficient to allow localization to PML-NBs and some DAXX-dependent H3K9me3-positive simple repeat sites.

REFERENCES

1. Solter D, Aronson J, Gilbert SF, McGrath J. Nuclear transfer in mouse embryos: activation of the embryonic genome. *Cold Spring Harbor symposia on quantitative biology*. 1985;50:45-50.
2. Cattanach BM, Kirk M. Differential activity of maternally and paternally derived chromosome regions in mice. *Nature*. 1985;315(6019):496-8.
3. Barton SC, Surani MA, Norris ML. Role of paternal and maternal genomes in mouse development. *Nature*. 1984;311(5984):374-6.
4. Surani MA, Barton SC, Norris ML. Development of reconstituted mouse eggs suggests imprinting of the genome during gametogenesis. *Nature*. 1984;308(5959):548-50.
5. McGrath J, Solter D. Completion of mouse embryogenesis requires both the maternal and paternal genomes. *Cell*. 1984;37(1):179-83.
6. Venter JC, Adams MD, Myers EW, Li PW, Mural RJ, Sutton GG, et al. The sequence of the human genome. *Science*. 2001;291(5507):1304-51.
7. Lander ES, Linton LM, Birren B, Nusbaum C, Zody MC, Baldwin J, et al. Initial sequencing and analysis of the human genome. *Nature*. 2001;409(6822):860-921.
8. Kornberg RD. Chromatin structure: a repeating unit of histones and DNA. *Science*. 1974;184(4139):868-71.
9. Oudet P, Gross-Bellard M, Chambon P. Electron microscopic and biochemical evidence that chromatin structure is a repeating unit. *Cell*. 1975;4(4):281-300.
10. Luger K, Mader AW, Richmond RK, Sargent DF, Richmond TJ. Crystal structure of the nucleosome core particle at 2.8 Å resolution. *Nature*. 1997;389(6648):251-60.
11. Davey CA, Sargent DF, Luger K, Maeder AW, Richmond TJ. Solvent mediated interactions in the structure of the nucleosome core particle at 1.9 Å resolution. *J Mol Biol*. 2002;319(5):1097-113.
12. Andrews AJ, Luger K. Nucleosome structure(s) and stability: variations on a theme. *Annu Rev Biophys*. 2011;40:99-117.
13. Luger K, Dechassa ML, Tremethick DJ. New insights into nucleosome and chromatin structure: an ordered state or a disordered affair? *Nat Rev Mol Cell Biol*. 2012;13(7):436-47.
14. Friedman N, Rando OJ. Epigenomics and the structure of the living genome. *Genome Res*. 2015;25(10):1482-90.
15. Zhu P, Li G. Structural insights of nucleosome and the 30-nm chromatin fiber. *Curr Opin Struct Biol*. 2016;36:106-15.
16. Li G, Reinberg D. Chromatin higher-order structures and gene regulation. *Current opinion in genetics & development*. 2011;21(2):175-86.
17. Risca VI, Greenleaf WJ. Unraveling the 3D genome: genomics tools for multiscale exploration. *Trends in genetics : TIG*. 2015;31(7):357-72.
18. Robinson PJ, Rhodes D. Structure of the '30 nm' chromatin fibre: a key role for the linker histone. *Curr Opin Struct Biol*. 2006;16(3):336-43.
19. McGhee JD, Rau DC, Charney E, Felsenfeld G. Orientation of the nucleosome within the higher order structure of chromatin. *Cell*. 1980;22(1 Pt 1):87-96.
20. Finch JT, Klug A. Solenoidal model for superstructure in chromatin. *Proceedings of the National Academy of Sciences of the United States of America*. 1976;73(6):1897-901.

REFERENCES

21. Dorigo B, Schalch T, Kulangara A, Duda S, Schroeder RR, Richmond TJ. Nucleosome arrays reveal the two-start organization of the chromatin fiber. *Science*. 2004;306(5701):1571-3.
22. Schalch T, Duda S, Sargent DF, Richmond TJ. X-ray structure of a tetranucleosome and its implications for the chromatin fibre. *Nature*. 2005;436(7047):138-41.
23. Quenet D, McNally JG, Dalal Y. Through thick and thin: the conundrum of chromatin fibre folding in vivo. *EMBO reports*. 2012;13(11):943-4.
24. Maeshima K, Hihara S, Eltsov M. Chromatin structure: does the 30-nm fibre exist in vivo? *Current opinion in cell biology*. 2010;22(3):291-7.
25. Eltsov M, Maclellan KM, Maeshima K, Frangakis AS, Dubochet J. Analysis of cryo-electron microscopy images does not support the existence of 30-nm chromatin fibers in mitotic chromosomes in situ. *Proceedings of the National Academy of Sciences of the United States of America*. 2008;105(50):19732-7.
26. Nishino Y, Eltsov M, Joti Y, Ito K, Takata H, Takahashi Y, et al. Human mitotic chromosomes consist predominantly of irregularly folded nucleosome fibres without a 30-nm chromatin structure. *The EMBO journal*. 2012;31(7):1644-53.
27. Fussner E, Ching RW, Bazett-Jones DP. Living without 30nm chromatin fibers. *Trends in biochemical sciences*. 2011;36(1):1-6.
28. Routh A, Sandin S, Rhodes D. Nucleosome repeat length and linker histone stoichiometry determine chromatin fiber structure. *Proceedings of the National Academy of Sciences of the United States of America*. 2008;105(26):8872-7.
29. Depken M, Schiessel H. Nucleosome shape dictates chromatin fiber structure. *Biophysical journal*. 2009;96(3):777-84.
30. Wong H, Victor JM, Mozziconacci J. An all-atom model of the chromatin fiber containing linker histones reveals a versatile structure tuned by the nucleosomal repeat length. *PLoS one*. 2007;2(9):e877.
31. Grigoryev SA, Arya G, Correll S, Woodcock CL, Schlick T. Evidence for heteromorphic chromatin fibers from analysis of nucleosome interactions. *Proceedings of the National Academy of Sciences of the United States of America*. 2009;106(32):13317-22.
32. Maeshima K, Imai R, Tamura S, Nozaki T. Chromatin as dynamic 10-nm fibers. *Chromosoma*. 2014;123(3):225-37.
33. Lieberman-Aiden E, van Berkum NL, Williams L, Imae M, Rogoyan A, Telling A, et al. Comprehensive mapping of long-range interactions reveals folding principles of the human genome. *Science*. 2009;326(5950):289-93.
34. Allis CD, Jenuwein T. The molecular hallmarks of epigenetic control. *Nature reviews Genetics*. 2016;17(8):487-500.
35. Trojer P, Reinberg D. Facultative heterochromatin: is there a distinctive molecular signature? *Molecular cell*. 2007;28(1):1-13.
36. Becker PB, Workman JL. Nucleosome remodeling and epigenetics. *Cold Spring Harbor perspectives in biology*. 2013;5(9).
37. Venkatesh S, Workman JL. Histone exchange, chromatin structure and the regulation of transcription. *Nat Rev Mol Cell Biol*. 2015;16(3):178-89.
38. Talbert PB, Henikoff S. Histone variants on the move: substrates for chromatin dynamics. *Nat Rev Mol Cell Biol*. 2017;18(2):115-26.

REFERENCES

39. Langst G, Manelyte L. Chromatin Remodelers: From Function to Dysfunction. *Genes*. 2015;6(2):299-324.
40. Lawrence M, Daujat S, Schneider R. Lateral Thinking: How Histone Modifications Regulate Gene Expression. *Trends in genetics : TIG*. 2016;32(1):42-56.
41. Avvakumov N, Nourani A, Cote J. Histone chaperones: modulators of chromatin marks. *Molecular cell*. 2011;41(5):502-14.
42. Eitoku M, Sato L, Senda T, Horikoshi M. Histone chaperones: 30 years from isolation to elucidation of the mechanisms of nucleosome assembly and disassembly. *Cellular and molecular life sciences : CMLS*. 2008;65(3):414-44.
43. Elsassner SJ, D'Arcy S. Towards a mechanism for histone chaperones. *Biochimica et biophysica acta*. 2013;1819(3-4):211-21.
44. Gurard-Levin ZA, Quivy JP, Almouzni G. Histone chaperones: assisting histone traffic and nucleosome dynamics. *Annual review of biochemistry*. 2014;83:487-517.
45. Hammond CM, Stromme CB, Huang H, Patel DJ, Groth A. Histone chaperone networks shaping chromatin function. *Nat Rev Mol Cell Biol*. 2017;18(3):141-58.
46. Mattioli F, D'Arcy S, Luger K. The right place at the right time: chaperoning core histone variants. *EMBO reports*. 2015;16(11):1454-66.
47. Bohmdorfer G, Wierzbicki AT. Control of Chromatin Structure by Long Noncoding RNA. *Trends in cell biology*. 2015;25(10):623-32.
48. Tirado-Magallanes R, Rebbani K, Lim R, Pradhan S, Benoukraf T. Whole genome DNA methylation: beyond genes silencing. *Oncotarget*. 2017;8(3):5629-37.
49. Bahar Halpern K, Vana T, Walker MD. Paradoxical role of DNA methylation in activation of FoxA2 gene expression during endoderm development. *The Journal of biological chemistry*. 2014;289(34):23882-92.
50. Yang X, Han H, De Carvalho DD, Lay FD, Jones PA, Liang G. Gene body methylation can alter gene expression and is a therapeutic target in cancer. *Cancer cell*. 2014;26(4):577-90.
51. Hu S, Wan J, Su Y, Song Q, Zeng Y, Nguyen HN, et al. DNA methylation presents distinct binding sites for human transcription factors. *eLife*. 2013;2:e00726.
52. Chodavarapu RK, Feng S, Bernatavichute YV, Chen PY, Stroud H, Yu Y, et al. Relationship between nucleosome positioning and DNA methylation. *Nature*. 2010;466(7304):388-92.
53. Jimenez-Useche I, Nurse NP, Tian Y, Kansara BS, Shim D, Yuan C. DNA methylation effects on tetra-nucleosome compaction and aggregation. *Biophysical journal*. 2014;107(7):1629-36.
54. Lev Maor G, Yearim A, Ast G. The alternative role of DNA methylation in splicing regulation. *Trends in genetics : TIG*. 2015;31(5):274-80.
55. Law JA, Jacobsen SE. Establishing, maintaining and modifying DNA methylation patterns in plants and animals. *Nature reviews Genetics*. 2010;11(3):204-20.
56. Smith ZD, Meissner A. DNA methylation: roles in mammalian development. *Nature reviews Genetics*. 2013;14(3):204-20.
57. Gopalakrishnan S, Sullivan BA, Trazzi S, Della Valle G, Robertson KD. DNMT3B interacts with constitutive centromere protein CENP-C to modulate DNA methylation and the histone code at centromeric regions. *Human molecular genetics*. 2009;18(17):3178-93.

REFERENCES

58. Breiling A, Lyko F. Epigenetic regulatory functions of DNA modifications: 5-methylcytosine and beyond. *Epigenetics & chromatin*. 2015;8:24.
59. Jeschke J, Collignon E, Fuks F. Portraits of TET-mediated DNA hydroxymethylation in cancer. *Current opinion in genetics & development*. 2016;36:16-26.
60. Raiber EA, Murat P, Chirgadze DY, Beraldi D, Luisi BF, Balasubramanian S. 5-Formylcytosine alters the structure of the DNA double helix. *Nature structural & molecular biology*. 2015;22(1):44-9.
61. Song CX, Szulwach KE, Dai Q, Fu Y, Mao SQ, Lin L, et al. Genome-wide profiling of 5-formylcytosine reveals its roles in epigenetic priming. *Cell*. 2013;153(3):678-91.
62. Wang L, Zhou Y, Xu L, Xiao R, Lu X, Chen L, et al. Molecular basis for 5-carboxycytosine recognition by RNA polymerase II elongation complex. *Nature*. 2015;523(7562):621-5.
63. Wu TP, Wang T, Seetin MG, Lai Y, Zhu S, Lin K, et al. DNA methylation on N(6)-adenine in mammalian embryonic stem cells. *Nature*. 2016;532(7599):329-33.
64. Cao J. The functional role of long non-coding RNAs and epigenetics. *Biological procedures online*. 2014;16:11.
65. Han P, Chang CP. Long non-coding RNA and chromatin remodeling. *RNA biology*. 2015;12(10):1094-8.
66. McBryant SJ, Adams VH, Hansen JC. Chromatin architectural proteins. *Chromosome research : an international journal on the molecular, supramolecular and evolutionary aspects of chromosome biology*. 2006;14(1):39-51.
67. Pan C, Fan Y. Role of H1 linker histones in mammalian development and stem cell differentiation. *Biochimica et biophysica acta*. 2016;1859(3):496-509.
68. Cubenas-Potts C, Corces VG. Architectural proteins, transcription, and the three-dimensional organization of the genome. *FEBS Lett*. 2015;589(20 Pt A):2923-30.
69. Mora A, Sandve GK, Gabrielsen OS, Eskeland R. In the loop: promoter-enhancer interactions and bioinformatics. *Briefings in bioinformatics*. 2016;17(6):980-95.
70. Bernardi G. Genome Organization and Chromosome Architecture. *Cold Spring Harbor symposia on quantitative biology*. 2015;80:83-91.
71. Gomez-Diaz E, Corces VG. Architectural proteins: regulators of 3D genome organization in cell fate. *Trends in cell biology*. 2014;24(11):703-11.
72. Ables ET, Drummond-Barbosa D. The steroid hormone ecdysone functions with intrinsic chromatin remodeling factors to control female germline stem cells in *Drosophila*. *Cell stem cell*. 2010;7(5):581-92.
73. Murawska M, Brehm A. CHD chromatin remodelers and the transcription cycle. *Transcription*. 2011;2(6):244-53.
74. Miccio A, Wang Y, Hong W, Gregory GD, Wang H, Yu X, et al. NuRD mediates activating and repressive functions of GATA-1 and FOG-1 during blood development. *The EMBO journal*. 2010;29(2):442-56.
75. Gerhold CB, Hauer MH, Gasser SM. INO80-C and SWR-C: guardians of the genome. *J Mol Biol*. 2015;427(3):637-51.
76. Bao Y, Shen X. INO80 subfamily of chromatin remodeling complexes. *Mutation research*. 2007;618(1-2):18-29.

REFERENCES

77. Bao Y, Shen X. SnapShot: Chromatin remodeling: INO80 and SWR1. *Cell*. 2011;144(1):158-e2.
78. Papamichos-Chronakis M, Watanabe S, Rando OJ, Peterson CL. Global regulation of H2A.Z localization by the INO80 chromatin-remodeling enzyme is essential for genome integrity. *Cell*. 2011;144(2):200-13.
79. Shen X, Mizuguchi G, Hamiche A, Wu C. A chromatin remodelling complex involved in transcription and DNA processing. *Nature*. 2000;406(6795):541-4.
80. Bannister AJ, Kouzarides T. Regulation of chromatin by histone modifications. *Cell research*. 2011;21(3):381-95.
81. Ng MK, Cheung P. A brief histone in time: understanding the combinatorial functions of histone PTMs in the nucleosome context. *Biochemistry and cell biology = Biochimie et biologie cellulaire*. 2016;94(1):33-42.
82. Xu YM, Du JY, Lau AT. Posttranslational modifications of human histone H3: an update. *Proteomics*. 2014;14(17-18):2047-60.
83. Helin K, Dhanak D. Chromatin proteins and modifications as drug targets. *Nature*. 2013;502(7472):480-8.
84. Jack AP, Hake SB. Getting down to the core of histone modifications. *Chromosoma*. 2014;123(4):355-71.
85. Lee KK, Workman JL. Histone acetyltransferase complexes: one size doesn't fit all. *Nat Rev Mol Cell Biol*. 2007;8(4):284-95.
86. Ropero S, Esteller M. The role of histone deacetylases (HDACs) in human cancer. *Molecular oncology*. 2007;1(1):19-25.
87. Guillemette B, Drogaris P, Lin HH, Armstrong H, Hiragami-Hamada K, Imhof A, et al. H3 lysine 4 is acetylated at active gene promoters and is regulated by H3 lysine 4 methylation. *PLoS genetics*. 2011;7(3):e1001354.
88. Liu CL, Kaplan T, Kim M, Buratowski S, Schreiber SL, Friedman N, et al. Single-nucleosome mapping of histone modifications in *S. cerevisiae*. *PLoS biology*. 2005;3(10):e328.
89. Karmodiya K, Krebs AR, Oulad-Abdelghani M, Kimura H, Tora L. H3K9 and H3K14 acetylation co-occur at many gene regulatory elements, while H3K14ac marks a subset of inactive inducible promoters in mouse embryonic stem cells. *BMC genomics*. 2012;13:424.
90. Calo E, Wysocka J. Modification of enhancer chromatin: what, how, and why? *Molecular cell*. 2013;49(5):825-37.
91. Wang Z, Zang C, Rosenfeld JA, Schones DE, Barski A, Cuddapah S, et al. Combinatorial patterns of histone acetylations and methylations in the human genome. *Nature genetics*. 2008;40(7):897-903.
92. Morris SA, Rao B, Garcia BA, Hake SB, Diaz RL, Shabanowitz J, et al. Identification of histone H3 lysine 36 acetylation as a highly conserved histone modification. *The Journal of biological chemistry*. 2007;282(10):7632-40.
93. Duan MR, Smerdon MJ. Histone H3 lysine 14 (H3K14) acetylation facilitates DNA repair in a positioned nucleosome by stabilizing the binding of the chromatin Remodeler RSC (Remodels Structure of Chromatin). *The Journal of biological chemistry*. 2014;289(12):8353-63.
94. Vazquez BN, Thackray JK, Simonet NG, Kane-Goldsmith N, Martinez-Redondo P, Nguyen T, et al. SIRT7 promotes genome integrity and modulates non-homologous end joining DNA repair. *The EMBO journal*. 2016;35(14):1488-503.

REFERENCES

95. Tessarz P, Kouzarides T. Histone core modifications regulating nucleosome structure and dynamics. *Nat Rev Mol Cell Biol.* 2014;15(11):703-8.
96. Rajagopalan M, Balasubramanian S, Ioshikhes I, Ramaswamy A. Structural dynamics of nucleosome mediated by acetylations at H3K56 and H3K115,122. *European biophysics journal : EBJ.* 2016.
97. Di Cerbo V, Mohn F, Ryan DP, Montellier E, Kacem S, Tropberger P, et al. Acetylation of histone H3 at lysine 64 regulates nucleosome dynamics and facilitates transcription. *eLife.* 2014;3:e01632.
98. Manohar M, Mooney AM, North JA, Nakkula RJ, Picking JW, Edon A, et al. Acetylation of histone H3 at the nucleosome dyad alters DNA-histone binding. *The Journal of biological chemistry.* 2009;284(35):23312-21.
99. Tropberger P, Pott S, Keller C, Kamieniarz-Gdula K, Caron M, Richter F, et al. Regulation of transcription through acetylation of H3K122 on the lateral surface of the histone octamer. *Cell.* 2013;152(4):859-72.
100. Tropberger P, Schneider R. Scratching the (lateral) surface of chromatin regulation by histone modifications. *Nature structural & molecular biology.* 2013;20(6):657-61.
101. Santos-Rosa H, Schneider R, Bannister AJ, Sherriff J, Bernstein BE, Emre NC, et al. Active genes are tri-methylated at K4 of histone H3. *Nature.* 2002;419(6905):407-11.
102. Schneider R, Bannister AJ, Myers FA, Thorne AW, Crane-Robinson C, Kouzarides T. Histone H3 lysine 4 methylation patterns in higher eukaryotic genes. *Nature cell biology.* 2004;6(1):73-7.
103. Becker JS, Nicetto D, Zaret KS. H3K9me3-Dependent Heterochromatin: Barrier to Cell Fate Changes. *Trends in genetics : TIG.* 2016;32(1):29-41.
104. Grossniklaus U, Paro R. Transcriptional silencing by polycomb-group proteins. *Cold Spring Harbor perspectives in biology.* 2014;6(11):a019331.
105. Voon HP, Gibbons RJ. Maintaining memory of silencing at imprinted differentially methylated regions. *Cellular and molecular life sciences : CMLS.* 2016;73(9):1871-9.
106. Brinkman AB, Roelofsen T, Pennings SW, Martens JH, Jenuwein T, Stunnenberg HG. Histone modification patterns associated with the human X chromosome. *EMBO reports.* 2006;7(6):628-34.
107. Wen H, Li Y, Xi Y, Jiang S, Stratton S, Peng D, et al. ZMYND11 links histone H3.3K36me3 to transcription elongation and tumour suppression. *Nature.* 2014;508(7495):263-8.
108. Casadio F, Lu X, Pollock SB, LeRoy G, Garcia BA, Muir TW, et al. H3R42me2a is a histone modification with positive transcriptional effects. *Proceedings of the National Academy of Sciences of the United States of America.* 2013;110(37):14894-9.
109. Jack AP, Bussemer S, Hahn M, Punzeler S, Snyder M, Wells M, et al. H3K56me3 is a novel, conserved heterochromatic mark that largely but not completely overlaps with H3K9me3 in both regulation and localization. *PloS one.* 2013;8(2):e51765.
110. Daujat S, Weiss T, Mohn F, Lange UC, Ziegler-Birling C, Zeissler U, et al. H3K64 trimethylation marks heterochromatin and is dynamically remodeled during

REFERENCES

- developmental reprogramming. *Nature structural & molecular biology*. 2009;16(7):777-81.
111. Ng HH, Ciccone DN, Morshead KB, Oettinger MA, Struhl K. Lysine-79 of histone H3 is hypomethylated at silenced loci in yeast and mammalian cells: a potential mechanism for position-effect variegation. *Proceedings of the National Academy of Sciences of the United States of America*. 2003;100(4):1820-5.
112. Guenther MG, Levine SS, Boyer LA, Jaenisch R, Young RA. A chromatin landmark and transcription initiation at most promoters in human cells. *Cell*. 2007;130(1):77-88.
113. Schubeler D, MacAlpine DM, Scalzo D, Wirbelauer C, Kooperberg C, van Leeuwen F, et al. The histone modification pattern of active genes revealed through genome-wide chromatin analysis of a higher eukaryote. *Genes & development*. 2004;18(11):1263-71.
114. Steger DJ, Lefterova MI, Ying L, Stonestrom AJ, Schupp M, Zhuo D, et al. DOT1L/KMT4 recruitment and H3K79 methylation are ubiquitously coupled with gene transcription in mammalian cells. *Molecular and cellular biology*. 2008;28(8):2825-39.
115. Bode AM, Dong Z. Inducible covalent posttranslational modification of histone H3. *Science's STKE : signal transduction knowledge environment*. 2005;2005(281):re4.
116. Nowak SJ, Corces VG. Phosphorylation of histone H3: a balancing act between chromosome condensation and transcriptional activation. *Trends in genetics : TIG*. 2004;20(4):214-20.
117. Sawicka A, Hartl D, Goiser M, Pusch O, Stocsits RR, Tamir IM, et al. H3S28 phosphorylation is a hallmark of the transcriptional response to cellular stress. *Genome Res*. 2014;24(11):1808-20.
118. Prigent C, Dimitrov S. Phosphorylation of serine 10 in histone H3, what for? *J Cell Sci*. 2003;116(Pt 18):3677-85.
119. Strahl BD, Allis CD. The language of covalent histone modifications. *Nature*. 2000;403(6765):41-5.
120. Rando OJ. Combinatorial complexity in chromatin structure and function: revisiting the histone code. *Current opinion in genetics & development*. 2012;22(2):148-55.
121. Bernstein BE, Mikkelsen TS, Xie X, Kamal M, Huebert DJ, Cuff J, et al. A bivalent chromatin structure marks key developmental genes in embryonic stem cells. *Cell*. 2006;125(2):315-26.
122. Voigt P, LeRoy G, Drury WJ, 3rd, Zee BM, Son J, Beck DB, et al. Asymmetrically modified nucleosomes. *Cell*. 2012;151(1):181-93.
123. Yung PY, Stuetzer A, Fischle W, Martinez AM, Cavalli G. Histone H3 Serine 28 Is Essential for Efficient Polycomb-Mediated Gene Repression in *Drosophila*. *Cell reports*. 2015;11(9):1437-45.
124. Lee JS, Shukla A, Schneider J, Swanson SK, Washburn MP, Florens L, et al. Histone crosstalk between H2B monoubiquitination and H3 methylation mediated by COMPASS. *Cell*. 2007;131(6):1084-96.
125. Talbert PB, Ahmad K, Almouzni G, Ausio J, Berger F, Bhalla PL, et al. A unified phylogeny-based nomenclature for histone variants. *Epigenetics & chromatin*. 2012;5:7.

REFERENCES

126. Muller S, Almouzni G. Chromatin dynamics during the cell cycle at centromeres. *Nature reviews Genetics*. 2017;18(3):192-208.
127. Marzluff WF, Wagner EJ, Duronio RJ. Metabolism and regulation of canonical histone mRNAs: life without a poly(A) tail. *Nature reviews Genetics*. 2008;9(11):843-54.
128. Bonisch C, Hake SB. Histone H2A variants in nucleosomes and chromatin: more or less stable? *Nucleic acids research*. 2012;40(21):10719-41.
129. Chen P, Wang Y, Li G. Dynamics of histone variant H3.3 and its coregulation with H2A.Z at enhancers and promoters. *Nucleus (Austin, Tex)*. 2014;5(1):21-7.
130. Jin C, Zang C, Wei G, Cui K, Peng W, Zhao K, et al. H3.3/H2A.Z double variant-containing nucleosomes mark 'nucleosome-free regions' of active promoters and other regulatory regions. *Nature genetics*. 2009;41(8):941-5.
131. Adam M, Robert F, Larochelle M, Gaudreau L. H2A.Z is required for global chromatin integrity and for recruitment of RNA polymerase II under specific conditions. *Molecular and cellular biology*. 2001;21(18):6270-9.
132. Raisner RM, Hartley PD, Meneghini MD, Bao MZ, Liu CL, Schreiber SL, et al. Histone variant H2A.Z marks the 5' ends of both active and inactive genes in euchromatin. *Cell*. 2005;123(2):233-48.
133. Xu Y, Ayrappetov MK, Xu C, Gursoy-Yuzugullu O, Hu Y, Price BD. Histone H2A.Z controls a critical chromatin remodeling step required for DNA double-strand break repair. *Molecular cell*. 2012;48(5):723-33.
134. Gursoy-Yuzugullu O, House N, Price BD. Patching Broken DNA: Nucleosome Dynamics and the Repair of DNA Breaks. *J Mol Biol*. 2016;428(9 Pt B):1846-60.
135. Meneghini MD, Wu M, Madhani HD. Conserved histone variant H2A.Z protects euchromatin from the ectopic spread of silent heterochromatin. *Cell*. 2003;112(5):725-36.
136. Rangasamy D, Greaves I, Tremethick DJ. RNA interference demonstrates a novel role for H2A.Z in chromosome segregation. *Nature structural & molecular biology*. 2004;11(7):650-5.
137. Nekrasov M, Amrichova J, Parker BJ, Soboleva TA, Jack C, Williams R, et al. Histone H2A.Z inheritance during the cell cycle and its impact on promoter organization and dynamics. *Nature structural & molecular biology*. 2012;19(11):1076-83.
138. Greaves IK, Rangasamy D, Ridgway P, Tremethick DJ. H2A.Z contributes to the unique 3D structure of the centromere. *Proceedings of the National Academy of Sciences of the United States of America*. 2007;104(2):525-30.
139. Chakravarthy S, Gundimella SK, Caron C, Perche PY, Pehrson JR, Khochbin S, et al. Structural characterization of the histone variant macroH2A. *Molecular and cellular biology*. 2005;25(17):7616-24.
140. Ratnakumar K, Duarte LF, LeRoy G, Hasson D, Smeets D, Vardabasso C, et al. ATRX-mediated chromatin association of histone variant macroH2A1 regulates alpha-globin expression. *Genes & development*. 2012;26(5):433-8.
141. Doyen CM, An W, Angelov D, Bondarenko V, Mietton F, Studitsky VM, et al. Mechanism of polymerase II transcription repression by the histone variant macroH2A. *Molecular and cellular biology*. 2006;26(3):1156-64.
142. Chang EY, Ferreira H, Somers J, Nusinow DA, Owen-Hughes T, Narlikar GJ. MacroH2A allows ATP-dependent chromatin remodeling by SWI/SNF and ACF

REFERENCES

- complexes but specifically reduces recruitment of SWI/SNF. *Biochemistry*. 2008;47(51):13726-32.
143. Angelov D, Molla A, Perche PY, Hans F, Cote J, Khochbin S, et al. The histone variant macroH2A interferes with transcription factor binding and SWI/SNF nucleosome remodeling. *Molecular cell*. 2003;11(4):1033-41.
144. Lavigne MD, Vatsellas G, Polyzos A, Mantouvalou E, Sianidis G, Maraziotis I, et al. Composite macroH2A/NRF-1 Nucleosomes Suppress Noise and Generate Robustness in Gene Expression. *Cell reports*. 2015;11(7):1090-101.
145. Gamble MJ, Frizzell KM, Yang C, Krishnakumar R, Kraus WL. The histone variant macroH2A1 marks repressed autosomal chromatin, but protects a subset of its target genes from silencing. *Genes & development*. 2010;24(1):21-32.
146. Chadwick BP, Willard HF. A novel chromatin protein, distantly related to histone H2A, is largely excluded from the inactive X chromosome. *The Journal of cell biology*. 2001;152(2):375-84.
147. Bao Y, Konesky K, Park YJ, Rosu S, Dyer PN, Rangasamy D, et al. Nucleosomes containing the histone variant H2A.Bbd organize only 118 base pairs of DNA. *The EMBO journal*. 2004;23(16):3314-24.
148. Doyen CM, Montel F, Gautier T, Menoni H, Claudet C, Delacour-Larose M, et al. Dissection of the unusual structural and functional properties of the variant H2A.Bbd nucleosome. *The EMBO journal*. 2006;25(18):4234-44.
149. Sansoni V, Casas-Delucchi CS, Rajan M, Schmidt A, Bonisch C, Thomae AW, et al. The histone variant H2A.Bbd is enriched at sites of DNA synthesis. *Nucleic acids research*. 2014;42(10):6405-20.
150. Tolstorukov MY, Goldman JA, Gilbert C, Ogryzko V, Kingston RE, Park PJ. Histone variant H2A.Bbd is associated with active transcription and mRNA processing in human cells. *Molecular cell*. 2012;47(4):596-607.
151. Fernandez-Capetillo O, Lee A, Nussenzweig M, Nussenzweig A. H2AX: the histone guardian of the genome. *DNA repair*. 2004;3(8-9):959-67.
152. Turinetto V, Giachino C. Multiple facets of histone variant H2AX: a DNA double-strand-break marker with several biological functions. *Nucleic acids research*. 2015;43(5):2489-98.
153. Santoro SW, Dulac C. The activity-dependent histone variant H2BE modulates the life span of olfactory neurons. *eLife*. 2012;1:e00070.
154. Urahama T, Horikoshi N, Osakabe A, Tachiwana H, Kurumizaka H. Structure of human nucleosome containing the testis-specific histone variant TSH2B. *Acta crystallographica Section F, Structural biology communications*. 2014;70(Pt 4):444-9.
155. Shinagawa T, Takagi T, Tsukamoto D, Tomaru C, Huynh LM, Sivaraman P, et al. Histone variants enriched in oocytes enhance reprogramming to induced pluripotent stem cells. *Cell stem cell*. 2014;14(2):217-27.
156. Boulard M, Gautier T, Mbele GO, Gerson V, Hamiche A, Angelov D, et al. The NH2 tail of the novel histone variant H2BFWT exhibits properties distinct from conventional H2B with respect to the assembly of mitotic chromosomes. *Molecular and cellular biology*. 2006;26(4):1518-26.
157. Churikov D, Siino J, Svetlova M, Zhang K, Gineitis A, Morton Bradbury E, et al. Novel human testis-specific histone H2B encoded by the interrupted gene on the X chromosome. *Genomics*. 2004;84(4):745-56.

REFERENCES

158. Shaytan AK, Landsman D, Panchenko AR. Nucleosome adaptability conferred by sequence and structural variations in histone H2A-H2B dimers. *Curr Opin Struct Biol.* 2015;32:48-57.
159. McKinley KL, Cheeseman IM. The molecular basis for centromere identity and function. *Nat Rev Mol Cell Biol.* 2016;17(1):16-29.
160. Black BE, Cleveland DW. Epigenetic centromere propagation and the nature of CENP-a nucleosomes. *Cell.* 2011;144(4):471-9.
161. Vardabasso C, Hasson D, Ratnakumar K, Chung CY, Duarte LF, Bernstein E. Histone variants: emerging players in cancer biology. *Cellular and molecular life sciences : CMLS.* 2014;71(3):379-404.
162. Rosin LF, Mellone BG. Centromeres Drive a Hard Bargain. *Trends in genetics : TIG.* 2017;33(2):101-17.
163. Tachiwana H, Kagawa W, Shiga T, Osakabe A, Miya Y, Saito K, et al. Crystal structure of the human centromeric nucleosome containing CENP-A. *Nature.* 2011;476(7359):232-5.
164. Panchenko T, Sorensen TC, Woodcock CL, Kan ZY, Wood S, Resch MG, et al. Replacement of histone H3 with CENP-A directs global nucleosome array condensation and loosening of nucleosome superhelical termini. *Proceedings of the National Academy of Sciences of the United States of America.* 2011;108(40):16588-93.
165. Howman EV, Fowler KJ, Newson AJ, Redward S, MacDonald AC, Kalitsis P, et al. Early disruption of centromeric chromatin organization in centromere protein A (Cenpa) null mice. *Proceedings of the National Academy of Sciences of the United States of America.* 2000;97(3):1148-53.
166. Zink LM, Hake SB. Histone variants: nuclear function and disease. *Current opinion in genetics & development.* 2016;37:82-9.
167. Buschbeck M, Hake SB. Variants of core histones and their roles in cell fate decisions, development and cancer. *Nat Rev Mol Cell Biol.* 2017.
168. Tachiwana H, Osakabe A, Kimura H, Kurumizaka H. Nucleosome formation with the testis-specific histone H3 variant, H3t, by human nucleosome assembly proteins in vitro. *Nucleic acids research.* 2008;36(7):2208-18.
169. Urahama T, Harada A, Maehara K, Horikoshi N, Sato K, Sato Y, et al. Histone H3.5 forms an unstable nucleosome and accumulates around transcription start sites in human testis. *Epigenetics & chromatin.* 2016;9:2.
170. Shi L, Wen H, Shi X. The Histone Variant H3.3 in Transcriptional Regulation and Human Disease. *J Mol Biol.* 2016.
171. Frank D, Doenecke D, Albig W. Differential expression of human replacement and cell cycle dependent H3 histone genes. *Gene.* 2003;312:135-43.
172. Bramlage B, Kosciessa U, Doenecke D. Differential expression of the murine histone genes H3.3A and H3.3B. *Differentiation; research in biological diversity.* 1997;62(1):13-20.
173. Hake SB, Garcia BA, Kauer M, Baker SP, Shabanowitz J, Hunt DF, et al. Serine 31 phosphorylation of histone variant H3.3 is specific to regions bordering centromeres in metaphase chromosomes. *Proceedings of the National Academy of Sciences of the United States of America.* 2005;102(18):6344-9.
174. Li M, Dong Q, Zhu B. Aurora Kinase B Phosphorylates Histone H3.3 at Serine 31 during Mitosis in Mammalian Cells. *J Mol Biol.* 2017.

REFERENCES

175. Wong LH, Ren H, Williams E, McGhie J, Ahn S, Sim M, et al. Histone H3.3 incorporation provides a unique and functionally essential telomeric chromatin in embryonic stem cells. *Genome Res.* 2009;19(3):404-14.
176. Chang FT, Chan FL, JD RM, Udugama M, Mayne L, Collas P, et al. CHK1-driven histone H3.3 serine 31 phosphorylation is important for chromatin maintenance and cell survival in human ALT cancer cells. *Nucleic acids research.* 2015;43(5):2603-14.
177. Tachiwana H, Osakabe A, Shiga T, Miya Y, Kimura H, Kagawa W, et al. Structures of human nucleosomes containing major histone H3 variants. *Acta crystallographica Section D, Biological crystallography.* 2011;67(Pt 6):578-83.
178. Chen P, Zhao J, Wang Y, Wang M, Long H, Liang D, et al. H3.3 actively marks enhancers and primes gene transcription via opening higher-ordered chromatin. *Genes & development.* 2013;27(19):2109-24.
179. Thakar A, Gupta P, Ishibashi T, Finn R, Silva-Moreno B, Uchiyama S, et al. H2A.Z and H3.3 histone variants affect nucleosome structure: biochemical and biophysical studies. *Biochemistry.* 2009;48(46):10852-7.
180. Jin C, Felsenfeld G. Nucleosome stability mediated by histone variants H3.3 and H2A.Z. *Genes & development.* 2007;21(12):1519-29.
181. Kraushaar DC, Jin W, Maunakea A, Abraham B, Ha M, Zhao K. Genome-wide incorporation dynamics reveal distinct categories of turnover for the histone variant H3.3. *Genome biology.* 2013;14(10):R121.
182. Braunschweig U, Hogan GJ, Pagie L, van Steensel B. Histone H1 binding is inhibited by histone variant H3.3. *The EMBO journal.* 2009;28(23):3635-45.
183. Placek BJ, Huang J, Kent JR, Dorsey J, Rice L, Fraser NW, et al. The histone variant H3.3 regulates gene expression during lytic infection with herpes simplex virus type 1. *Journal of virology.* 2009;83(3):1416-21.
184. Tamura T, Smith M, Kanno T, Dasenbrock H, Nishiyama A, Ozato K. Inducible deposition of the histone variant H3.3 in interferon-stimulated genes. *The Journal of biological chemistry.* 2009;284(18):12217-25.
185. Yang JH, Song Y, Seol JH, Park JY, Yang YJ, Han JW, et al. Myogenic transcriptional activation of MyoD mediated by replication-independent histone deposition. *Proceedings of the National Academy of Sciences of the United States of America.* 2011;108(1):85-90.
186. Hodl M, Basler K. Transcription in the absence of histone H3.3. *Current biology : CB.* 2009;19(14):1221-6.
187. Jang CW, Shibata Y, Starmer J, Yee D, Magnuson T. Histone H3.3 maintains genome integrity during mammalian development. *Genes & development.* 2015;29(13):1377-92.
188. Banaszynski LA, Wen D, Dewell S, Whitcomb SJ, Lin M, Diaz N, et al. Hira-dependent histone H3.3 deposition facilitates PRC2 recruitment at developmental loci in ES cells. *Cell.* 2013;155(1):107-20.
189. Sakai A, Schwartz BE, Goldstein S, Ahmad K. Transcriptional and developmental functions of the H3.3 histone variant in *Drosophila*. *Current biology : CB.* 2009;19(21):1816-20.
190. Goldberg AD, Banaszynski LA, Noh KM, Lewis PW, Elsaesser SJ, Stadler S, et al. Distinct factors control histone variant H3.3 localization at specific genomic regions. *Cell.* 2010;140(5):678-91.

REFERENCES

191. Ray-Gallet D, Woolfe A, Vassias I, Pellentz C, Lacoste N, Puri A, et al. Dynamics of histone H3 deposition in vivo reveal a nucleosome gap-filling mechanism for H3.3 to maintain chromatin integrity. *Molecular cell*. 2011;44(6):928-41.
192. Ahmad K, Henikoff S. The histone variant H3.3 marks active chromatin by replication-independent nucleosome assembly. *Molecular cell*. 2002;9(6):1191-200.
193. Millau JF, Gaudreau L. CTCF, cohesin, and histone variants: connecting the genome. *Biochemistry and cell biology = Biochimie et biologie cellulaire*. 2011;89(5):505-13.
194. de Dieuleveult M, Yen K, Hmitou I, Depaux A, Boussouar F, Bou Dargham D, et al. Genome-wide nucleosome specificity and function of chromatin remodellers in ES cells. *Nature*. 2016;530(7588):113-6.
195. Elsaesser SJ, Goldberg AD, Allis CD. New functions for an old variant: no substitute for histone H3.3. *Current opinion in genetics & development*. 2010;20(2):110-7.
196. Szenker E, Ray-Gallet D, Almouzni G. The double face of the histone variant H3.3. *Cell research*. 2011;21(3):421-34.
197. Udugama M, FT MC, Chan FL, Tang MC, Pickett HA, JD RM, et al. Histone variant H3.3 provides the heterochromatic H3 lysine 9 tri-methylation mark at telomeres. *Nucleic acids research*. 2015;43(21):10227-37.
198. Elsasser SJ, Noh KM, Diaz N, Allis CD, Banaszynski LA. Histone H3.3 is required for endogenous retroviral element silencing in embryonic stem cells. *Nature*. 2015;522(7555):240-4.
199. Sadic D, Schmidt K, Groh S, Kondofersky I, Ellwart J, Fuchs C, et al. Atrx promotes heterochromatin formation at retrotransposons. *EMBO reports*. 2015;16(7):836-50.
200. Morozov VM, GavriloVA EV, Ogryzko VV, Ishov AM. Dualistic function of Daxx at centromeric and pericentromeric heterochromatin in normal and stress conditions. *Nucleus (Austin, Tex)*. 2012;3(3):276-85.
201. Santenard A, Ziegler-Birling C, Koch M, Tora L, Bannister AJ, Torres-Padilla ME. Heterochromatin formation in the mouse embryo requires critical residues of the histone variant H3.3. *Nature cell biology*. 2010;12(9):853-62.
202. Takai H, Smogorzewska A, de Lange T. DNA damage foci at dysfunctional telomeres. *Current biology : CB*. 2003;13(17):1549-56.
203. Bush KM, Yuen BT, Barrilleaux BL, Riggs JW, O'Geen H, Cotterman RF, et al. Endogenous mammalian histone H3.3 exhibits chromatin-related functions during development. *Epigenetics & chromatin*. 2013;6(1):7.
204. Yuen BT, Bush KM, Barrilleaux BL, Cotterman R, Knoepfler PS. Histone H3.3 regulates dynamic chromatin states during spermatogenesis. *Development (Cambridge, England)*. 2014;141(18):3483-94.
205. Tang MC, Jacobs SA, Matisse DM, Soh YM, Graham AN, Tran A, et al. Contribution of the two genes encoding histone variant h3.3 to viability and fertility in mice. *PLoS genetics*. 2015;11(2):e1004964.
206. Couldrey C, Carlton MB, Nolan PM, Colledge WH, Evans MJ. A retroviral gene trap insertion into the histone 3.3A gene causes partial neonatal lethality, stunted growth, neuromuscular deficits and male sub-fertility in transgenic mice. *Human molecular genetics*. 1999;8(13):2489-95.

REFERENCES

207. Park SM, Choi EY, Bae M, Kim S, Park JB, Yoo H, et al. Histone variant H3F3A promotes lung cancer cell migration through intronic regulation. *Nature communications*. 2016;7:12914.
208. Graber MW, Schweinfest CW, Reed CE, Papas TS, Baron PL. Isolation of differentially expressed genes in carcinoma of the esophagus. *Annals of surgical oncology*. 1996;3(2):192-7.
209. Schwartzentruber J, Korshunov A, Liu XY, Jones DT, Pfaff E, Jacob K, et al. Driver mutations in histone H3.3 and chromatin remodelling genes in paediatric glioblastoma. *Nature*. 2012;482(7384):226-31.
210. Wu G, Broniscer A, McEachron TA, Lu C, Paugh BS, Becksfort J, et al. Somatic histone H3 alterations in pediatric diffuse intrinsic pontine gliomas and non-brainstem glioblastomas. *Nature genetics*. 2012;44(3):251-3.
211. Behjati S, Tarpey PS, Presneau N, Scheipl S, Pillay N, Van Loo P, et al. Distinct H3F3A and H3F3B driver mutations define chondroblastoma and giant cell tumor of bone. *Nature genetics*. 2013;45(12):1479-82.
212. Lewis PW, Muller MM, Koletsky MS, Cordero F, Lin S, Banaszynski LA, et al. Inhibition of PRC2 activity by a gain-of-function H3 mutation found in pediatric glioblastoma. *Science*. 2013;340(6134):857-61.
213. Chan KM, Fang D, Gan H, Hashizume R, Yu C, Schroeder M, et al. The histone H3.K27M mutation in pediatric glioma reprograms H3K27 methylation and gene expression. *Genes & development*. 2013;27(9):985-90.
214. Justin N, Zhang Y, Tarricone C, Martin SR, Chen S, Underwood E, et al. Structural basis of oncogenic histone H3K27M inhibition of human polycomb repressive complex 2. *Nature communications*. 2016;7:11316.
215. Lu C, Jain SU, Hoelper D, Bechet D, Molden RC, Ran L, et al. Histone H3K36 mutations promote sarcomagenesis through altered histone methylation landscape. *Science*. 2016;352(6287):844-9.
216. Fang D, Gan H, Lee JH, Han J, Wang Z, Riester SM, et al. The histone H3.K36M mutation reprograms the epigenome of chondroblastomas. *Science*. 2016;352(6291):1344-8.
217. Steffen PA, Ringrose L. What are memories made of? How Polycomb and Trithorax proteins mediate epigenetic memory. *Nat Rev Mol Cell Biol*. 2014;15(5):340-56.
218. Wiedemann SM, Mildner SN, Bonisch C, Israel L, Maiser A, Matheisl S, et al. Identification and characterization of two novel primate-specific histone H3 variants, H3.X and H3.Y. *The Journal of cell biology*. 2010;190(5):777-91.
219. Kujirai T, Horikoshi N, Sato K, Maehara K, Machida S, Osakabe A, et al. Structure and function of human histone H3.Y nucleosome. *Nucleic acids research*. 2016.
220. Kim JM, Kim K, Punj V, Liang G, Ulmer TS, Lu W, et al. Linker histone H1.2 establishes chromatin compaction and gene silencing through recognition of H3K27me3. *Scientific reports*. 2015;5:16714.
221. Gibbons RJ, McDowell TL, Raman S, O'Rourke DM, Garrick D, Ayyub H, et al. Mutations in ATRX, encoding a SWI/SNF-like protein, cause diverse changes in the pattern of DNA methylation. *Nature genetics*. 2000;24(4):368-71.

REFERENCES

222. Voon HP, Wong LH. New players in heterochromatin silencing: histone variant H3.3 and the ATRX/DAXX chaperone. *Nucleic acids research*. 2016;44(4):1496-501.
223. Voon HP, Hughes JR, Rode C, De La Rosa-Velazquez IA, Jenuwein T, Feil R, et al. ATRX Plays a Key Role in Maintaining Silencing at Interstitial Heterochromatic Loci and Imprinted Genes. *Cell reports*. 2015;11(3):405-18.
224. He Q, Kim H, Huang R, Lu W, Tang M, Shi F, et al. The Daxx/Atrx Complex Protects Tandem Repetitive Elements during DNA Hypomethylation by Promoting H3K9 Trimethylation. *Cell stem cell*. 2015;17(3):273-86.
225. Wong LH, McGhie JD, Sim M, Anderson MA, Ahn S, Hannan RD, et al. ATRX interacts with H3.3 in maintaining telomere structural integrity in pluripotent embryonic stem cells. *Genome Res*. 2010;20(3):351-60.
226. Lovejoy CA, Li W, Reisenweber S, Thongthip S, Bruno J, de Lange T, et al. Loss of ATRX, genome instability, and an altered DNA damage response are hallmarks of the alternative lengthening of telomeres pathway. *PLoS genetics*. 2012;8(7):e1002772.
227. Ritchie K, Seah C, Moulin J, Isaac C, Dick F, Berube NG. Loss of ATRX leads to chromosome cohesion and congression defects. *The Journal of cell biology*. 2008;180(2):315-24.
228. Gibbons RJ, Picketts DJ, Villard L, Higgs DR. Mutations in a putative global transcriptional regulator cause X-linked mental retardation with alpha-thalassemia (ATR-X syndrome). *Cell*. 1995;80(6):837-45.
229. Jiao Y, Shi C, Edil BH, de Wilde RF, Klimstra DS, Maitra A, et al. DAXX/ATRX, MEN1, and mTOR pathway genes are frequently altered in pancreatic neuroendocrine tumors. *Science*. 2011;331(6021):1199-203.
230. Heaphy CM, de Wilde RF, Jiao Y, Klein AP, Edil BH, Shi C, et al. Altered telomeres in tumors with ATRX and DAXX mutations. *Science*. 2011;333(6041):425.
231. Marinoni I, Kurrer AS, Vassella E, Dettmer M, Rudolph T, Banz V, et al. Loss of DAXX and ATRX are associated with chromosome instability and reduced survival of patients with pancreatic neuroendocrine tumors. *Gastroenterology*. 2014;146(2):453-60.e5.
232. Amorim JP, Santos G, Vinagre J, Soares P. The Role of ATRX in the Alternative Lengthening of Telomeres (ALT) Phenotype. *Genes*. 2016;7(9).
233. Belotserkovskaya R, Oh S, Bondarenko VA, Orphanides G, Studitsky VM, Reinberg D. FACT facilitates transcription-dependent nucleosome alteration. *Science*. 2003;301(5636):1090-3.
234. Aguilar-Gurrieri C, Larabi A, Vinayachandran V, Patel NA, Yen K, Reja R, et al. Structural evidence for Nap1-dependent H2A-H2B deposition and nucleosome assembly. *The EMBO journal*. 2016;35(13):1465-82.
235. Bowman A, Ward R, Wiechens N, Singh V, El-Mkami H, Norman DG, et al. The histone chaperones Nap1 and Vps75 bind histones H3 and H4 in a tetrameric conformation. *Molecular cell*. 2011;41(4):398-408.
236. Jasencakova Z, Scharf AN, Ask K, Corpet A, Imhof A, Almouzni G, et al. Replication stress interferes with histone recycling and predeposition marking of new histones. *Molecular cell*. 2010;37(5):736-43.
237. Keck KM, Pemberton LF. Histone chaperones link histone nuclear import and chromatin assembly. *Biochimica et biophysica acta*. 2013;1819(3-4):277-89.

REFERENCES

238. English CM, Adkins MW, Carson JJ, Churchill ME, Tyler JK. Structural basis for the histone chaperone activity of Asf1. *Cell*. 2006;127(3):495-508.
239. Ray-Gallet D, Quivy JP, Scamps C, Martini EM, Lipinski M, Almouzni G. HIRA is critical for a nucleosome assembly pathway independent of DNA synthesis. *Molecular cell*. 2002;9(5):1091-100.
240. Tagami H, Ray-Gallet D, Almouzni G, Nakatani Y. Histone H3.1 and H3.3 complexes mediate nucleosome assembly pathways dependent or independent of DNA synthesis. *Cell*. 2004;116(1):51-61.
241. Tang Y, Poustovoitov MV, Zhao K, Garfinkel M, Canutescu A, Dunbrack R, et al. Structure of a human ASF1a-HIRA complex and insights into specificity of histone chaperone complex assembly. *Nature structural & molecular biology*. 2006;13(10):921-9.
242. Abascal F, Corpet A, Gurard-Levin ZA, Juan D, Ochsenbein F, Rico D, et al. Subfunctionalization via adaptive evolution influenced by genomic context: the case of histone chaperones ASF1a and ASF1b. *Molecular biology and evolution*. 2013;30(8):1853-66.
243. Natsume R, Eitoku M, Akai Y, Sano N, Horikoshi M, Senda T. Structure and function of the histone chaperone CIA/ASF1 complexed with histones H3 and H4. *Nature*. 2007;446(7133):338-41.
244. Agez M, Chen J, Guerois R, van Heijenoort C, Thuret JY, Mann C, et al. Structure of the histone chaperone ASF1 bound to the histone H3 C-terminal helix and functional insights. *Structure (London, England : 1993)*. 2007;15(2):191-9.
245. Schwabish MA, Struhl K. Asf1 mediates histone eviction and deposition during elongation by RNA polymerase II. *Molecular cell*. 2006;22(3):415-22.
246. Huang H, Stromme CB, Saredi G, Hodl M, Strandsby A, Gonzalez-Aguilera C, et al. A unique binding mode enables MCM2 to chaperone histones H3-H4 at replication forks. *Nature structural & molecular biology*. 2015;22(8):618-26.
247. Elsasser SJ, Huang H, Lewis PW, Chin JW, Allis CD, Patel DJ. DAXX envelops a histone H3.3-H4 dimer for H3.3-specific recognition. *Nature*. 2012;491(7425):560-5.
248. Structure of the variant histone H3.3-H4 heterodimer in complex with its chaperone DAXX. 2012.
249. Gaillard PH, Martini EM, Kaufman PD, Stillman B, Moustacchi E, Almouzni G. Chromatin assembly coupled to DNA repair: a new role for chromatin assembly factor I. *Cell*. 1996;86(6):887-96.
250. Smith S, Stillman B. Purification and characterization of CAF-I, a human cell factor required for chromatin assembly during DNA replication in vitro. *Cell*. 1989;58(1):15-25.
251. Shibahara K, Stillman B. Replication-dependent marking of DNA by PCNA facilitates CAF-1-coupled inheritance of chromatin. *Cell*. 1999;96(4):575-85.
252. Krude T. Chromatin assembly factor 1 (CAF-1) colocalizes with replication foci in HeLa cell nuclei. *Experimental cell research*. 1995;220(2):304-11.
253. Marheineke K, Krude T. Nucleosome assembly activity and intracellular localization of human CAF-1 changes during the cell division cycle. *The Journal of biological chemistry*. 1998;273(24):15279-86.
254. Martini E, Roche DM, Marheineke K, Verreault A, Almouzni G. Recruitment of phosphorylated chromatin assembly factor 1 to chromatin after UV irradiation of human cells. *The Journal of cell biology*. 1998;143(3):563-75.

REFERENCES

255. Volk A, Crispino JD. The role of the chromatin assembly complex (CAF-1) and its p60 subunit (CHAF1b) in homeostasis and disease. *Biochimica et biophysica acta*. 2015;1849(8):979-86.
256. Hoek M, Stillman B. Chromatin assembly factor 1 is essential and couples chromatin assembly to DNA replication in vivo. *Proceedings of the National Academy of Sciences of the United States of America*. 2003;100(21):12183-8.
257. Nabatiyan A, Krude T. Silencing of chromatin assembly factor 1 in human cells leads to cell death and loss of chromatin assembly during DNA synthesis. *Molecular and cellular biology*. 2004;24(7):2853-62.
258. Ye X, Franco AA, Santos H, Nelson DM, Kaufman PD, Adams PD. Defective S phase chromatin assembly causes DNA damage, activation of the S phase checkpoint, and S phase arrest. *Molecular cell*. 2003;11(2):341-51.
259. . !!! INVALID CITATION !!! (230).
260. Yang J, Zhang X, Feng J, Leng H, Li S, Xiao J, et al. The Histone Chaperone FACT Contributes to DNA Replication-Coupled Nucleosome Assembly. *Cell reports*. 2016;14(5):1128-41.
261. Adam S, Polo SE, Almouzni G. Transcription recovery after DNA damage requires chromatin priming by the H3.3 histone chaperone HIRA. *Cell*. 2013;155(1):94-106.
262. Zhang H, Gan H, Wang Z, Lee JH, Zhou H, Ordog T, et al. RPA Interacts with HIRA and Regulates H3.3 Deposition at Gene Regulatory Elements in Mammalian Cells. *Molecular cell*. 2017;65(2):272-84.
263. Rai TS, Puri A, McBryan T, Hoffman J, Tang Y, Pchelintsev NA, et al. Human CABIN1 is a functional member of the human HIRA/UBN1/ASF1a histone H3.3 chaperone complex. *Molecular and cellular biology*. 2011;31(19):4107-18.
264. Ricketts MD, Marmorstein R. A Molecular Prospective for HIRA Complex Assembly and H3.3-Specific Histone Chaperone Function. *J Mol Biol*. 2016.
265. Ricketts MD, Frederick B, Hoff H, Tang Y, Schultz DC, Singh Rai T, et al. Ubinuclein-1 confers histone H3.3-specific-binding by the HIRA histone chaperone complex. *Nature communications*. 2015;6:7711.
266. Pchelintsev NA, McBryan T, Rai TS, van Tuyn J, Ray-Gallet D, Almouzni G, et al. Placing the HIRA histone chaperone complex in the chromatin landscape. *Cell reports*. 2013;3(4):1012-9.
267. Drane P, Ouararhni K, Depaux A, Shuaib M, Hamiche A. The death-associated protein DAXX is a novel histone chaperone involved in the replication-independent deposition of H3.3. *Genes & development*. 2010;24(12):1253-65.
268. Lewis PW, Elsaesser SJ, Noh KM, Stadler SC, Allis CD. Daxx is an H3.3-specific histone chaperone and cooperates with ATRX in replication-independent chromatin assembly at telomeres. *Proceedings of the National Academy of Sciences of the United States of America*. 2010;107(32):14075-80.
269. Roberts C, Sutherland HF, Farmer H, Kimber W, Halford S, Carey A, et al. Targeted mutagenesis of the Hira gene results in gastrulation defects and patterning abnormalities of mesoendodermal derivatives prior to early embryonic lethality. *Molecular and cellular biology*. 2002;22(7):2318-28.
270. Michaelson JS, Bader D, Kuo F, Kozak C, Leder P. Loss of Daxx, a promiscuously interacting protein, results in extensive apoptosis in early mouse development. *Genes & development*. 1999;13(15):1918-23.

REFERENCES

271. DeNizio JE, Elsasser SJ, Black BE. DAXX co-folds with H3.3/H4 using high local stability conferred by the H3.3 variant recognition residues. *Nucleic acids research*. 2014;42(7):4318-31.
272. Delbarre E, Ivanauskiene K, Kuntziger T, Collas P. DAXX-dependent supply of soluble (H3.3-H4) dimers to PML bodies pending deposition into chromatin. *Genome Res*. 2013;23(3):440-51.
273. Salomoni P. The PML-Interacting Protein DAXX: Histone Loading Gets into the Picture. *Frontiers in oncology*. 2013;3:152.
274. Corpet A, Olbrich T, Gwerder M, Fink D, Stucki M. Dynamics of histone H3.3 deposition in proliferating and senescent cells reveals a DAXX-dependent targeting to PML-NBs important for pericentromeric heterochromatin organization. *Cell cycle (Georgetown, Tex)*. 2014;13(2):249-67.
275. Chang FT, McGhie JD, Chan FL, Tang MC, Anderson MA, Mann JR, et al. PML bodies provide an important platform for the maintenance of telomeric chromatin integrity in embryonic stem cells. *Nucleic acids research*. 2013;41(8):4447-58.
276. Pan WW, Zhou JJ, Liu XM, Xu Y, Guo LJ, Yu C, et al. Death domain-associated protein DAXX promotes ovarian cancer development and chemoresistance. *The Journal of biological chemistry*. 2013;288(19):13620-30.
277. Singhi AD, Liu TC, Roncaioli JL, Cao D, Zeh HJ, Zureikat AH, et al. Alternative Lengthening of Telomeres and Loss of DAXX/ATRX Expression Predicts Metastatic Disease and Poor Survival in Patients with Pancreatic Neuroendocrine Tumors. *Clinical cancer research : an official journal of the American Association for Cancer Research*. 2017;23(2):600-9.
278. Pipinikas CP, Dibra H, Karpathakis A, Feber A, Novelli M, Oukrif D, et al. Epigenetic dysregulation and poorer prognosis in DAXX-deficient pancreatic neuroendocrine tumours. *Endocrine-related cancer*. 2015;22(3):L13-8.
279. Slatter TL, Hsia H, Samaranyaka A, Sykes P, Clow WB, Devenish CJ, et al. Loss of ATRX and DAXX expression identifies poor prognosis for smooth muscle tumours of uncertain malignant potential and early stage uterine leiomyosarcoma. *The journal of pathology Clinical research*. 2015;1(2):95-105.
280. Latreille D, Bluy L, Benkirane M, Kiernan RE. Identification of histone 3 variant 2 interacting factors. *Nucleic acids research*. 2014;42(6):3542-50.
281. Rappsilber J, Mann M, Ishihama Y. Protocol for micro-purification, enrichment, pre-fractionation and storage of peptides for proteomics using StageTips. *Nature protocols*. 2007;2(8):1896-906.
282. Cox J, Mann M. MaxQuant enables high peptide identification rates, individualized p.p.b.-range mass accuracies and proteome-wide protein quantification. *Nature biotechnology*. 2008;26(12):1367-72.
283. Tyanova S, Temu T, Sinitcyn P, Carlson A, Hein MY, Geiger T, et al. The Perseus computational platform for comprehensive analysis of (prote)omics data. *Nature methods*. 2016;13(9):731-40.
284. Keilhauer EC, Hein MY, Mann M. Accurate protein complex retrieval by affinity enrichment mass spectrometry (AE-MS) rather than affinity purification mass spectrometry (AP-MS). *Molecular & cellular proteomics : MCP*. 2015;14(1):120-35.
285. Langmead B, Salzberg SL. Fast gapped-read alignment with Bowtie 2. *Nature methods*. 2012;9(4):357-9.

REFERENCES

286. Bulut-Karslioglu A, De La Rosa-Velazquez IA, Ramirez F, Barenboim M, Onishi-Seebacher M, Arand J, et al. Suv39h-dependent H3K9me3 marks intact retrotransposons and silences LINE elements in mouse embryonic stem cells. *Molecular cell*. 2014;55(2):277-90.
287. Feng J, Liu T, Qin B, Zhang Y, Liu XS. Identifying ChIP-seq enrichment using MACS. *Nature protocols*. 2012;7(9):1728-40.
288. Gentleman RC, Carey VJ, Bates DM, Bolstad B, Dettling M, Dudoit S, et al. Bioconductor: open software development for computational biology and bioinformatics. *Genome biology*. 2004;5(10):R80.
289. Love MI, Huber W, Anders S. Moderated estimation of fold change and dispersion for RNA-seq data with DESeq2. *Genome biology*. 2014;15(12):550.
290. Machanick P, Bailey TL. MEME-ChIP: motif analysis of large DNA datasets. *Bioinformatics (Oxford, England)*. 2011;27(12):1696-7.
291. Ramirez F, Dundar F, Diehl S, Gruning BA, Manke T. deepTools: a flexible platform for exploring deep-sequencing data. *Nucleic acids research*. 2014;42(Web Server issue):W187-91.
292. Hahne F, Ivanek R. Visualizing Genomic Data Using Gviz and Bioconductor. *Methods in molecular biology (Clifton, NJ)*. 2016;1418:335-51.
293. Chang CC, Naik MT, Huang YS, Jeng JC, Liao PH, Kuo HY, et al. Structural and functional roles of Daxx SIM phosphorylation in SUMO paralog-selective binding and apoptosis modulation. *Molecular cell*. 2011;42(1):62-74.
294. Escobar-Cabrera E, Okon M, Lau DK, Dart CF, Bonvin AM, McIntosh LP. Characterizing the N- and C-terminal Small ubiquitin-like modifier (SUMO)-interacting motifs of the scaffold protein DAXX. *The Journal of biological chemistry*. 2011;286(22):19816-29.
295. Lin DY, Huang YS, Jeng JC, Kuo HY, Chang CC, Chao TT, et al. Role of SUMO-interacting motif in Daxx SUMO modification, subnuclear localization, and repression of sumoylated transcription factors. *Molecular cell*. 2006;24(3):341-54.
296. Michod D, Bartesaghi S, Khelifi A, Bellodi C, Berliocchi L, Nicotera P, et al. Calcium-dependent dephosphorylation of the histone chaperone DAXX regulates H3.3 loading and transcription upon neuronal activation. *Neuron*. 2012;74(1):122-35.
297. Brazina J, Svadlenka J, Macurek L, Andera L, Hodny Z, Bartek J, et al. DNA damage-induced regulatory interplay between DAXX, p53, ATM kinase and Wip1 phosphatase. *Cell cycle (Georgetown, Tex)*. 2015;14(3):375-87.
298. Ecsedy JA, Michaelson JS, Leder P. Homeodomain-interacting protein kinase 1 modulates Daxx localization, phosphorylation, and transcriptional activity. *Molecular and cellular biology*. 2003;23(3):950-60.
299. Kwon JE, La M, Oh KH, Oh YM, Kim GR, Seol JH, et al. BTB domain-containing speckle-type POZ protein (SPOP) serves as an adaptor of Daxx for ubiquitination by Cul3-based ubiquitin ligase. *The Journal of biological chemistry*. 2006;281(18):12664-72.
300. Tang J, Qu L, Pang M, Yang X. Daxx is reciprocally regulated by Mdm2 and Hausp. *Biochemical and biophysical research communications*. 2010;393(3):542-5.
301. Ciccarone F, Zampieri M, Caiafa P. PARP1 orchestrates epigenetic events setting up chromatin domains. *Seminars in cell & developmental biology*. 2017;63:123-34.

REFERENCES

302. Hein MY, Hubner NC, Poser I, Cox J, Nagaraj N, Toyoda Y, et al. A human interactome in three quantitative dimensions organized by stoichiometries and abundances. *Cell*. 2015;163(3):712-23.
303. Heintzman ND, Stuart RK, Hon G, Fu Y, Ching CW, Hawkins RD, et al. Distinct and predictive chromatin signatures of transcriptional promoters and enhancers in the human genome. *Nature genetics*. 2007;39(3):311-8.
304. Vermeulen M, Timmers HT. Grasping trimethylation of histone H3 at lysine 4. *Epigenomics*. 2010;2(3):395-406.
305. Timms RT, Tchasovnikarova IA, Antrobus R, Dougan G, Lehner PJ. ATF7IP-Mediated Stabilization of the Histone Methyltransferase SETDB1 Is Essential for Heterochromatin Formation by the HUSH Complex. *Cell reports*. 2016;17(3):653-9.
306. Lubber CA, Cox J, Lauterbach H, Fancke B, Selbach M, Tschopp J, et al. Quantitative proteomics reveals subset-specific viral recognition in dendritic cells. *Immunity*. 2010;32(2):279-89.
307. Eberl HC, Spruijt CG, Kelstrup CD, Vermeulen M, Mann M. A map of general and specialized chromatin readers in mouse tissues generated by label-free interaction proteomics. *Molecular cell*. 2013;49(2):368-78.
308. Schotta G, Ebert A, Reuter G. SU(VAR)3-9 is a conserved key function in heterochromatic gene silencing. *Genetica*. 2003;117(2-3):149-58.
309. Peters AH, O'Carroll D, Scherthan H, Mechtler K, Sauer S, Schofer C, et al. Loss of the Suv39h histone methyltransferases impairs mammalian heterochromatin and genome stability. *Cell*. 2001;107(3):323-37.
310. Kaustov L, Ouyang H, Amaya M, Lemak A, Nady N, Duan S, et al. Recognition and specificity determinants of the human cbx chromodomains. *The Journal of biological chemistry*. 2011;286(1):521-9.
311. Canzio D, Larson A, Narlikar GJ. Mechanisms of functional promiscuity by HP1 proteins. *Trends in cell biology*. 2014;24(6):377-86.
312. Hsieh FK, Kulaeva OI, Patel SS, Dyer PN, Luger K, Reinberg D, et al. Histone chaperone FACT action during transcription through chromatin by RNA polymerase II. *Proceedings of the National Academy of Sciences of the United States of America*. 2013;110(19):7654-9.
313. Liu CP, Xiong C, Wang M, Yu Z, Yang N, Chen P, et al. Structure of the variant histone H3.3-H4 heterodimer in complex with its chaperone DAXX. *Nature structural & molecular biology*. 2012;19(12):1287-92.
314. Hake SB, Allis CD. Histone H3 variants and their potential role in indexing mammalian genomes: the "H3 barcode hypothesis". *Proceedings of the National Academy of Sciences of the United States of America*. 2006;103(17):6428-35.
315. Li Q, Zhou H, Wurtele H, Davies B, Horazdovsky B, Verreault A, et al. Acetylation of histone H3 lysine 56 regulates replication-coupled nucleosome assembly. *Cell*. 2008;134(2):244-55.
316. Su D, Hu Q, Li Q, Thompson JR, Cui G, Fazly A, et al. Structural basis for recognition of H3K56-acetylated histone H3-H4 by the chaperone Rtt106. *Nature*. 2012;483(7387):104-7.
317. Choi SH, Worswick S, Byun HM, Shear T, Soussa JC, Wolff EM, et al. Changes in DNA methylation of tandem DNA repeats are different from interspersed repeats in cancer. *International journal of cancer*. 2009;125(3):723-9.

REFERENCES

318. Ross JP, Rand KN, Molloy PL. Hypomethylation of repeated DNA sequences in cancer. *Epigenomics*. 2010;2(2):245-69.
319. Su J, Shao X, Liu H, Liu S, Wu Q, Zhang Y. Genome-wide dynamic changes of DNA methylation of repetitive elements in human embryonic stem cells and fetal fibroblasts. *Genomics*. 2012;99(1):10-7.
320. Zhang K, Gao Y, Li J, Burgess R, Han J, Liang H, et al. A DNA binding winged helix domain in CAF-1 functions with PCNA to stabilize CAF-1 at replication forks. *Nucleic acids research*. 2016;44(11):5083-94.
321. Sauer PV, Timm J, Liu D, Sitbon D, Boeri-Erba E, Velours C, et al. Insights into the molecular architecture and histone H3-H4 deposition mechanism of yeast Chromatin assembly factor 1. *eLife*. 2017;6.
322. Connelly KE, Dykhuizen EC. Compositional and functional diversity of canonical PRC1 complexes in mammals. *Biochimica et biophysica acta*. 2017;1860(2):233-45.
323. Chittock EC, Latwiel S, Miller TC, Muller CW. Molecular architecture of polycomb repressive complexes. *Biochem Soc Trans*. 2017;45(1):193-205.
324. Gao Z, Zhang J, Bonasio R, Strino F, Sawai A, Parisi F, et al. PCGF homologs, CBX proteins, and RYBP define functionally distinct PRC1 family complexes. *Molecular cell*. 2012;45(3):344-56.
325. Vermeulen M, Eberl HC, Matarese F, Marks H, Denissov S, Butter F, et al. Quantitative interaction proteomics and genome-wide profiling of epigenetic histone marks and their readers. *Cell*. 2010;142(6):967-80.
326. Tsunaka Y, Fujiwara Y, Oyama T, Hirose S, Morikawa K. Integrated molecular mechanism directing nucleosome reorganization by human FACT. *Genes & development*. 2016;30(6):673-86.
327. Okada M, Okawa K, Isobe T, Fukagawa T. CENP-H-containing complex facilitates centromere deposition of CENP-A in cooperation with FACT and CHD1. *Molecular biology of the cell*. 2009;20(18):3986-95.
328. Persson J, Ekwall K. Chd1 remodelers maintain open chromatin and regulate the epigenetics of differentiation. *Experimental cell research*. 2010;316(8):1316-23.
329. Petty E, Pillus L. Balancing chromatin remodeling and histone modifications in transcription. *Trends in genetics : TIG*. 2013;29(11):621-9.
330. Siggins L, Cordeddu L, Ronnerblad M, Lennartsson A, Ekwall K. Transcription-coupled recruitment of human CHD1 and CHD2 influences chromatin accessibility and histone H3 and H3.3 occupancy at active chromatin regions. *Epigenetics & chromatin*. 2015;8(1):4.
331. Li H, Ilin S, Wang W, Duncan EM, Wysocka J, Allis CD, et al. Molecular basis for site-specific read-out of histone H3K4me3 by the BPTF PHD finger of NURF. *Nature*. 2006;442(7098):91-5.
332. Wysocka J, Swigut T, Xiao H, Milne TA, Kwon SY, Landry J, et al. A PHD finger of NURF couples histone H3 lysine 4 trimethylation with chromatin remodelling. *Nature*. 2006;442(7098):86-90.
333. Kukimoto I, Elderkin S, Grimaldi M, Oelgeschlager T, Varga-Weisz PD. The histone-fold protein complex CHRAC-15/17 enhances nucleosome sliding and assembly mediated by ACF. *Molecular cell*. 2004;13(2):265-77.

REFERENCES

334. Loyola A, Huang JY, LeRoy G, Hu S, Wang YH, Donnelly RJ, et al. Functional analysis of the subunits of the chromatin assembly factor RSF. *Molecular and cellular biology*. 2003;23(19):6759-68.
335. Pessina F, Lowndes NF. The RSF1 histone-remodelling factor facilitates DNA double-strand break repair by recruiting centromeric and Fanconi Anaemia proteins. *PLoS biology*. 2014;12(5):e1001856.
336. Doyon Y, Selleck W, Lane WS, Tan S, Cote J. Structural and functional conservation of the NuA4 histone acetyltransferase complex from yeast to humans. *Molecular and cellular biology*. 2004;24(5):1884-96.
337. Murr R, Vaissiere T, Sawan C, Shukla V, Herceg Z. Orchestration of chromatin-based processes: mind the TRRAP. *Oncogene*. 2007;26(37):5358-72.
338. Fuchs M, Gerber J, Drapkin R, Sif S, Ikura T, Ogryzko V, et al. The p400 complex is an essential E1A transformation target. *Cell*. 2001;106(3):297-307.
339. Pradhan SK, Su T, Yen L, Jacquet K, Huang C, Cote J, et al. EP400 Deposits H3.3 into Promoters and Enhancers during Gene Activation. *Molecular cell*. 2016;61(1):27-38.
340. Yao W, King DA, Beckwith SL, Gowans GJ, Yen K, Zhou C, et al. The INO80 Complex Requires the Arp5-Ies6 Subcomplex for Chromatin Remodeling and Metabolic Regulation. *Molecular and cellular biology*. 2016;36(6):979-91.
341. Schubert HL, Wittmeyer J, Kasten MM, Hinata K, Rawling DC, Heroux A, et al. Structure of an actin-related subcomplex of the SWI/SNF chromatin remodeler. *Proceedings of the National Academy of Sciences of the United States of America*. 2013;110(9):3345-50.
342. Yang X, Zaurin R, Beato M, Peterson CL. Swi3p controls SWI/SNF assembly and ATP-dependent H2A-H2B displacement. *Nature structural & molecular biology*. 2007;14(6):540-7.
343. Chen L, Conaway RC, Conaway JW. Multiple modes of regulation of the human Ino80 SNF2 ATPase by subunits of the INO80 chromatin-remodeling complex. *Proceedings of the National Academy of Sciences of the United States of America*. 2013;110(51):20497-502.
344. Vedadi M, Blazer L, Eram MS, Baryshte-Lovejoy D, Arrowsmith CH, Hajian T. Targeting human SET1/MLL family of proteins. *Protein Sci*. 2017;26(4):662-76.
345. Herz HM, Hu D, Shilatifard A. Enhancer malfunction in cancer. *Molecular cell*. 2014;53(6):859-66.
346. Jozwik KM, Chernukhin I, Serandour AA, Nagarajan S, Carroll JS. FOXA1 Directs H3K4 Monomethylation at Enhancers via Recruitment of the Methyltransferase MLL3. *Cell reports*. 2016;17(10):2715-23.
347. Shinsky SA, Monteith KE, Viggiano S, Cosgrove MS. Biochemical reconstitution and phylogenetic comparison of human SET1 family core complexes involved in histone methylation. *The Journal of biological chemistry*. 2015;290(10):6361-75.
348. Silva AC, Xu X, Kim HS, Fillingham J, Kislinger T, Mennella TA, et al. The replication-independent histone H3-H4 chaperones HIR, ASF1, and RTT106 cooperate to maintain promoter fidelity. *The Journal of biological chemistry*. 2012;287(3):1709-18.

REFERENCES

349. Alabert C, Barth TK, Reveron-Gomez N, Sidoli S, Schmidt A, Jensen ON, et al. Two distinct modes for propagation of histone PTMs across the cell cycle. *Genes & development*. 2015;29(6):585-90.
350. Kujirai T, Horikoshi N, Xie Y, Taguchi H, Kurumizaka H. Identification of the amino acid residues responsible for stable nucleosome formation by histone H3.Y. *Nucleus (Austin, Tex)*. 2017:1-10.
351. Lahiri S, Sun N, Buck A, Imhof A, Walch A. MALDI imaging mass spectrometry as a novel tool for detecting histone modifications in clinical tissue samples. *Expert review of proteomics*. 2016;13(3):275-84.
352. Lahiri S, Sun N, Solis-Mezarino V, Fedisch A, Ninkovic J, Feuchtinger A, et al. In situ detection of histone variants and modifications in mouse brain using imaging mass spectrometry. *Proteomics*. 2016;16(3):437-47.

ABBREVIATIONS

ABBREVIATIONS

5caC	5-carboxylcytosine
5fC	5-formylcytosine
5hmC	5-hydroxymethylcytosine (5hmC)
5mC	5-methylcytosine
AA	Amino acid
ADP	Adenosine diphosphate
ALT	Alternative lengthening of telomeres
ASF1	Anti-silencing function 1
ATP	Adenosine triphosphate
ATRX	α -thalassaemia/mental retardation X-linked
BPTF	Bromodomain PHD finger transcription factor
BSA	Bovine serum albumin
CABIN1	Calcineurin binding protein 1
CAF-1	Chromatin assembly factor 1
CBX	Chromobox protein homolog
CHD	Chromodomain helicase DNA-binding protein
ChIP	Chromatin immunoprecipitation
CHRAC1	Chromatin accessibility complex 1
CPI	Complete protease inhibitor
CTCF	CCCTC-binding factor Culture
DAPI	4',6-Diamidino-2-phenylindole
DAXX	Death domain-associated protein
DMEM	Dulbecco's modified eagle medium
DMSO	Dimethylsulfoxide
DSB	Double strand break
DTT	Dithiothreitol
EZH2	Enhancer of Zeste 2
FACT	Facilitates chromatin transcription
FCS	Fetal calf serum
FSC	Forward scatter
G2	Gap 2
GEO	Gene expression omnibus
GFP	Green fluorescent protein
H/DX-MS	Hydrogen/deuterium exchange mass spectrometry
H2A.Bbd	H2A Barr body deficient
HAT	Histone acetyltransferase

ABBREVIATIONS

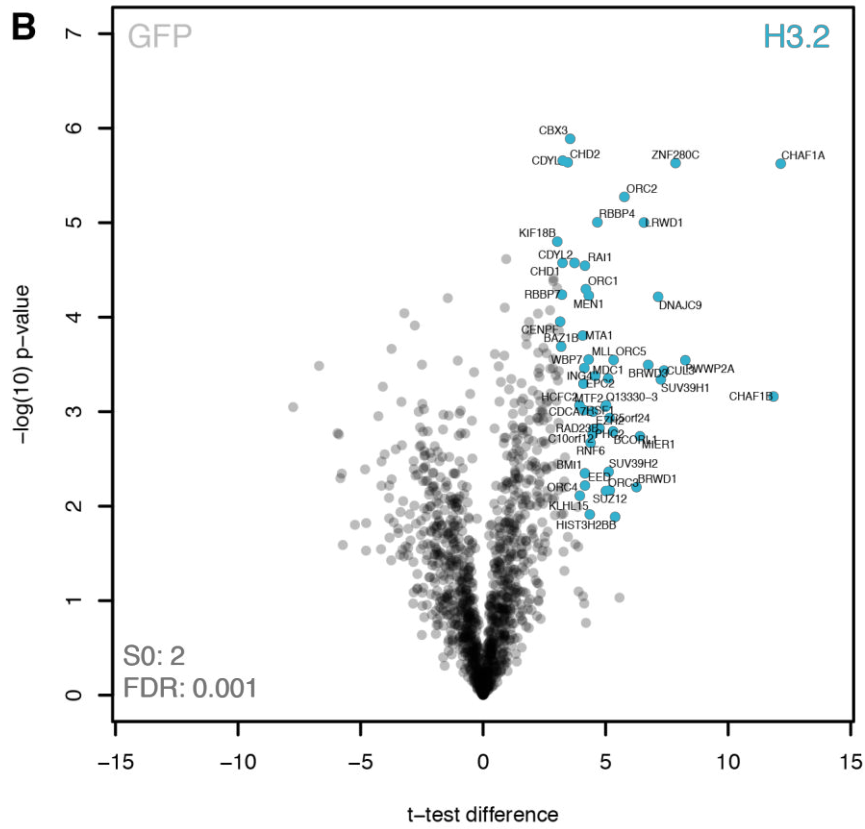
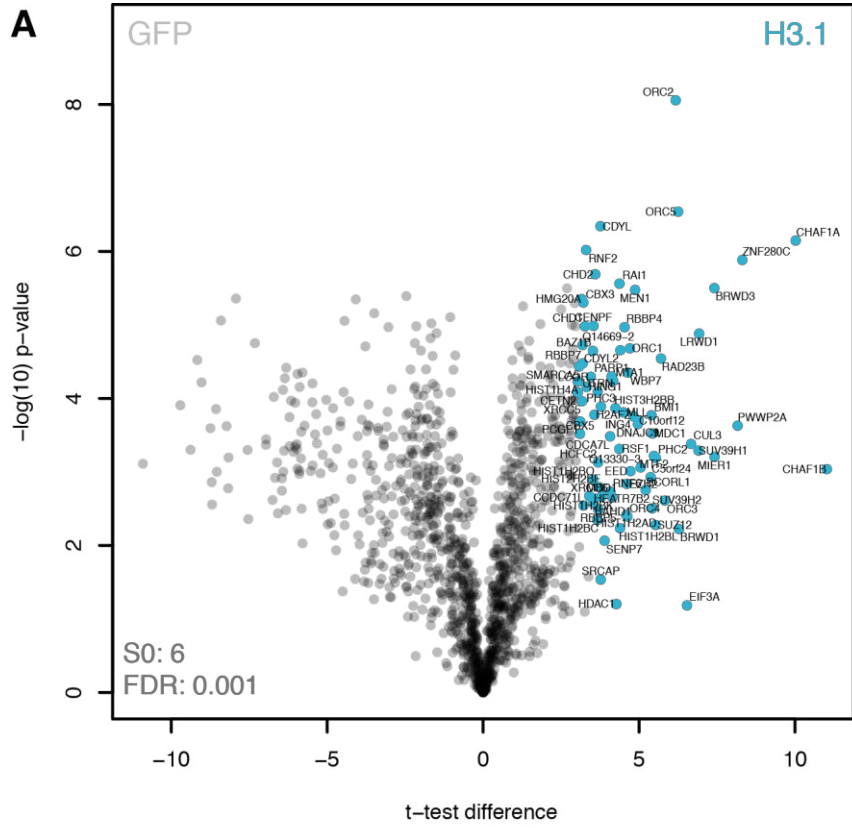
HBD	Histone-binding domain
HDAC	Histone deacetylase
HEPES	2-[4-(2-hydroxyethyl)piperazin-1-yl]ethanesulfonic acid
HFD	Histone fold domain
HIRA	Histone regulatory homologue A
HP1	Heterochromatin binding protein 1
IF	Immunofluorescence
IPTG	Isopropyl- β -D-thiogalactopyranoside
KAT	Lysine acetyltransferase
lncRNAs	Long noncoding RNAs
MCM	Minichromosome maintenance
MEFs	Mouse embryonic fibroblasts
mESC	Mouse embryonic stem cell
MLL3	Mixed-lineage leukemia 3
MNase	Micrococcal nuclease
MS	Mass spectrometry
NAD	Nicotinamide adenine dinucleotide
NAP1	Nucleosome assembly protein 1
NASP	Nuclear autoantigenic sperm protein
NB	Nuclear body
Nb	Nonbound
NCP	Nucleosome core particle
Neo	Neomycin
NSCs	Neural stem cell
nt	Nucleotide
panNET	Pancreatic neuroendocrine tumor
PARP1	Poly (ADP-ribose) polymerase 1
PBS	Phosphate buffered saline
PCGF	Polycomb group finger
PCNA	Proliferating cell nuclear antigen
PCR	Polymerase chain reaction
PHC	Polyhomeotic-like protein
PHD	Plant homeodomain finger
PML	Promyelocytic leukemia
PRC	Polycomb Repressive Complex protein
PTM	Posttranslational modification
RbAp46	Retinoblastoma-associated protein 46
RbAp48	Retinoblastoma-associated protein 48

ABBREVIATIONS

RPA	Replication protein A
RSF1	Remodeling and spacing factor 1
RT	Room temperature
SDS	Sodium dodecyl sulfate
SETD1A	SET domain containing 1A
SILAC	Stable isotope labeling of amino acids in cell culture
Spt16	Suppressor of Ty16
SSC	Sideward scatter
SSRP1	Structure specific recognition protein 1
SUMO	Small ubiquitin like modifier
SUV39H	Suppressor of variegation 3-9
TBE	Tris borate EDTA
TE	Tris EDTA
TERRA	Telomere repeat-containing RNA
TF	Transcription factor
TFA	Trifluoroacetic acid
TIFs	Telomere dysfunctional induced foci
TRRAP	Transformation/transcription associated
TSA	Trichostatin A
TSS	Transcriptional start sites
UBN1	Ubinuclein 1
UTR	Untranslated region

APPENDIX

APPENDIX



APPENDIX

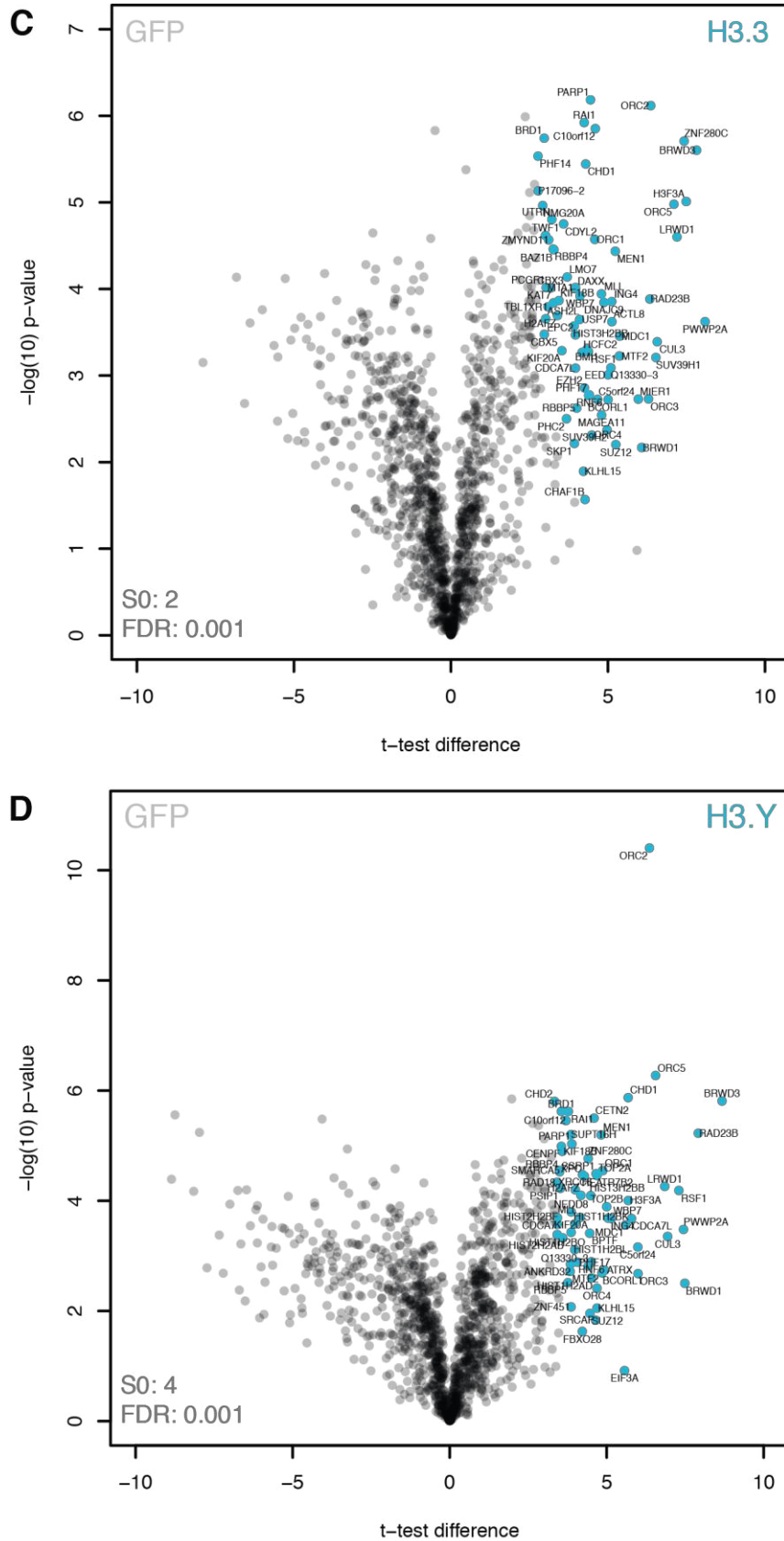


Figure A.1: Identification of proteins enriched on eGFP-H3 variant-containing mononucleosomes obtained by label-free quantitative mass spectrometry compared to eGFP immunoprecipitations. Mononucleosomes of eGFP and eGFP-H3.1 (A), -H3.2 (B), -H3.3 (C) and -H3.Y (D) expressing cell lines were generated and subjected to immunoprecipitations with GFP-trap_M beads. Comparing

APPENDIX

interactors of eGFP and H3 variants served to identify and exclude background binders. Enrichment differences were obtained from two-sample t-tests and are displayed by plotting p-values and t-test differences in volcano plots. Permutation-based FDR cutoff was utilized to identify significantly enriched proteins. These proteins are labeled in the plot.

